Development of Re(I) Photocatalysts for the Photochemical Reduction of Atmospheric CO_2

by

Elizabeth Anne Murphy

A thesis submitted in partial fulfillment of the requirements for the degree of

Master of Science

Department of Chemistry
University of Alberta

ABSTRACT

Three new Re(I) photocatalysts were prepared by synthesizing imidazole and imidazolium dyes based on carbazolyl dicyanobenzene derivatives and physically linking them to a Re metal centre for the photochemical reduction of CO_2. The imidazolium dyes were of interest because they are precursors to free non-heterocyclic compounds which can be generated by deprotonation. All three photocatalysts, Re-**2**, Re-**8**, and Re-**9**, were successful in the reduction of CO_2, yielding CO as a reduction product and methane as a side product. The CO_2 reduction reactions with each catalyst began with an initial burst in activity followed by a decrease due to the precipitation of a solid in the reaction solution that reflected/blocked incident light. One of the Re-NHC photocatalysts, Re-**8**, resulted in the highest activity out of the three compounds, with an initial turnover frequency of 47 h^{-1}. The source of the produced methane was identified as the cleavage of a methyl group from the electron donor, 1,3-dimethyl-2-phenyl-2,3-dihydro-1H-benzimidazole, by a radical reaction chain unrelated to the reduction of CO_2. These compounds show promising results as photocatalysts for the reduction of CO_2 to CO and can be translated to heterogeneous systems via electro-polymerization of the carbazole moieties on to indium-tin oxide and carbon electrodes.

ACKNOWLEDGEMENTS

The journey to completing and submitting this thesis was not easy and required the assistance of many individuals. I would first like to thank Ryan Mercer for his endless support and graciousness in both my academic and personal life over these past two years of graduate school. I would also like to thank my parents, Steven and Karen, as well as my sisters Cassandra and Juliette for always raising my spirits and providing encouragement. To my lab mates, past and present, thank you for your guidance and support in my research. Thank you to my friends back home, especially Jessica Giggins, and to my new friends here in Edmonton, specifically Lexi Enns, for their never-ending support and constant reassurance over the years. Finally, thank you to Dr. Steven H. Bergens for his immense contribution to my chemistry knowledge, technical skills and overall confidence in the lab. I would also like to acknowledge Dr. Lundgren and Dr. Tykwinski for their participation in my supervisory committee and their contribution to my graduate school experience. Thank you for everyone, including those not mentioned by name, who contributed to this experience and to the completion of this program, you did not go unnoticed.

TABLE OF CONTENTS

LIST OF TABLES

LIST OF FIGURES

LIST OF SCHEMES

LIST OF SYMBOLS AND ABBREVIATIONS

• – radical

˚C – degree Celsius

$\Delta \mathbf{E_{ST}}$ – energy difference between singlet and triplet excited states

BI^+ – 1,2-dimethyl-2-phenylbenzimidazolium bicarbonate

BIH – 1,3-dimethyl-2-phenyl-2,3-dihydro-1H-benzimidazole

bpy – 2,2'-bipyridine

br s – broad singlet

CCS – carbon capture and storage

CDCB – carbazole dicyanobenzene

CN – cyano group

COF – covalent organic framework

comp m – complex multiplet

d – doublet

DCM – dichloromethane

dd – doublet of doublet

ddd – doublet of doublet of doublet

DFT – density functional theory

dmb – 2-((3',5'-dimethyl-4'-hydroxyphenyl)azo)benzoic acid

dt – doublet of triplet

Eq - equivalents

Fac – facial

FTIR – Fourier transform infrared

GC-MS – gas chromatography with mass spectroscopy detector

GC-TCD – gas chromatography with thermal conductivity detector

HER – hydrogen evolution reaction

HOMO – highest occupied molecular orbital

HPLC – high-performance liquid chromatography

hr/h – hour

HRMS – high-resolution mass spectrometry

IR – infrared

ISC – intersystem crossing

LED – light-emitting diode

LUMO – lowest unoccupied molecular orbital

M – molar

m – multiplet

MeCN – acetonitrile

min - minute

mL – millilitre

MLCT – metal-to-ligand charge transfer

mM – millimolar

mmol – millimoles

MOF – molecular organic framework

mol – moles

n – mole

N^N – diimine ligand

NADH – nicotinamide adenine nucleotide

NADPH – nicotinamide adenine nucleotide phosphate

NHC – non-heterocyclic carbene

nm – nanometer

NMR – nuclear magnetic resonance

NTO – natural transition orbitals

OEOS – one-electron oxidized species

OERS – one-electron reduced species

OLED – organic light-emitting diode

OPP – oligo(*p*-phenylene)

P(O-*i*Pr)$_3$ – triisopropyl phosphite

P(OEt)$_3$ – triethyl phosphite

Phen – 1,10-phenanthroline

ppm – part per million

ppy – 2-phenylpyridine

PS - photosensitizer

PS* – excited photosensitizer

RDS – rate-determining step

s – singlet

S_0 – ground state

S_1 – lowest energy singlet excited state

SCN – thiocyanate

SOC – spin orbit coupling

SV – Stern-Volmer

T – time

t – triplet

T_1 – lowest energy triplet excited state

TADF – thermally-active delayed fluorescence

td – triplet of doublet

THF – tetrahydrofuran

TMB – 1,3,5-trimethoxybenzene standard

TOF – turnover frequency

TON_{CH4} – CH_4 turnover number

TON_{CO} – CO turnover number

tpy – terpyridine

µL – microlitre

UV – ultraviolet

V – volume

1. INTRODUCTION

1.1 Environmental Impacts of Excess Atmospheric CO_2

In recent times, a major environmental concern is the progressive global warming of planet Earth. The increasing temperature of our planet is a serious rising issue as it can have severe consequences, such as the melting of ice at the Earth's pole, rapid rising sea levels and increased precipitation across the globe.[1] Carbon dioxide, CO_2, is the main greenhouse gas present in the atmosphere leading to global climate change. Excessive CO_2 emissions build up in the atmosphere and absorb and re-emit infrared light from the Earth which raises global temperatures, resulting in ocean acidification.[1] The latest measurement of atmospheric CO_2 by NASA was determined to be 420 ppm, compared to 396 ppm in March 2013. Already, this shows an increase of 24 ppm in only 10 years.[2] According to NASA, human activities have increased the atmospheric CO_2 level by 50% in less than 200 years, making it 150% of its value from 1750.[2] The Intergovernmental Panel on Climate Change (IPCC) Special Report on the impacts of global warming predicts that the atmospheric CO_2 content could reach 590 ppm by 2100, leading to a global mean temperature increase of 1.9 ˚C.[3] A global mean temperature increase of this nature would lead to many devastating environmental impacts, as mentioned above.

1.2 Utilization of CO_2

Fossil fuels represent the major conventional energy source across the world due to their stability, availability, and high energy density.[4] The excessive use and burning of fossil fuels results in large volumes of CO_2 emissions and, in turn, has raised atmospheric CO_2 levels by 100 ppm over the previous century.[4] As a result, the CO_2 emissions from fossil fuel combustion is the single major cause of global warming and climate change.[4] Additionally, the excessive use of fossil fuels will result in their inevitable depletion meaning we will be forced to find a substitute renewable

energy to meet the increasing energy demand of the human population. There are several strategies that have been developed to mitigate the effect of global warming on our planet, with the direct reduction of CO_2 emissions released into the atmosphere being the most efficient and direct route to change.[1] The direct reduction of CO_2 emission, carbon capture and sequestration (CCS) of CO_2 and utilization of atmospheric CO_2 are three strategies that can be explored to decrease overall CO_2 emissions.[1] However, it would be incredibly challenging to lower CO_2 emissions from human activities due to the increasing global population and the continuous demand for a high quality of life.[1] Options to decrease emissions caused by humans involve drastic changes in behaviour and consumption, improving current agricultural processes and the development of efficient renewable energy sources.[5] These strategies would take a long time period to successfully implement and have an effect on the current environmental status. Direct air capture and the capture of CO_2 at the source, as well as underground or undersea storage of the gas, are technologies with high readiness levels and have begun being implemented in some facilities around Alberta.[5] The Government of Alberta has invested $1.24 billion into the Quest and Alberta Carbon Trunk Line (ACTL), which have safely captured over 10.5 million tonnes of CO_2 since 2015.[6] The billions of dollars invested in CCS technology by the Government of Alberta not only serves as a strategy to mitigate the impact of CO_2 on the climate, but also to help make CCS technologies more accessible and to share knowledge in order to help future CCS projects across the globe benefit from discoveries learned in Alberta.[6] Although, the capacity of CCS technology does present some limitations, including a high energy requirement for the compression and transportation of the gas, as well as serious environmental risks of leakage.[1] Despite this, scientists are beginning to consider atmospheric CO_2 as a potential sustainable building block for an alternative source of energy.

A major challenge we are currently facing is the development of ways to use resources more efficiently and new ways to harvest carbon. In nature, plants convert CO_2 into energy-rich carbohydrates using sunlight as the energy source and water as reductant in a photosynthetic process (*scheme 1A, 1B*).[7]

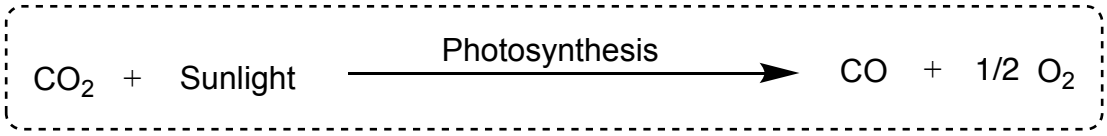

Scheme 1A. *Overall reaction scheme of photosynthetic reduction of CO_2 to CO.*

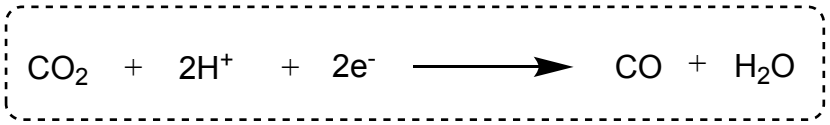

Scheme 1B. *Half-reaction of the production of CO by photosynthesis.*

The direct use of solar energy to convert atmospheric CO_2 into solar fuels and chemicals presents a potential opportunity to substitute fossil fuels and solution to the energy crisis.[8] As a result, the development of systems with the ability to convert CO_2 into energy-rich compounds with solar energy as the only energy input is extremely desirable. In theory, solar power is an infinite energy source that could be incredibly useful if harnessed efficiently given that it is cheap, abundant, and ecologically clean and safe.[4,9] Despite this, certain technologies will always rely on fossil fuels as the main energy source, such as long-range transportation including commercial airplanes and jets. The reduction of captured CO_2 into useful products promotes carbon-neutral processes and can be achieved in many ways, such as biological, thermal, electrochemical, and photochemical systems.[4] Both the electrochemical and photochemical systems allow for the conversion of CO_2 into C_1 intermediates, such as formic acid (HCOOH) and carbon monoxide (CO), which can be further processed into valuable chemicals.[8,10] This will be discussed in detail further on. The concept of solar-driven reduction of CO_2 into valuable chemicals is gaining increasing attention as it presents a promising approach to address global warming and the energy

crisis we are currently facing. Both indirect and direct conversion technologies have been introduced recently. Indirect conversion technologies, such as conversion of biomass into biofuel or the hydrogenation of CO_2 into energy-rich molecules, describes a system in which the reaction uses hydrogen from solar water splitting photocatalysts or the electrolysis of water.[11,12] Direct conversion technologies describe the reduction of CO_2 in the presence of a catalyst via electrochemical or photochemical reactions.[13] These systems are advantageous over indirect conversion technologies as there is no requirement for an intermediate energy carrier.[10]

CO_2 is an extremely stable molecule to reduction that has a linear molecular geometry in its ground state and a net dipole moment of 0.[5] The carbon-oxygen double bonds have a high dissociation energy around 750 kJ/mol, meaning high energy input is required for the molecule to undergo homolytic bond cleavage.[9] Carbon is in its highest possible oxidation state in CO_2 which results in limited opportunity for electron transfers and chemical transformations to occur.[9] However, this also means that reduction of CO_2 can lead to many different products, varying from CO and methane (CH_4) to higher hydrocarbons in the gaseous phase.[9] Photocatalysis for the reduction of CO_2 can provide an approach to encourage the molecule to bend its linear geometry to create dipole moments and generate chemical reactivity.[5] The one-electron reduction of CO_2 generates a radical anion ($CO_2^{\bullet}$) with thermodynamically unfavourable high reduction potential.[10] One the other hand, two-electron and greater-than-two-electron reduction of CO_2 generates more stable, energy-rich products at low potentials (*figure 1*).[10] The two-electron reduction generates carbon monoxide (CO) and formic acid (HCOOH), while the 4-, 6- and 8-electron reduction of CO_2 produce formaldehyde (HCHO), methanol (CH_3OH) and CH_4, respectively.[10] CO and HCOOH are both useful and desirable reduction products that can be used in further chemical processes. CO can be easily converted into liquid hydrocarbons using the Fischer-Tropsch

reaction.[14] HCOOH is a useful liquid storage material for H_2 as it can be easily converted to H_2.[15] Both heterogeneous and homogeneous systems that absorb visible light and promote electron transfer have been developed for the reduction of CO_2. Excitation of the system by one photon typically induces only one-electron transfer as opposed to a multi-electron transfer that is required to reduce CO_2 into high-value products.[16] For this reason, catalysts that can convert one-electron transfer into multi-electron transfer are necessary to generate products that are useful in further chemical and industrial processes from CO_2.[11] Additionally, the two-electron reduction of CO_2 is thermally unfavourable compared to H_2 formation in aqueous conditions.[10] This means that the hydrogen evolution reaction (HER) competes with the reduction of CO_2 in the presence of water.[10] Reported photocatalytic systems for the reduction of CO_2 face low energy conversion efficiency, uncontrollable selectivity and instability, and competing HER in aqueous conditions.[9] For the reasons mentioned above, there is a need to design and develop highly active photocatalytic systems that demonstrate high selectivity and conversion efficiency, that cannot readily reduce H^+ to H_2, and that drive multi-electron reduction processes.

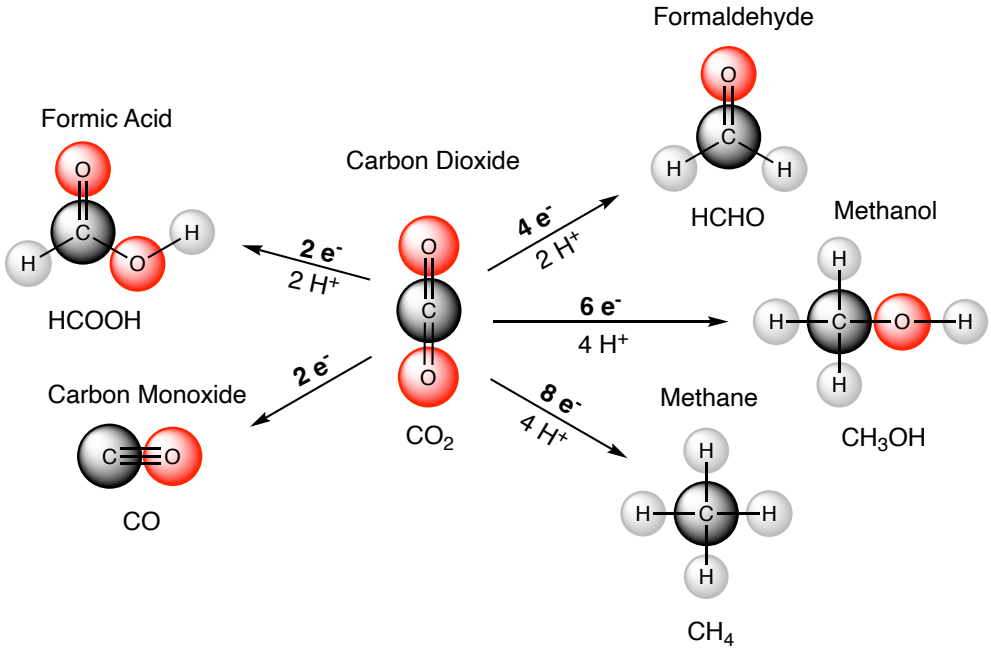

Figure 1. *Potential products from reduction of CO_2 in 2-, 4-, 6- and 8-electron reduction pathways.*

1.3 Metal Complexes for Reduction of CO_2

Metal complexes provide many accessible redox states in the central metal and the ligands, making the multi-electron reduction process feasible and demonstrating potential use in photoactive systems for the reduction of CO_2.[9] The metal-complex-catalyzed reduction of CO_2 is initiated by generating a low-valent unsaturated metal complex by reducing the catalyst which then allows it to interact with CO_2.[9,10] These systems can be divided into two main categories depending on how the electron is supplied to the catalyst: electrochemical and photochemical. In an electrochemical system, the electrons are injected into the catalyst from the electrode.[10] This allows for relatively fast electron injection speeds that can be controlled by potentials applied to the electrode.[10] In photochemical systems, the catalyst accepts an electron from an excited photosensitizer (PS) molecule to generate the reduced catalyst species.[17] Photochemical CO_2 reduction systems will be discussed in detail in the following section.

1.4 Metal Complex-Catalyzed Photochemical CO_2 Reduction

There are three main components in photochemical systems for the reduction of CO_2: the photosensitizer (PS), the catalyst, and the electron donor (D).[7] As mentioned previously, the catalyst must be reduced by the PS to generate a low valent metal complex that can interact with CO_2. The first step in this process can involve the PS molecule absorbing a photon and getting promoted to its excited state (PS*) which then initiates an electron transfer to the catalyst via reductive or oxidative quenching (*scheme 2*).[7,10] Reductive quenching is the process in which the excited PS* is reductively quenched by an electron donor D, generating the reduced $PS^{\bullet-}$.[7,10] Oxidative quenching is the process in which the excited state PS* directly gives an electron to the catalyst, generating the one-electron oxidized species (OEOS) $PS^{\bullet+}$.[10] The oxidized $PS^{\bullet+}$ is reduced back to PS by the electron donor, D.[7,10] This quenching process is rare, as the catalyst typically

requires the reduced PS to have a higher reduction potential than the corresponding excited PS*.[10] In addition, the concentration of the catalyst is limited and usually low whereas the electron donor concentration can be increased easily, making the oxidative quenching of the PS* by the catalyst unfavourable. The one-electron reduced species (OERS) of the catalyst is generated by the sequential processes of excitation of PS to PS*, quenching of PS* by an electron donor D to $PS^{\bullet-}$ which then allows reduction of the catalyst by electron capture from OERS of PS.[16] After the reduction of the catalyst, a CO ligand can dissociate from the metal centre permitting the coordination of a CO_2 molecule to the open site.[16] The absorption of one photon of the PS induces a one-electron transfer to the catalyst. As mentioned previously, multi-electron transfers are required for the reduction of CO_2 meaning another electron source is required.[17] Another cycle of excitation and quenching of the PS is necessary to provide a second electron to the catalyst, making the second electron injection slower. Again, this is the main limitation of photochemical systems compared to electrochemical systems where the electron injection rate can be controlled and is significantly faster.

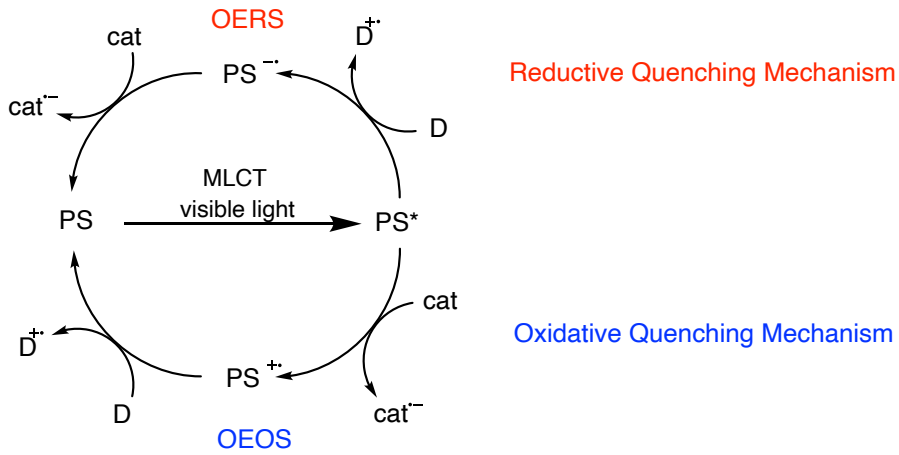

Scheme 2. *Reductive and oxidative quenching mechanisms upon excitation of the photosensitizer (PS) by visible light. This electron-relay cycle from the PS to the catalyst generates the reduced catalyst that can then undergo the catalytic reaction cycle.*

1.5 Factors that Affect Photochemical CO_2 Reduction Reactions

The photochemical CO_2 reaction involves an electron relay cycle in which an electron is transferred to the catalyst from PS and a catalytic cycle in which the reduced catalyst reacts with CO_2.[18,19] As a result, the rate-determining step (RDS) of the process is dependent on the reaction conditions. If the RDS occurs in the catalytic cycle, then the CO_2 reduction rate is proportional to the concentration of the catalyst.[10] Increasing the concentration of the catalyst results in an increase in reaction rate until it becomes saturated and no longer has an impact.[18,19] At this point, the RDS moves to the electron relay cycle where it depends on the formation rate of $PS^{\bullet-}$.[18,19] This rate is heavily dependent on the nature of the electron donor D and the PS, making them important factors in the catalytic and electron relay cycle.[10]

1.5.1 Electron Donor

The purpose of the electron donor is to quench the excited PS* which initiates the electron transfer process. The electron donor is consumed during this reaction, making it a sacrificial electron donor.[7] Most sacrificial electron donors that are utilized for the photochemical reduction of CO_2 include different amines, NADH-model compounds, and ascorbate (*figure 2*).[7] The most widely used electron donors are triethylamine (TEA) and triethanolamine (TEOA) in high amounts, as well as 1-benzyl-1,4-dihydronicotinamide (BNAH) and 1,3-dimethyl-2-phenyl-2,3-dihydro-1H-benzimidazole (BIH).[10]

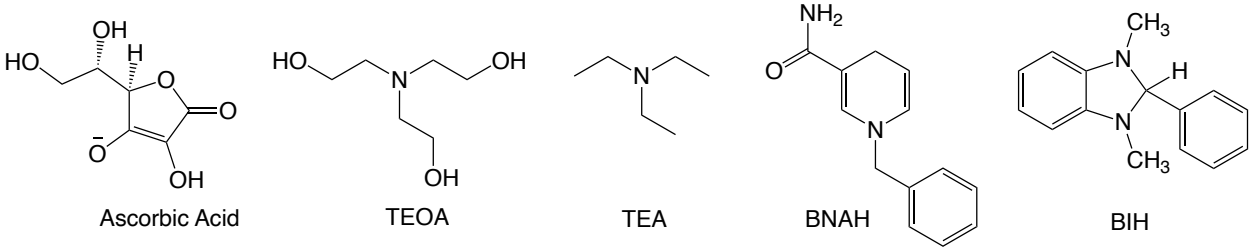

Figure 2. *Structure of common electron donors applied in CO_2 reduction reactions.*

These compounds are useful for CO_2 reduction reactions because they release a proton in their one-electron oxidized species (OEOS) which is important for the suppression of back-electron transfer from OERS of the PS to the OEOS of the electron donor D.[10] For some electron donors, the deprotonation of the OEOS of the electron donor has strong reductive power that can be enough to reduce the PS, the catalyst or even an intermediate making them capable of working as two-electron donors.[10] In natural photosynthesis, there are physically separate compartments responsible for the splitting of water and the reduction of CO_2 with NADPH or NADH.[7] BNAH is a model compound for NADH, which acts as a redox mediator in natural photosynthesis, and is known as both a one-electron and two-electron donor in photocatalytic CO_2 reduction (*scheme 3A*).[20] The one-electron oxidation of BNAH induces deprotonation to $BNA^{\bullet}$ which acts as a more powerful reductant.[10] However, it has been found to dimerize to BNA_2 following two-electron reduction.[21] The accumulation of BNA_2 in the reaction solution has been found to interfere with and deactivate the photocatalytic activity.[21] BIH, another widely used electron donor, demonstrates even stronger reduction power than BNAH and shows no dimerization due to steric hindrance (*scheme 3B*).[22,23] The one-electron oxidation of BIH induces deprotonation from BIH to $BI^{\bullet}$ that can be further reduced to its fully oxidized form, BI.[10] BIH presents many advantages over other electron donors as it can donate two electrons and one proton, has not been found to interfere with the photocatalytic reaction and demonstrates improved turnover numbers (TON)/quantum yield with rhenium (I) complexes.[22,24]

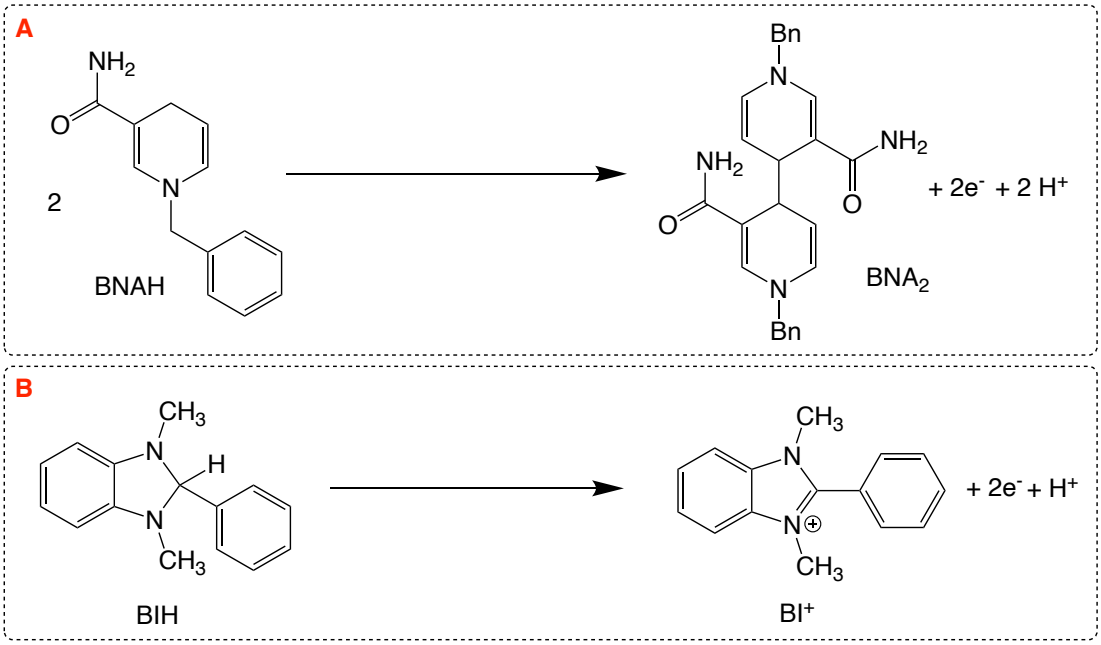

Scheme 3. *A) Dimerization of BNAH upon 2-electron oxidation and deprotonation in CO_2 reduction reactions. B) Formation of BI^+ upon 2-electron oxidation and deprotonation of BIH in CO_2 reduction reactions.*

1.5.2 Photosensitizer

In redox photocatalysis, the role of the photosensitizer (PS) is to mediate the electron transfer from the electron donor D to the catalyst by photoexcitation.[25] As a result, the PS should exhibit preferable absorption in the visible region to efficiently utilize solar light and have stronger absorption at the excitation wavelength than other molecules in the reaction mixture, such as the electron donor D and the catalyst.[25] Additionally, the PS is required to have long emission lifetimes and a highly stable OERS produced following the electron transfer to efficiently undergo the reductive quenching process.[25] The development of organic chromophores as PS is desirable for photoredox catalysis as they are sustainable alternatives to the noble metal complexes that make up a majority of reported PS.[7] Organic chromophores are typically fluorescent with the emissive excited state being a singlet which prevents high efficiency of the electron transfer process following excitation.[7] As long-lived states are beneficial for this process, many strategies have been developed to increase spin orbit coupling (SOC) and to enhance the population of the triplet

excited state.[7] The triplet excited state T_1 to ground state S_0 is a spin-forbidden process, making the excited state lifetime of T_1 orders of magnitude longer than the initially populated singlet excited state S_1 (*figure 3*).[26] Organic chromophores with high triplet quantum yields and long triplet lifetimes have wide applications in many areas of chemistry, including use as energy donors in photocatalysis, for solar energy harvesting, as low cost organic light-emitting diodes (OLEDs) and several others.[27–34] Therefore, the past decade has seen the design and development of more powerful triplet sensitizers gain a lot of attention. Triplet states can be generated via intersystem crossing (ISC) of the lowest excited singlet state S_1 and requires mixing between singlet and triplet wavefunctions.[26] ISC is about 2–3 orders of magnitude slower than radiative or non-radiative decay of the singlet excited state S_1 because energy and time is needed to flip the electron spin.[26] The population of triplet excited states is mostly dependent on the strength of SOC and the energy difference between S_1 and T_1 (ΔE_{ST}).[35] The main factor that influences the interaction between an electron's spin and orbital motions (SOC) is the atom size, with SOC being enhanced in larger atoms.[35] This is referred to as the "heavy atom effect".[35] The molecular structural engineering of organic chromophores, including manipulation of the energies of S_1 and T_1 to bring them closer to one another, can allow for the promotion of triplet excited states.[36] The heavy atom effect, the design of molecules and complexes with small ΔE_{ST}, and the development of donor-acceptor dyads that generate triplet excited states following excitation and charge recombination are some of the strategies that have been applied to generate chromophores/PS with increased emission lifetimes.[7,26] Phosphorescent metal complexes, organic molecules, and delayed-fluorescence complexes have been reported in the literature as PS for homogeneous photocatalytic CO_2 reduction systems.[24,25,37]

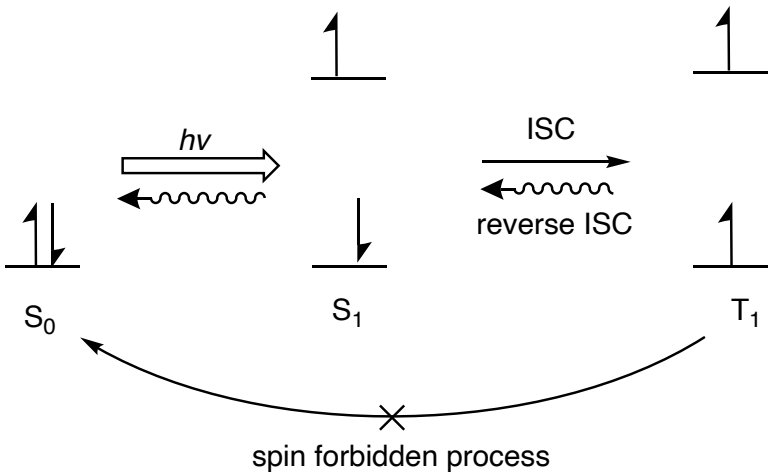

Figure 3. *Depiction of the relationship between ground state (S_0), the lowest excited singlet state (S_1) and the lowest excited triplet state (T_1) upon absorption of energy.*

The chromophores and photosensitizers reported in literature can be classified into several different groups (*figure 4*). The most widely used photosensitizers are Ru(II) polypyridine complexes because they have relatively long lifetimes that last several hundred nanoseconds and are photochemically stable except in aqueous solutions.[25] Both $[Ru(bpy)_3]^{2+}$, where bpy is 2,2'-bipyridine, and $[Ru(dmb)_3]^{2+}$, where dmb is 4,4'-dimethyl-2,2'-bipyridine, are well-known PS in photocatalyzed CO_2 reduction reactions because of their strong absorption in the visible region and their ability to undergo rapid and efficient ISC to produce triplet metal-to-ligand charge transfer (^{3}MLCT) excited states following photoexcitation.[25,38–40] Os(II) polypyridine complexes are similar to the Ru(II) polypyridine complexes and have also been employed as the PS in the photochemical reduction of CO_2. $[Os^{II}(N^N)_3]^{2+}$-type compounds, where N^N is a diimine ligand, show absorption at lower wavelengths of the visible light spectrum, closer to 700 nm, compared to the corresponding Ru(II) complexes.[25,41] They are able to use a much wider wavelength range of visible light as ^{3}MLCT absorption bands are present at 540–730 nm that are not seen for the Ru-polypyridine complexes.[25,41] However, the Os(II) complexes have shorter emission lifetimes and more negative reduction potentials in excited states than the respective Ru(II) complexes.[25] As a

result, stronger electron donors, such as benzimidazole derivatives, are required to reductively quench the PS*.[25] Cyclometalated Ir(III) complexes, such as *fac*-[Ir(ppy)$_3$] and [Ir(ppy)$_2$(bpy)]$^+$ where ppy is 2-phenylpyridine, have been used as PS for both CO_2 reduction and hydrogen evolution reaction (HER).[25,42–46] These compounds have been shown to demonstrate absorption at shorter wavelengths compared to the Ru(II) complexes, strong oxidation power of the excited states and high stability under photocatalytic reaction conditions.[25] There are two general classes of these PS, including [Ir(C^N^C)$_2$(N^N)]$^+$ and *fac*-[Ir(C^N^C)$_3$] where C^N^C is a cyclometalated ring and N^N is a diimine ligand.[25] Rhenium(I) complexes have gained a lot of attention as PS for CO_2 reduction reactions[47], with *fac*-[Re(N^N)(CO)$_3$(PR$_3$)]$^+$, where N^N is a diimine ligand, being recently reported as a good PS for the conversion of CO_2 to CO.[48] The PAr$_3$ ligand with Ar representing an aryl group also showed good PS properties, including high formation quantum yields of OERS, OERS durability and photostability.[48] Metal porphyrins and chlorophylls have been found to show two strong absorption bands in the visible region.[25] Porphyrin complexes with Pd(II) centres can generate triplet excited states with a long lifetime of several hundred microseconds via ISC.[25] Many Pd-porphyrins and other derivatives show PS abilities similar to the Ru(II)-polypyridine complexes mentioned above.[25] Porphyrins with Zn(II) centres have shorter excited state lifetimes, ranging from picoseconds to nanoseconds but can be applied as PS in supramolecular complexes in which they are attached to the catalyst.[49,50]

Finally, organic compounds with long-lived excited lifetimes have been used as organic photosensitizers in CO_2 reduction.[25] The triplet excited state of phenazine, a metabolite produced by bacteria, can be made by excitation in good yield.[51–53] Oligo(*p*-phenylenes) (OPPs) also demonstrate strong reduction power that is large enough to reduce CO_2 by electron transfer and produce CO_2 radical anions, but can only absorb within the UV region.[52,54,55] The design of small

organic molecules as heavy-atom-free triplet PS is challenging. While some aromatic hydrocarbons, such as *p*-terphenyl and phenazine, show effective ISC, the modification of chemical structures can result in unpredictable changes in their photophysical properties.[36] There is a need to develop more environmentally and economically friendly organic dye PS; however, small organic chromophores often show decreased efficiency for photoredox reactions.[56] Compared to metal-based PS, organic dyes can exhibit weak SOC and lower populations of the triplet excited state (T_1).[56] Other than introducing heavy atoms to increase SOC and the population of the T_1 excited state, an alternative approach involves triplet generation via charge recombination of spatially separated donor-acceptor dyads.[56]

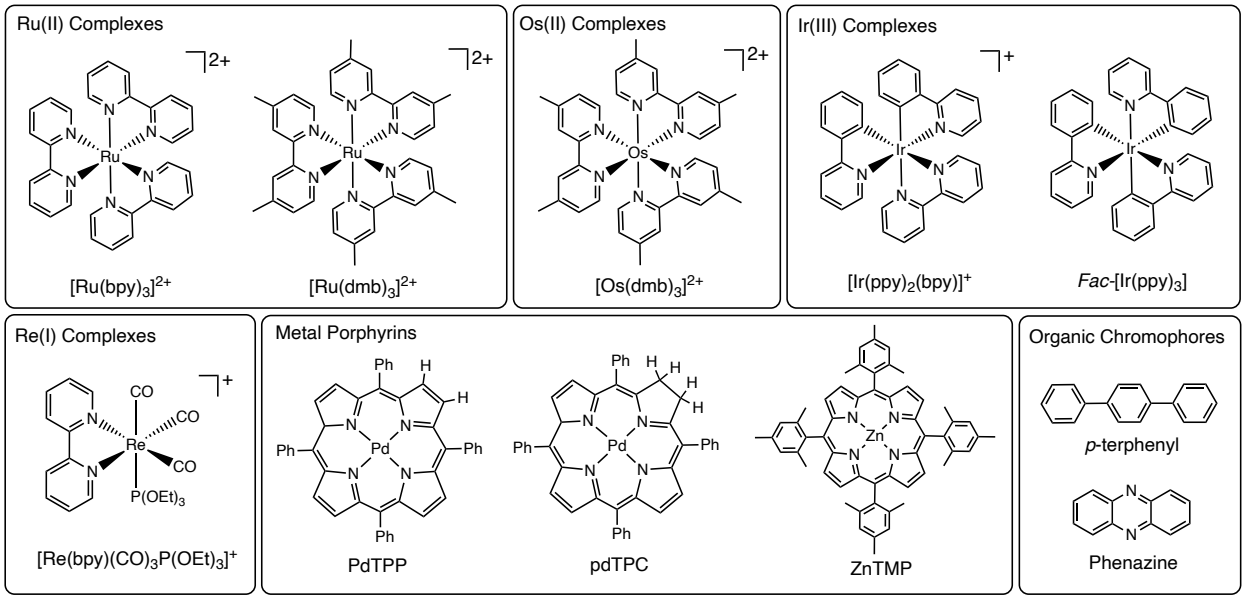

Figure 4. *Common photosensitizers used for CO_2 reduction reactions.*

1.4.3 Other Factors

In addition to the electron donor and the PS, three other factors can influence the outcome of CO_2 reduction reactions. The reaction solvent has a significant impact on these reactions as the solvent molecules can coordinate transiently to the vacant site on the catalyst where CO_2 reacts.[10] As a result, the use of strongly coordinating solvents is avoided. A commonly used solvent in

photocatalytic CO_2 reduction reactions is dimethylformamide (DMF) with dimethylacetamide (DMA) and N-methyl-2-pyrrolidone (NMP) used as alternatives due to their low coordinating ability and increased solubility of CO_2.[57,58] Acetonitrile (MeCN) is the most commonly used solvent for these reactions despite its lower activity compared to DMF.[57] While the reason behind this remains unclear, it likely has to do with having an increased coordinating ability over DMF.[10] Finally, the CO_2 concentration in the reaction mixture and the temperature have also been shown to have an impact on the ratio of products observed following the CO_2 reduction reaction.[10,59,60] A higher CO_2 concentration has been found to favour CO production over HCOOH.[60]

1.6 CO_2 Reduction Catalysts

The catalyst for the photochemical reduction of CO_2 has a variety of roles ranging from accepting electrons from the PS* in oxidative quenching or $PS^{\bullet-}$ in reductive quenching, the accumulation of multiple electrons and the activation of CO_2.[25] It is also important that the catalyst has very little or no ability to evolve H_2 as it competes with CO_2 reduction in aqueous conditions.[7,25] In the past, noble metals, such as Ru, Re and Ir have been used as metal centres in CO_2 reduction catalysts.[8] These metals are impractical due to their low abundance and high cost, making their substitution with non-noble metals for both catalysts and PS of high interest.[8] First row transition metals like Mn, Fe, Co and Ni are highly abundant, more sustainable and low cost, making them significantly more appealing for new efficient photocatalysts.[7]

1.6.1 Classification of CO_2 Reduction Catalysts

To date, a majority of reported catalyst systems can be classified into six main categories: Re(I) complexes, Ru(II) complexes, Co(II) complexes, Mn(I) complexes, Ni(II) complexes, Ir(III) complexes and metal porphyrins (*figure 5*).[25] Re(I) carbonyl diimine compounds of the *fac*-$[Re(N\hat{}N)(CO)_3C]^+$-type (X = Cl^-, Br^-, MeCN, pyridine, PR_3, etc.) have been shown to selectively

produce CO from reduction of CO_2 and can also act as PS.[25] Ru(II) complexes can be further divided into two types: *cis*–$[Ru(N^N)_2(CO)_2]^{2+}$ and *cis,trans*-$Ru(N^N)(CO)_2Cl_2$.[18,19,60–62] These compounds have been applied for CO_2 reduction and have been shown to polymerize in photocatalytic conditions via dissociation of N^N or Cl^- ligand from the OERS.[18,19,61] Like Ru(II) complexes, Co(II) complexes can also be separated into two types: $[Co(N^N)_n]^{2+}$ and $[Co(macrocycle)]^{2+}$ where macrocycle is a tetraaza-macrocycle, typically cyclam.[63–67] These types of catalysts have been found to product CO from CO_2 along with substantial H_2, which is undesirable despite being an earth-abundant catalyst.[25] A wide variety of Mn(I) complexes have been investigated in recent times as a more sustainable alternative to Re(I) complexes. *Fac*-$Mn(bpy)(CO)_3Br$ has been shown to work as a catalyst for both electrochemical and photochemical CO_2 reduction.[68–70] Ni(II) tetraaza-macrocycle complexes with the general formula $[Ni(macrocycle)]^{2+}$ have been shown to work as selective CO_2 reduction catalysts with H_2 evolution suppression in electrochemical systems.[71,72] However, both CO and H_2 are observed in photochemical reaction conditions with these complexes as catalyst.[71,72] Ir(III) complexes have also emerged recently as potential CO_2 reduction catalysts with $[Ir(tpy)(ppy)Cl]^+$, where tpy is 2,2':6',2''-terpyridine and ppy is 2-phenylpyridine, being recently reported as a CO_2 reduction catalyst for the production of CO in the absence of a PS.[73,74] Finally, metal porphyrins with Co or Fe have been successfully applied in CO_2 reduction reactions in the absence and presence of a PS.[75–78] The review "Photocatalytic reduction of CO_2 using metal complexes" by Ishitani *et al.* provides a comprehensive list of all major photocatalysts employed in the reduction of CO_2, as well as the reaction conditions and activity.[25]

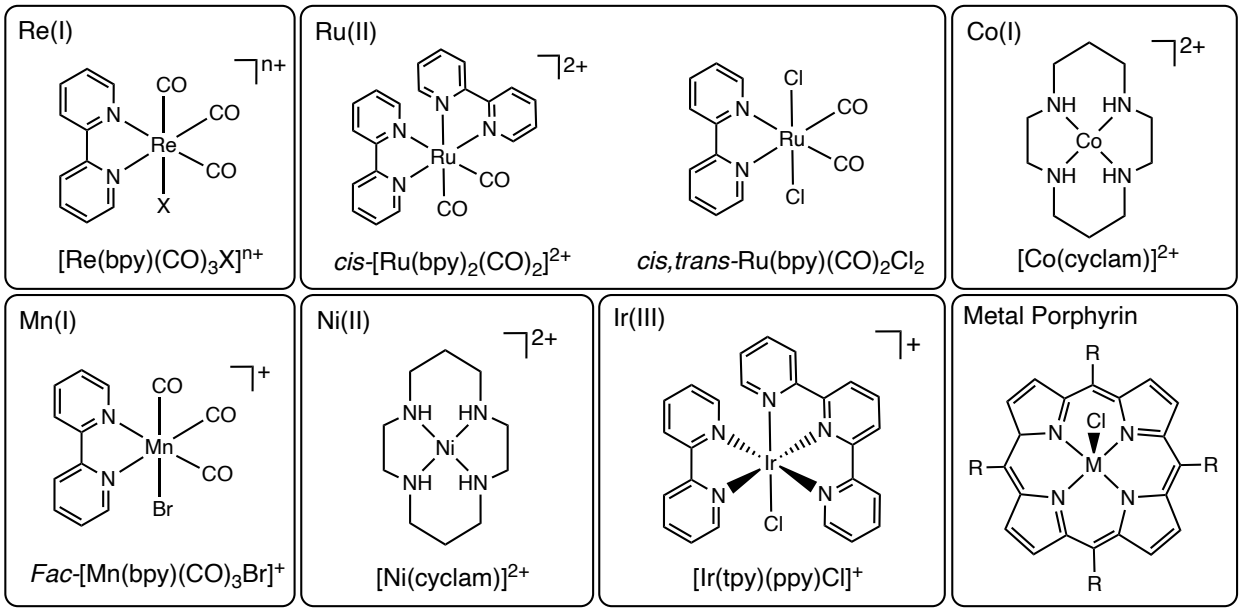

Figure 5. *Common groups of photocatalysts employed for the reduction of CO_2 with a sacrificial electron donor and a photosensitizer.*

1.6.2 Re(I) CO_2 Reduction Catalysts

Evidently, a wide variety of complexes have been investigated for their application in CO_2 reduction reactions. Some systems demonstrate more benefits over others, with Re(I) complexes presenting many advantages over the other systems mentioned. Re(I) complexes have shown high product selectivity and high reduction efficiency by producing CO from CO_2 almost exclusively while suppressing H_2 evolution even in aqueous conditions.[10] These types of compounds have been investigated for almost a century, with the first Re(I) carbonyl compound, $ReCl(phen)(CO)_3$ where phen is 1,10-phenanthroline, being synthesized by Hieber *et al.* in 1941.[79] A few years later, both Wrighton and Meyer investigated the lowest excited states of similar complexes and found emitting states with significant triplet character.[80,81] In 1983, Lehn, Ziessel and Hawecker were the first to use Re(I) complexes for photocatalytic CO_2 reduction.[21] They demonstrated the application of *fac*-$Re(bpy)(CO)_3X$ where X = Cl^-, Br^- as PS in DMF under visible light irradiation with $[Co(bpy)_3]^{2+}$ as the catalyst. The complex produced CO with very high selectivity and efficiency even in the absence of the Co catalyst.[21] As a result, they were able to demonstrate the first use of

fac-Re(bpy)$(CO)_3$X as a homogeneous catalyst to produce CO from CO_2.[21] This development resulted in Re(I) compounds gaining substantially more attention as catalysts for the reduction of CO_2 and lead to the development of many derivatives. A few years later, Ziessel, Lehn and Hawecker demonstrated the efficient use of *fac*-Re(bpy)$(CO)_3$Cl as an efficient homogeneous catalyst for both the electrochemical and photochemical reduction of CO_2 with the use of a tertiary amine to quench the excited state.[82] A significant amount of research at this time was then aimed at researching the photophysical properties and light induced energy/electron transfer processes of many Re(I) complexes with varying diimine ligands such as 1,10-phenanthroline, phenanthroline derivatives, different α-diimine and bidentate ligands, in the absence of a bidentate ligand, along with changing the X ligand to Br^-, Cl^- and pyridine.[83–89] Several groups also found that the use of phosphine ligands, such as $P(OEt)_3$ and $P(O\text{-}i\text{-}Pr)_3$, and varying pyridine derivatives in these complexes can lead to efficient photocatalytic reduction of CO_2 as well.[90–93] In 2006, Kurz *et al.* demonstrated that the [Re(bpy)$(CO)_3$X] catalyst can be easily modified by replacing the X ligand with SCN^-, Br^-, CN^- and H_2O.[94] The activity of the catalyst was retained and even enhanced with some ligands despite altering the spectroscopic and electrochemical properties.[94] This work extensively illustrated the tunability of these types of complexes for CO_2 reduction reactions. Takeda *et al.* used these same complexes ($[Re(bpy)(CO)_3X]^+$, X = SCN^-, CN^-, Cl^-) to investigate the reaction mechanism by comparing the three systems.[95] They found the most active catalyst was the X = SCN^- complex, giving 30 TON_{CO} after 25 hours, while the X = Cl^- complex gave half this activity and X = CN^- complex was inactive.[95] In 2011, Chauvin *et al*. found a similar catalyst with improved catalytic activity, giving 30 TON_{CO} after approximately 4.2 hours.[96] The most efficient system up to this date was reported in 2013 by Ishitani *et al*.[47] They synthesized a series of ring-shaped Re(I) complexes with varying lengths of bridging ligands and varying Re(I) units that

functioned as efficient and durable photosensitizers.[47] The combination of the Re-ring photosensitizer with a *fac*-[Re(bpy)$(CO)_3$(MeCN)]$^+$ catalyst was highly efficient for CO_2 reduction to CO, giving 526 TON_{CO} after 16 hours.[47] The photophysical properties of the Re-rings were easily varied by changing the cavity size, with a smaller central cavity leading to intramolecular π-π interactions and longer excited state lifetimes.[47] This combination of PS and catalyst resulted in a CO_2 reduction reaction with a quantum yield of 82%, one of the highest quantum yields reported in literature.[47] In the last few years, there has been a shift in focus towards the development of Ru-Re assembled photocatalysts, entrapment of the PS and photocatalyst in molecular-organic frameworks (MOFs), tethering these catalysts together in the form of covalent organic frameworks (COFs) and many more advanced applications of these photocatalytic systems.[97–103] Some more recent works include the investigation of different promoters and their effects on Mn, Re and Ru catalysts, such as [Re(bpy)$(CO)_3$Cl][104], and the study of *fac*-[Re(N^N)$(CO)_3$Cl] complexes where N^N is a 1,10-phenanthroline ligand with its 4,7 positions substituted with either carbazole, indole and pyrrole.[105] The latter work found exceptionally high photocatalytic performance for all three substituted systems in comparison to 1,10-phenanthroline, with the pyrrole-substituted ligand showing the highest efficiency at 125 TON_{CO} after 24 hours.[105] The majority of the CO_2 photoreduction systems mentioned above utilized a light source, such as a mercury (Hg) lamp or a xenon (Xe) lamp, with a UV light cut-off filter. While the specific wavelength cut-off for each system varied slightly, the filters remained around 400 nm, such as 436, 400, 380, 380 and 365 nm.[47,93–95,98] The presence of the light filters prevented any high-energy UV light from reaching the reaction and assured that the systems were operating under purely visible light, which is a principal objective in most of this work.

1.7 Overview of Project Goals

This project details the development, synthesis and evaluation of photocatalytic efficiency of the visible-light driven CO_2 reduction catalyst $[Re(bpy)(CO)_3X]^+$ where X = carbazole dicyanobenzene (CDCB) derivatives synthesized within the group (*figure 6*). The carbazole dicyanobenzene derivatives, 3Cz-IPN imidazole (**2**), the benzyl imidazolium dye (**3**) and the isopropyl imidazolium dye (**4**) were synthesized based on the 4Cz-IPN compounds first synthesized by Uoyama *et al.*[106] The three organic dye molecules were attached to a Re(I) metal centre through the imidazole moiety in an attempt to increase photocatalytic efficiency and TON_{CO} from CO_2 in order to develop more efficient atmospheric CO_2 reduction photocatalytic systems.

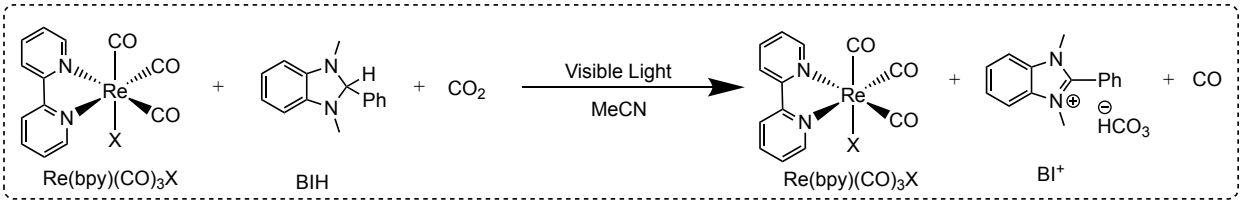

Scheme 4. *Reaction scheme overview of the work developed throughout this project. $Re(bpy)(CO)_3X$ where X represents organic dyes synthesized within the group attached to the Re centre to act as both the photocatalyst and photosensitizer in the reduction of CO_2.*

2 – DESIGN AND SYNTHESIS OF ORGANIC DYES

2.1 RATIONALE

The research achieved throughout this project was based on the development and synthesis of novel organic carbazolyl dicyanobenzene (CDCB) derivatives (*figure 6*) that show potential as PS in photochemical CO_2 reduction reaction systems.

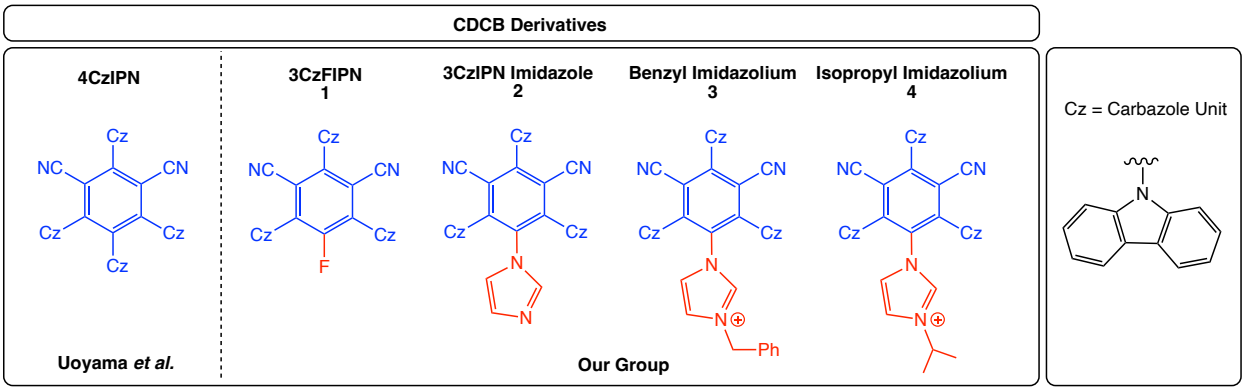

Figure 6. *Overview of the CDCB-derivative dyes synthesized within our group.*

Uoyama *et al.* successfully applied a novel pathway to achieve high electroluminescence efficiency using simple aromatic compounds that demonstrate thermally activated delayed fluorescence (TADF).[106] TADF is a process in which molecular species in the non-emitting excited state T_1 utilize thermal energy from its surroundings to change states and undergo light emission (*figure 7*).[107] The transition of an excited molecular species in the triplet state T_1 to the ground state S_0 is a theoretically forbidden process called phosphorescence.[107] Instead, reverse ISC (RISC) from T_1 to S_1 generates the final emissive singlet excited state S_1 which only then returns to S_0 and emits light.[107] The energy level of the S_1 excited state is typically higher in energy than the T_1 excited state, requiring energy input to undergo RISC which renders this process thermally-activated.[107] They were able to successfully design organic molecules with a small energy gap between the S_1 and T_1 excited states (ΔE_{ST}) to enhance the triplet excited state population as well as T_1 to S_1 reverse ISC. As mentioned previously, excited states are attainable by intramolecular

charge transfer between spatially separate donor and acceptor moieties within a system. The combination of a small ΔE_{ST} with a moderate radiative decay rate allows to overcome competitive non-radiative decay pathways and produces highly luminescent TADF materials.[106] However, the two properties conflict so the overlap of the HOMO and the LUMO must be carefully balanced in the design of these compounds.[106] In order to enhance photoluminescence, any change in molecular conformation between S_0 and S_1 excited states should be restrained to suppress non-radiative decay pathways and limited orbital overlap results in almost no emission.[106]

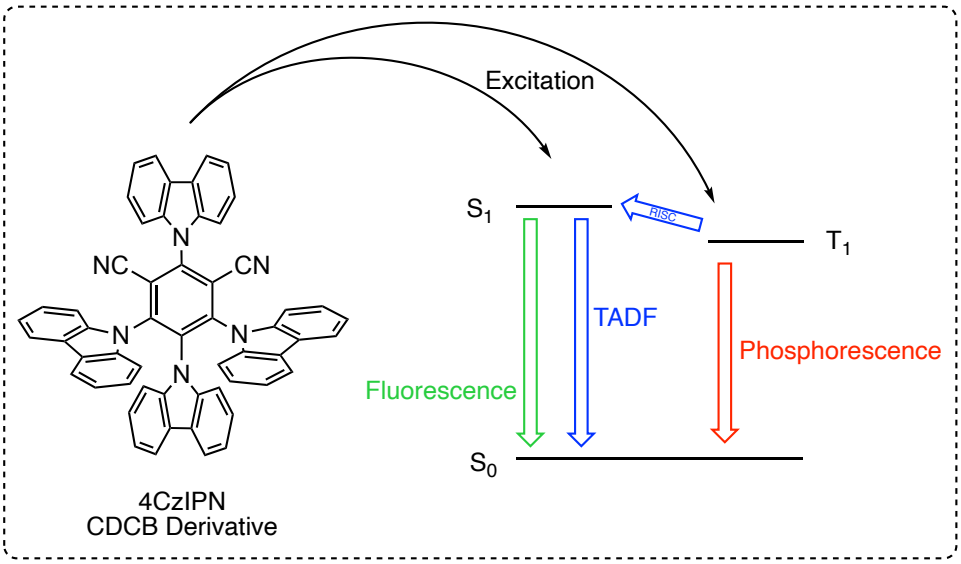

Figure 7. *Schematic depiction of the energy transfer processes that 4CzIPN and other CDCB derivatives undergo following excitation. TADF involves RISC from T_1 to S_1, followed by light emission from S_1 to S_0, as indicated by the blue arrows.*

Uoyama *et al.* reported a series of highly efficient TADF emitters based on CDCBs involving carbazolyl groups as electron donors and a dicyanobenzene moiety as the electron acceptor.[106] In the synthesized TADF emitters, the carbazolyl units are distorted from the dicyanobenzene plane due to steric hindrance. They also found that altering the number of carbazolyl groups or introducing new substituents can easily tune the emission wavelengths of the CDCB emitter by changing electron-donating ability of the peripheral groups. As a result, highly efficient TADF emitters with a wide range of emission colours can be easily achieved through

CDCB derivatives. Under nitrogen, the delayed fluorescence occurring via reverse ISC of 4CzIPN (1,2,3,5-tetrakis(carbazol-9-yl)-4,6-dicyanobenzene) was more than two orders of magnitude larger than the prompt fluorescence.[106] As well, the steady-state photoluminescence spectrum of 4CzIPN in toluene showed an intense green emission with a maximum at 507 nm and a very small Stokes shift of 47 nm.[106] Emission produced by intramolecular charge transfer between donor and acceptor units typically shows a large Stokes shift. DFT calculations were also carried out to study the geometry of the S_0 state of 4CzIPN. The highest occupied natural transition orbitals (NTOs) were delocalized over the four carbazole groups and the lowest occupied NTO was found on the dicyanobenzene moiety.[106] The steric hindrance between the carbazolyl and dicyanobenzene moieties produces a large dihedral angle of 60˚ between the carbazolyl and dicyanobenzene planes.[106] This makes the highest occupied and lowest unoccupied NTOs spatially separated, and it limits conformational lability, enhancing T_1 to S_1 reverse ISC. The Stokes shift of S_1 in 4CzIPN is small compared to typical charge transfer systems.

2.2 RESULTS

To generate new CDCB derivatives, the fluorine atoms at the 2,4,6 positions of tetrafluoroisophthalonitrile were selectively replaced with carbazole groups in a low temperature reaction, yielding 5-fluoro-2,4,6-tris(carbazol-9-yl)benzene-1,3-dicarbonitrile (3CzFIPN, **1**) in 90% yield (*scheme 5*). The conjugation of the negative charge in the Meisenheimer intermediate with the nitrile groups is likely the driving force in the regioselectivity seen with the carbazole group placement.[108] The novel CDCB-derivative dye 1-(2,4,6-tri(9*H*-carbazol-9-yl)benzene-1,3-dicarbonitrile)imidazole (3CzIPN imidazole, **2**) was then synthesized from compound **1**. The imidazole group was first deprotonated with excess cesium carbonate then reacted with **1** to replace the remaining fluorine (*scheme 5*). This yields 3CzIPN imidazole **2**, our organic dye, in 95% yield

which can then be used for a wide range of reactions. The syntheses for compounds **1** and **2** are straightforward and use relatively inexpensive materials. Both reactions can be carried out in air and produce the compounds in high yield. The progress of the reaction from **1** to **2** can be easily monitored via ^{19}F NMR through the disappearance of the singlet at –111 ppm seen for compound **1** but not compound **2** (*figure 8*). Additionally, the successful attachment of the imidazole group to the dicyanobenzene ring can be confirmed by the appearance of three distinct singlet peaks correlating to the imidazole protons at 6.54, 6.15, and 5.87 ppm in the ^{1}H NMR spectrum (*figure 8*).

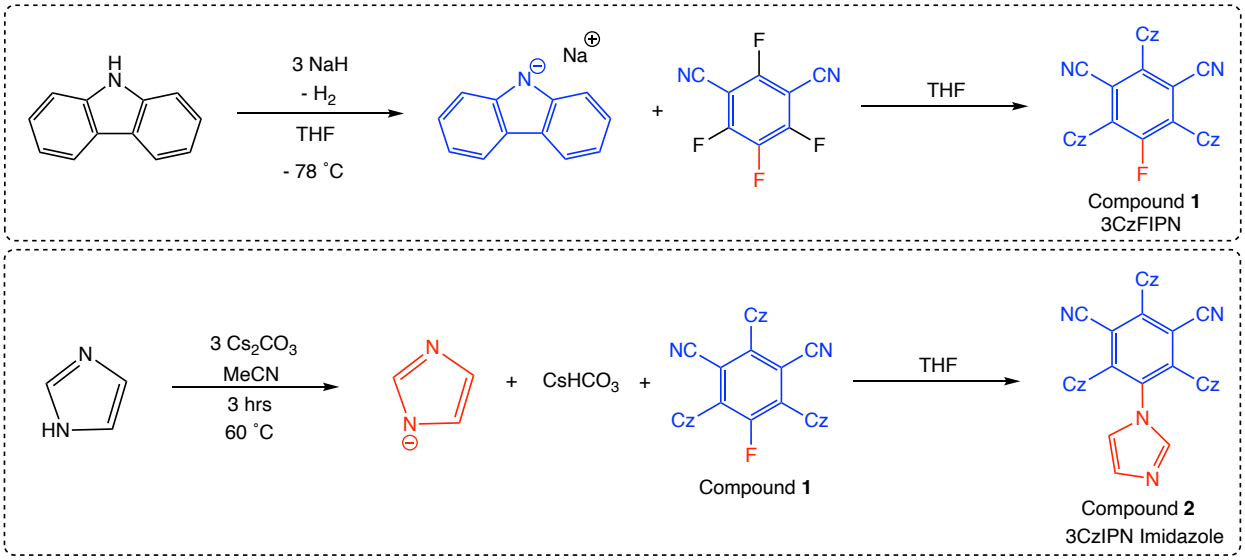

Scheme 5. *Reaction scheme for the synthesis of compound* ***1*** *and* ***2*** *from tetrafluoroisophthalonitrile.*

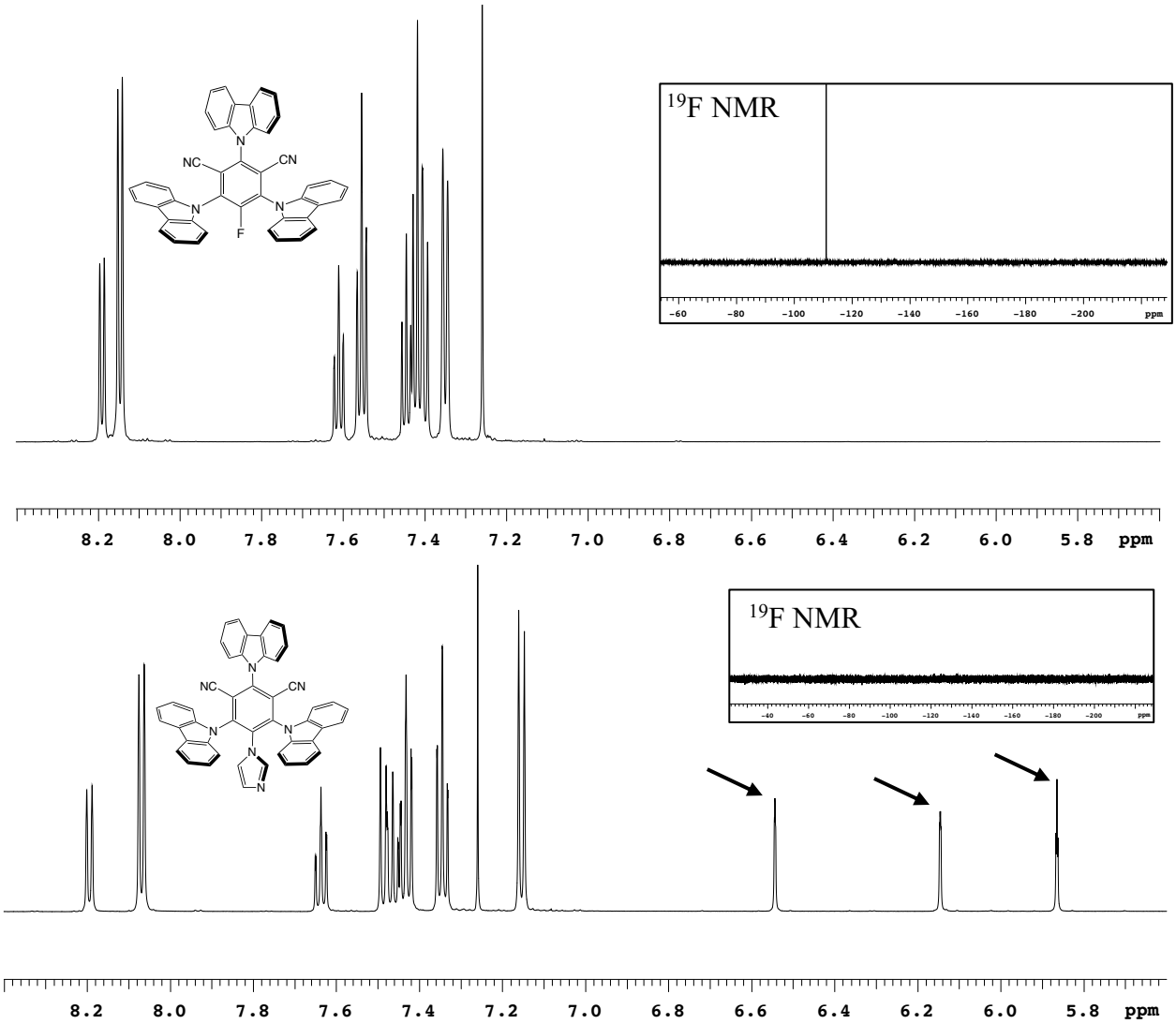

Figure 8. *^{1}H and ^{19}F NMR spectra of compound **1** (top) and **2** (bottom) showing a successful replacement of the fluorine atom by the imidazole group. The characteristic imidazole peaks are indicated by black arrows.*

However, there were minor complications that came up throughout these syntheses. The presence of excess carbazole in the preparation of **1** resulted in a small amount of tetracarbazolyl product while insufficient carbazole led to a small amount of the difluoro product (*scheme 6*). Both side-products are difficult to remove, making the product challenging to purify.

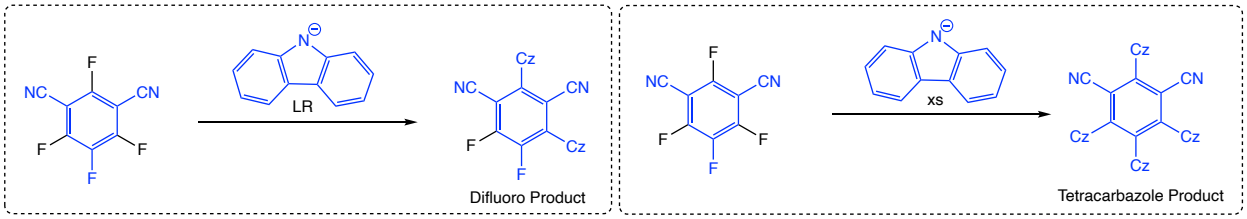

Scheme 6. *Reaction scheme for the synthesis of compound* ***1*** *in the presence of insufficient and excess carbazole reagent.*

Different variations of column chromatography and crystallizations were attempted for the purification of **1** and **2**, with crystallizations showing the most success. Flash chromatography in air using different solvent mixtures, such as hexane/ethyl acetate and hexane/DCM, and different stationary phase materials, such as silica and neutral alumina, was used to attempt to purify **1** and **2** (*table 1*). While column chromatography was only attempted on compound **1** once, it showed promising results with a 98% recovery of pure compound. However, the purification of compound **2** by chromatography was significantly less successful, with the highest percent recovery being only 56%. The results for flash chromatography using neutral alumina demonstrate some consistency (*attempts 2, 3 and 4, table 1*), except for the final attempt which resulted in a 0.3% recovery of the product. In this attempt, a different type of neutral alumina that may not have been suitable for flash chromatography was used as the stationary phase. The eluent moved through this stationary phase at a significantly slower place, leaving the product on the column for an extended period of time. The use of a light source to identify different elution bands in addition to the extended time on the column may have led to product decomposition by photodegradation or polymerization of the compound, explaining the significant loss in yield. All other flash chromatography attempts were carried out with HPLC flash grade neutral alumina, leading to more successful results.

Table 1. *Summary of attempts to purify compounds **1** and **2** by flash column chromatography.*

	Eluent	Stationary Phase	Loading	Starting Weight	Yield	% Recovery
(**1**) 3CzFIPN						
1	90% hexane/ethyl acetate	Neutral alumina	Dry	3.52 g	3.45 g	98%
(**2**) 3Cz-IPN Imidazole						
1	50% hexane/ethyl acetate	Silica	DCM	1.0159 g	0.5648 g	56%
2	50% hexane/ethyl acetate	Neutral alumina	Dry	0.5171 g	0.1129 g	22%
3	90% hexane/ethyl acetate	Neutral alumina	Dry	1.5 g	0.3762 g	25%
4	50% hexane/ethyl acetate	Neutral alumina	Dry	1.3 g	0.4600 g	35%
5*	50% hexane/ethyl acetate	Neutral alumina	Dry	1.5 g	0.0046 g	0.3%

The presence of tetracarbazole product in compound **1** is not a major issue as it has no impact on the synthesis of compound **2**. However, the presence of difluoro product resulting from a lack of carbazole in the reaction does interfere with the following synthesis as any excess deprotonated imidazole can replace both fluorine groups resulting in a di-imidazole product. An excess of carbazole reagent can easily prevent the formation of this product, yielding the tetracarbazole product that can be either removed via purification methods or carried through the next synthesis. In addition, compound **1** can also be purified via crystallization with DCM/ether. This did lead to a decrease in yield but provided a much simpler pathway for purification. As column chromatography was not successful for the purification of **2**, we were required to use a crystallization with acetone/ether to remove any tetracarbazole impurities. Crystallization of **2** by dissolving in minimal acetone followed by the slow addition of excess ether (1:5) resulted in successful purification of this compound.

Following the synthesis of **2**, photoluminescence data in 0.1 mM acetonitrile (MeCN) and dichloromethane (DCM) solutions was obtained to evaluate its potential role as a photosensitizer

(*figure 9*). The DCM solution demonstrated significantly higher excitation and emission intensity compared to the MeCN solution at the same concentration. Both solutions demonstrated an absorption maximum at 400 nm while the emission maxima were slightly different for each solvent. The DCM solution showed an emission maximum around 545 nm whereas the MeCN emission maximum was closer to 570 nm. In most cases, the energy of the absorbed photon is higher than the energy of the emitted photon, and this energy different is referred to as the Stokes shift. The Stokes shift is determined by calculating the difference between the excitation maximum and the emission maximum, making it 145 nm for the DCM solution and 170 nm for the MeCN solution (*table 2*).

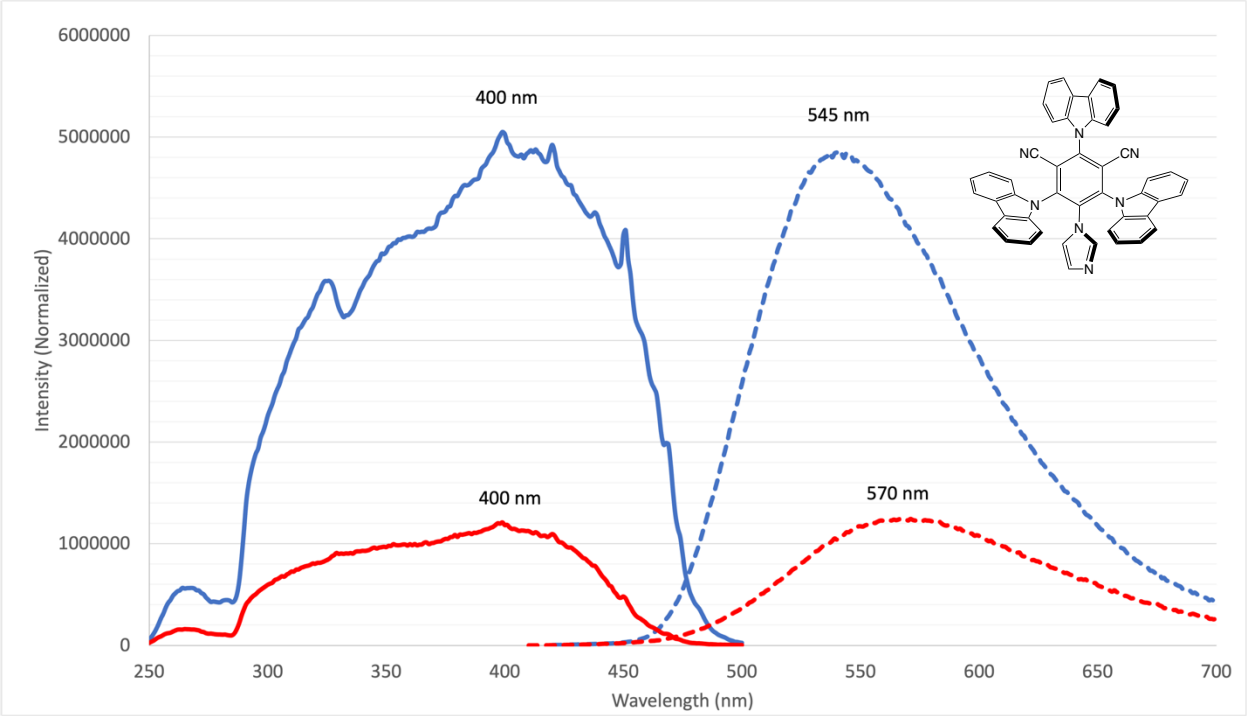

Figure 9. *Excitation and emission spectrum of 0.1 mM 3CzIPN imidazole (**2**) in DCM and MeCN. The blue trace represents the DCM solution, and the red trace represents the MeCN solution. Excitation data is marked by a solid line. Emission data is represented by a dashed line.*

Next, two imidazolium derivatives of compound **1** were prepared in which substituents were attached to the imidazole nitrogen. The first derivative was synthesized by treating compound **2** with excess benzyl bromide at 120 ˚C over 2 hours (*scheme 7*). This generated the benzyl

imidazolium bromide that was then reacted with a slight excess of silver tetrafluoroborate in MeCN for 1 hour to obtain the benzyl imidazolium-tetrafluoroborate salt compound (**3**) (*scheme 7*). The second derivative was synthesized in a similar reaction where compound **2** was treated with excess 2-iodopropane at 110 ˚C for 3.5 hours to generate the isopropyl imidazolium-iodide salt (*scheme 7*). This compound was then directly treated with a slight excess of silver tetrafluoroborate to generate the isopropyl imidazolium-tetrafluoroborate salt compound (**4**) (*scheme 7*).

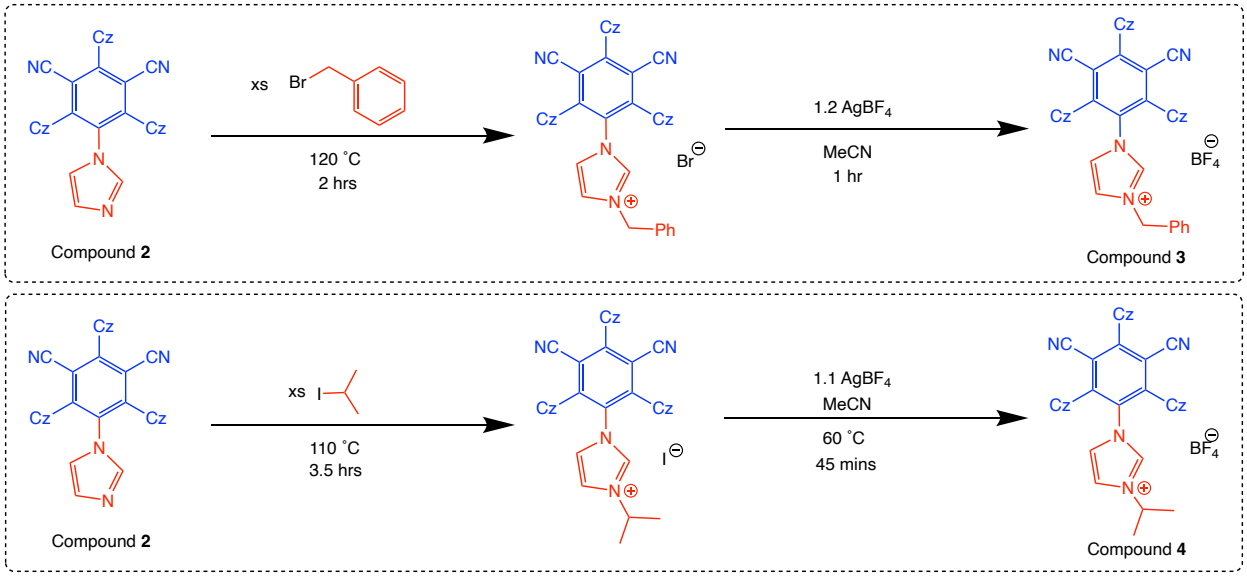

Scheme 7. *Reaction scheme for the synthesis of **2** (top) and **3** (bottom) from compound **2**.*

Both syntheses produced the desired product in high yield and high purity, making them attractive synthetic procedures. The products were washed with ether to remove any remaining benzyl bromide or 2-iodopropane, removing the need for additional purification processes. These imidazolium dye compounds were prepared because they are precursors to free NHC complexes that will be used to generate new photocatalysts further in this project.

Photoluminescence data was obtained for the imidazolium derivatives **3** and **4** in MeCN and DCM (*table 2, figure 10 and 11*). Both compounds showed increased excitation and emission intensity in DCM compared to MeCN which was also observed for 3CzIPN imidazole. The

excitation maximum for both compounds remained at 400 nm in the two solvents, however, the emission maximum was shifted depending on the compound and the solvent. For compound **3**, the emission maximum was around 580 nm in DCM and 600 nm in MeCN. For the compound **4**, the emission maximum was closer to 570 nm in DCM and 590 nm in MeCN. For all three compounds, the MeCN solutions induced higher wavelength emission maxima compared to the DCM solutions.

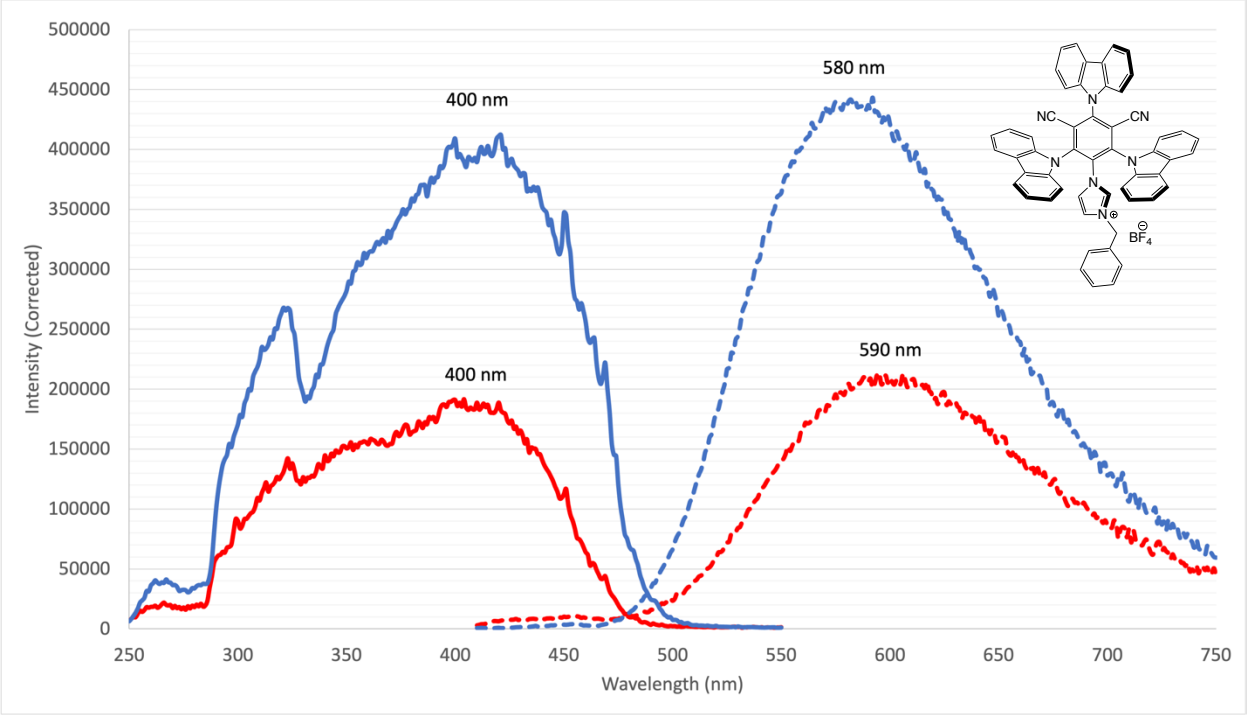

Figure 10. *Excitation and emission spectrum of 0.1 mM **3** in DCM and MeCN. The blue trace represents the DCM solution, and the red trace represents the MeCN solution. Excitation data is marked by a solid line. Emission data is represented by a dashed line.*

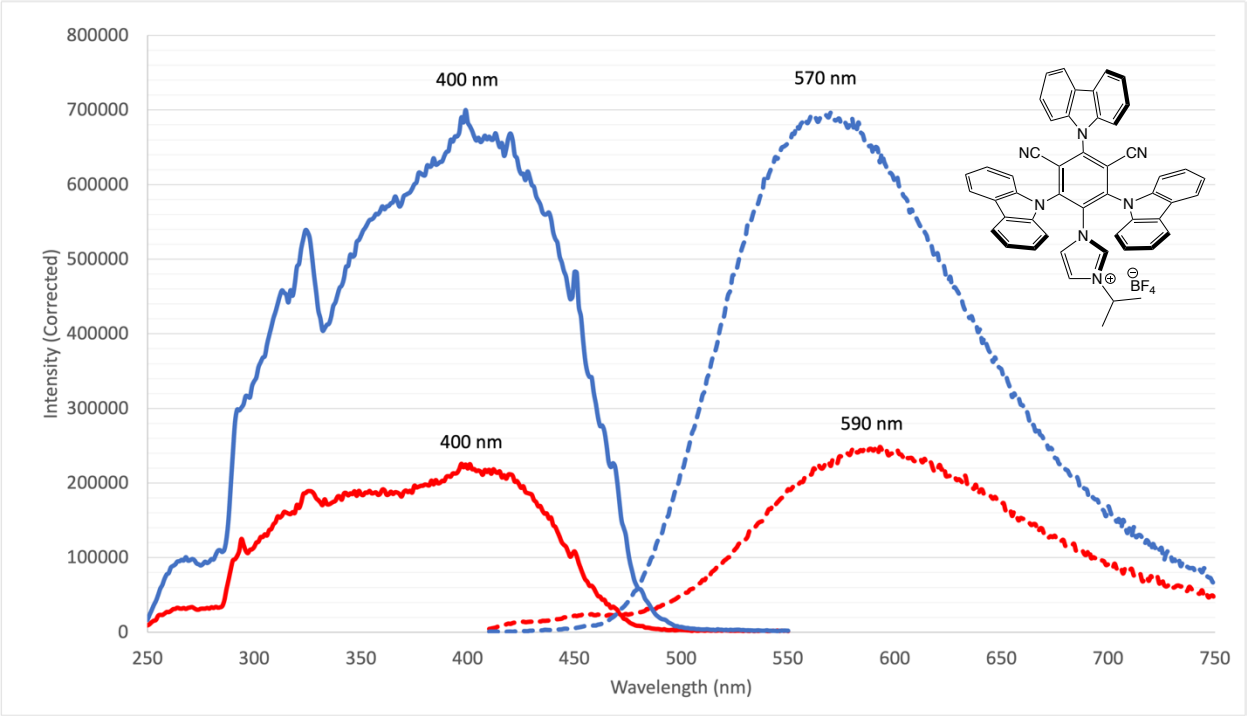

Figure 11. *Excitation and emission spectrum of 0.1 mM* ***4*** *in DCM and MeCN. The blue trace represents the DCM solution, and the red trace represents the MeCN solution. Excitation data is marked by a solid line. Emission data is represented by a dashed line.*

Table 2: *Summary of photoluminescence data collected for compounds* ***2****,* ***3*** *and* ***4****, and their calculated Stokes shifts.*

	DCM			**MeCN**		
	Excitation (nm)	*Emission (nm)*	*Stokes Shift (nm)*	*Excitation (nm)*	*Emission (nm)*	*Stokes Shift (nm)*
2	400	545	145	400	570	170
3	400	580	180	400	600	200
4	400	570	170	400	590	190

2.3 DISCUSSION

All three ligands were synthesized successfully based on the 4CzIPN TADF emitter developed by Uoyama *et al*. Compounds **3** and **4** were prepared as they are precursors to free NHC complexes that can be generated via deprotonation of the carbene carbon and can then undergo a variety of important chemical reactions. The fluorescence data obtained allowed for the evaluation of these compounds as potential photosensitizers in CO_2 reduction reactions. All three compounds showed a larger Stokes shift in MeCN as expected due to its increased polarity (*table 3*). The solvent molecules that surround the chromophore in solution have dipole moments that can interact with the dipole moments of the chromophore.[109] Upon excitation of the chromophore to its lowest excited singlet state S_1, excess vibrational energy is released to the surrounding solvent molecules as it relaxes to the lowest vibrational energy level.[109] The solvent molecules assist in stabilizing and lowering the excited state energy level in a process termed solvent relaxation in which the solvent molecules re-orient around the excited chromophore.[109] The further stabilization of the excited state reduced the energy separation from the ground state which results in a red shift to higher emission wavelengths. For this reason, more polar solvents lead to an increased Stokes shift due to the larger reduction of the energy level of the excited state compared to less polar solvents. This trend was observed for all three compounds, with a decreased Stokes shift arising in the DCM solutions.

Table 3: *Polarity index of solvents used for photoluminescence data acquisition of the three photosensitizers synthesized.*[110]

Solvent	Polarity Index
Dichloromethane (DCM)	3.1
Acetonitrile (MeCN)	5.8

2.4 CONCLUSION

Three new organic CDCB derivatives were developed and synthesized, 3CzIPN imidazole (**2**), the benzyl imidazolium-tetrafluoroborate salt derivative (**3**) and the isopropyl imidazolium-tetrafluoroborate salt derivative (**4**), with compounds **3** and **4** being precursors to free NHC complexes. These compounds were all prepared through simple and efficient synthetic procedures, with relatively inexpensive and sustainable materials. Any challenges encountered for the purification of 3CzIPN imidazole were overcome, with the acetone/ether crystallization yielding the best results. Once 3CzIPN imidazole was purified, the following syntheses required no additional purification methods. Photoluminescence data of these dyes revealed important information regarding their potential activity as photosensitizers. While none of the new dyes had a smaller Stokes shift than the 4CzIPN parent dye, these compounds still showed promising characteristics for their application as photosensitizers in CO_2 reduction systems.

3 – DEVELOPMENT OF NOVEL RE(I) PHOTOCATALYSTS

3.1 RATIONALE

The parent dye, 4CzIPN, and its derivatives[106] possess characteristics that are suitable for its use as photosensitizers in the photochemical reduction of CO_2. More specifically, the excitation of 4CzIPN by visible light initiates an intramolecular charge transfer excitation process generating two singly occupied molecular orbitals (SOMO) with redox properties and lifetimes that allow for photoredox reactions (*figure 12*).[106] The absorption of light in the visible region, ~ 460 nm for 4CzIPN, promotes an electron from the highest occupied molecular orbital (HOMO), localized on the carbazole rings, to a π^* acceptor orbital on the dicyanobenzene ring. This process is an intramolecular charge transfer from the relatively electron-rich donor moiety to the electron-deficient acceptor moiety, the dicyanobenzene ring. This excitation leads to formation of the lowest energy S_1 excited state. 4CzIPN is a conformationally rigid molecule and the dihedral angles between the carbazole groups and the dicyanobenzene ring prevent significant π-conjugation between them. As mentioned in the previous section, the molecular design of 4CzIPN results in a small energy difference between the excited singlet (S_1) and triplet (T_1) states (ΔE_{ST}). This small energy gap is one factor that allows for rapid ISC from S_1 to T_1. The T_1 excited state is a sufficiently long-lived excited state and the redox potentials of the SOMOs are appropriate to undergo a number of redox and energy transfer (e.g., Dexter energy transfer) reactions. This combination of features for 4CzIPN and its derivatives is ideal for chromophores and photosensitizers.

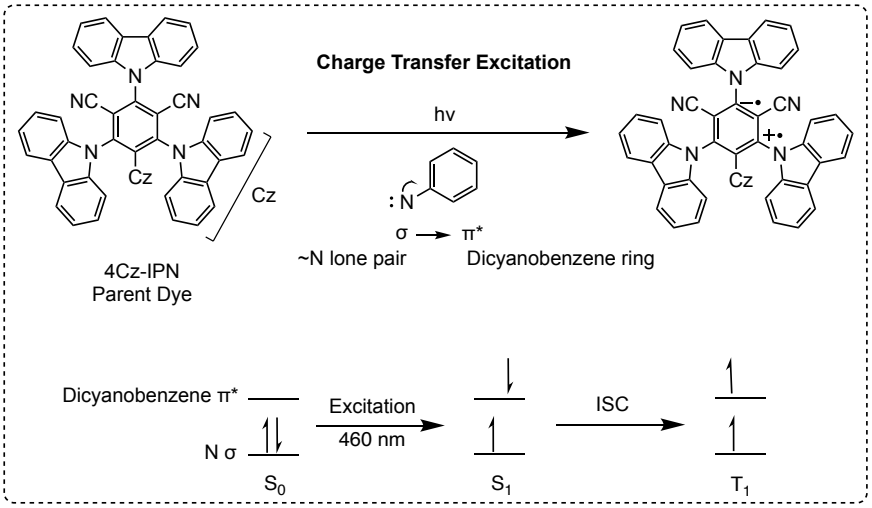

Figure 12. *Overview of the charge transfer excitation process that occurs in 4CzIPN upon absorption of visible light.*

Compound **2** (3CzIPN imidazole) is of similar structure to 4CzIPN except that it possesses an imidazole group in the meta position to the cyano groups on the benzene ring (*figure 13*). The imidazole group is a well-known ligand. Two other derivatives were prepared for this study: the benzyl imidazolium-BF_4^- salt (**3)** and the isopropyl imidazolium-BF_4^- salt (**4**). These imidazolium compounds were prepared as they are pre-cursors to N-heterocyclic carbenes (NHCs) (*figure 13*). Benzyl and isopropyl groups are common functionalities in NHC ligands because their preparations tend to be straightforward. Also, these groups have sufficient steric bulk to prevent dimerization of the free NHC, but not bulky enough to prevent coordination to metal centres and subsequent catalysis. Finally, the steric forces within these bulky functionalized dyes will likely function in a manner like those discussed previously for 4CzIPN (*figure* 13). More specifically, the dihedral angles between the rings will presumably minimise π-conjugation between them, and the geometries of the excited states will not be significantly different from the ground state. Experiments were carried out during the course of this study to prepare Re(I) complexes of these new imidazole- and NHC-dyes to investigate these predictions and to determine the photocatalytic activity of the compounds towards visible-light driven CO_2 reduction.

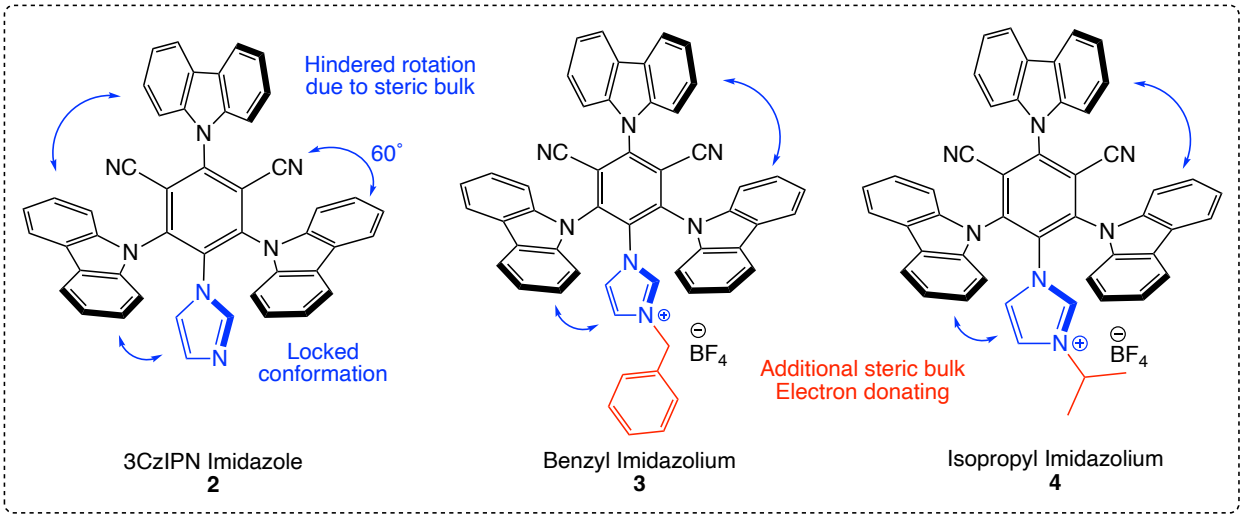

Figure 13. *Chemical structure of the three organic dyes: 3CzIPN imidazole (**2**), benzyl imidazolium-tetrafluoroborate salt (**3**) and isopropyl imidazolium-tetrafluoroborate salt (**4**). The steric hindrance of the carbazole rings locks the molecule into one conformation and forms a 60˚ dihedral angle between the carbazole moieties and the dicyanobenzene ring plane.*

3.2 RESULTS

To develop novel Re(I) catalysts and study their activity towards CO_2 photoreduction, the plan was to covalently link the catalyst and the organic PS together to promote intramolecular electron transfer. As mentioned previously, catalysts for the reduction of CO_2 must be reduced by the excited PS to generate a low-valent unsaturated complex that can interact with CO_2. The majority of photocatalytic CO_2 reductions with molecular transition metal catalysts are carried out in low concentration solutions of both the catalyst and PS. The reductions are believed to occur by multi-electron transfer steps between a short-lived excited state of the PS and catalytic intermediates. The number of electron transfer steps and the number of intermediates involved typically depend on the number of electrons utilized by the reduction of CO_2. In principle, physically linking the PS and the transition-metal catalyst would result in faster electron transfer and higher quantum efficiencies. Previous work in the group involved the homogeneous photochemical reduction of CO_2 with *fac*-Re(bpy)$(CO)_3$Cl as the catalyst and 3CzIPN imidazole **2** as the PS, both dissolved in MeCN with BIH (1,3-dimethyl-2-phenyl-2,3-dihydro-1H-

benzimidazole) as the sacrificial electron donor (*scheme 8*). BIH is a common sacrificial electron donor for photocatalytic reactions, as mentioned previously. For this project, the catalyst and dyes were linked together to determine whether the photocatalytic activity would be increased.

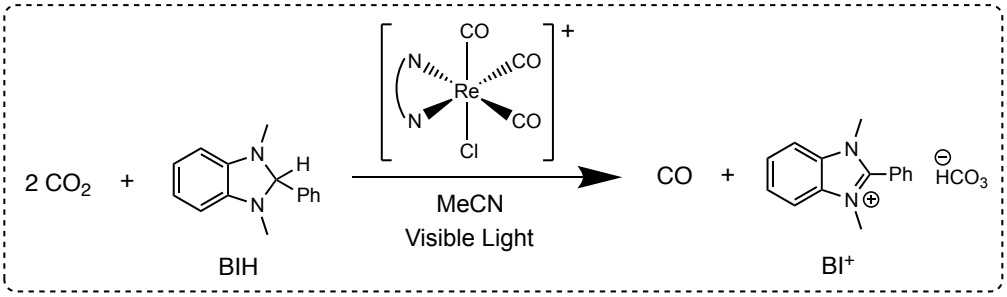

Scheme 8. *Overview of the homogeneous photochemical CO_2 reduction with fac-Re(bpy)(CO)$_3$Cl catalyst, 3CzIPN imidazole PS and BIH in solution. This reaction details the use of separate catalyst and PS molecules and was achieved prior to covalently linking the two compounds together.*

Like similar reactions reported in the literature[111–114], chloride abstraction from *fac*-Re(bpy)(CO)$_3$Cl by a slight excess of $AgBF_4$ in acetone generates the cationic Re-acetone complex (**5**) and an AgCl precipitate (*scheme 9*). This reaction was first carried out on an NMR scale. The solubility of the Re precursor, *fac*-Re(bpy)(CO)$_3$Cl, in acetone was low, but addition of the $AgBF_4$ acetone solution, sonication, and monitoring by ^{1}H NMR spectroscopy showed the reaction was complete after 1.5 hours to form a yellow solution with an AgCl precipitate. The identity of the Re-acetone complex **5** was confirmed by comparing its ^{1}H and ^{13}C NMR spectra to the MeCN solvent-cation reported in the literature.[103] Acetone was used for this study because it is more labile than MeCN when bonded to d-electron rich metal centres. *Figure 14* shows the ^{1}H NMR of the soluble products in d_6-acetone. There are two minor components in solution that are likely the BF_4^- compound **6**, and the aquo compound **7** formed by trace water either in the solvent or in the $AgBF_4$. No attempts were made to isolate these species or identify the minor components further, but it is noted that addition of excess water converts them all into the putative aquo compound **7** (*scheme 10, figure S39*). Solutions of **5** were stable over time at room temperature, but no attempt was made

to isolate it. The product solutions were utilized immediately upon preparation for reactions with the coordinating 3CzIPN derivatives.

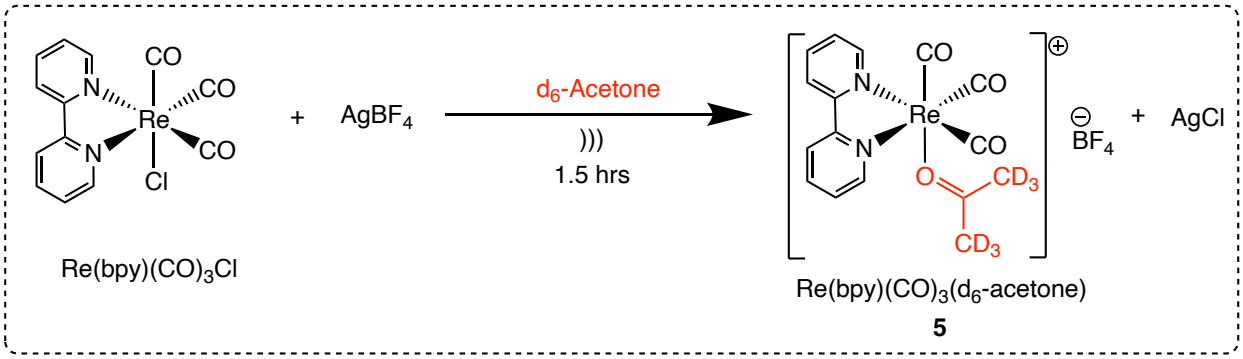

Scheme 9. *Reaction scheme of the removal of the Cl^- ligand in $Re(bpy)(CO)_3Cl$ by $AgBF_4$ in d_6-acetone.*

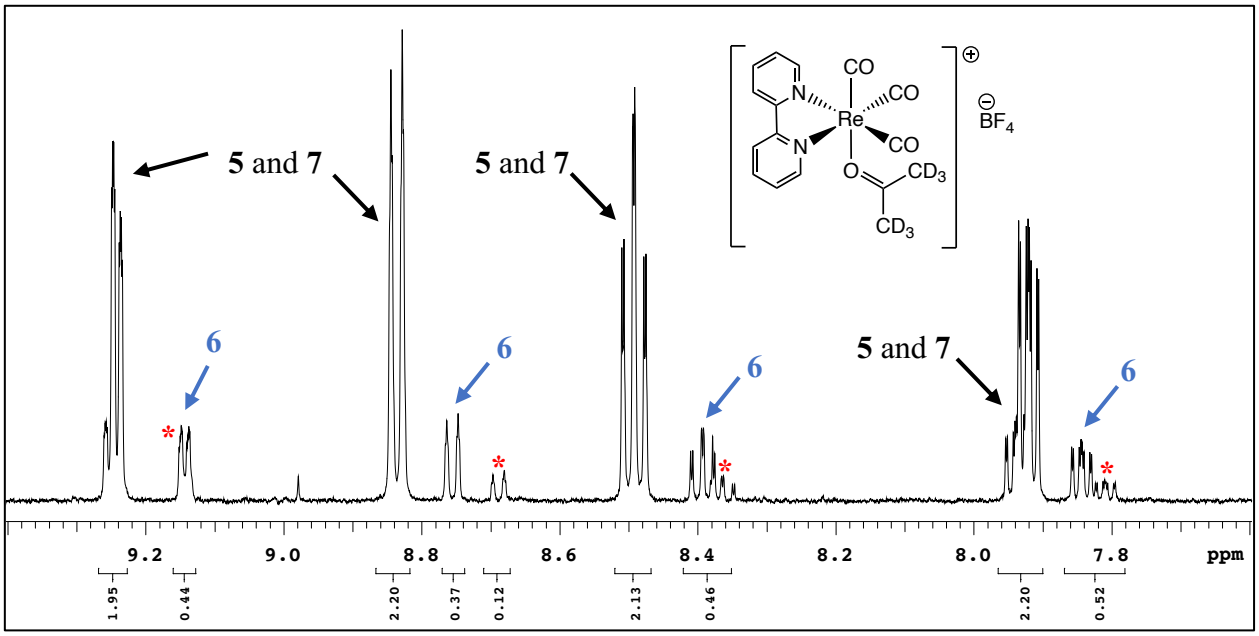

Figure 14. *^1H NMR spectrum of the $Re(bpy)(CO)_3(d_6$-acetone) complex **5** following chloride abstraction by $AgBF_4$ in d_6-acetone. The four large peaks correspond to a mixture of complexes **5** and **7** that is entirely converted to **7** upon addition of D_2O. The minor peaks, indicated by blue arrows, correspond to complex **6** that was also converted to **7** with D_2O addition. The other minor peaks highlighted by a red asterisk is postulated to belong to a hydroxide complex that does not react upon addition of D_2O or any organic dyes.*

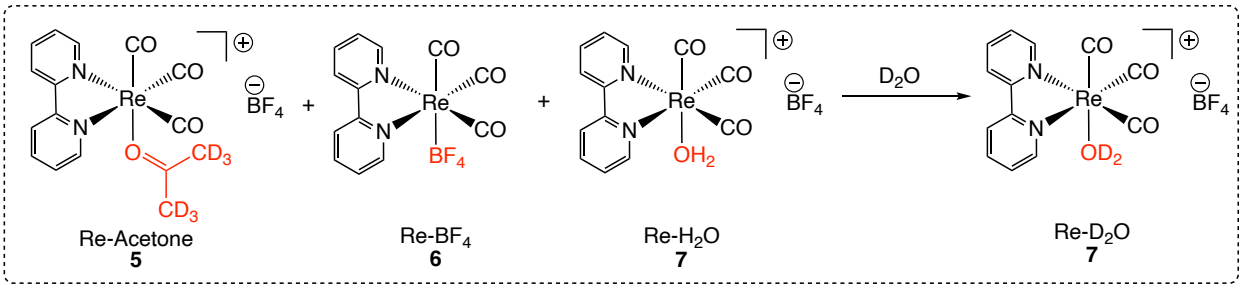

Scheme 10. *Conversion of the various complexes formed during the reaction between Re(bpy)(CO)$_3$Cl and AgBF$_4$ to the aquo complex **7** upon addition of D$_2$O.*

The reaction between the Re-acetone complex **5** and the 3CzIPN imidazole ligand **2** was incomplete and formed a mixture of starting materials and products (~ 60%, estimated) after 24 hours at room temperature. Inspection of molecular models and the crystal structure of the free imidazole show there is significant crowding in these molecules. The displacement products form slowly at room temperature and exist as a kinetic mixture of rotamers. Indeed, heating the reaction at 60 ˚C for ~ 18 hours further drove it nearly to completion. As well, the heating converted the products into a mixture with a major rotamer, as evidence by the convergence of the imidazole peaks in the ^{1}H NMR spectrum into three major peaks at 7.09, 6.37 and 6.15 ppm (*scheme 11, figure 15*). As expected, minor rotamers were still present after heating.

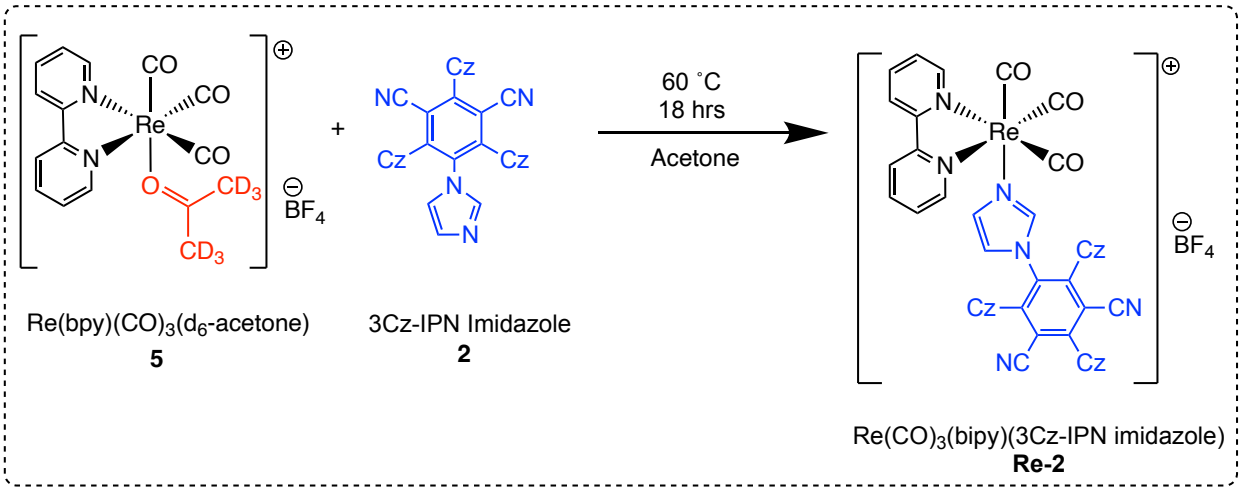

Scheme 11. *Reaction scheme of the synthesis of Re-**2** by heating the mixture of Re-acetone and 3CzIPN imidazole (**2**).*

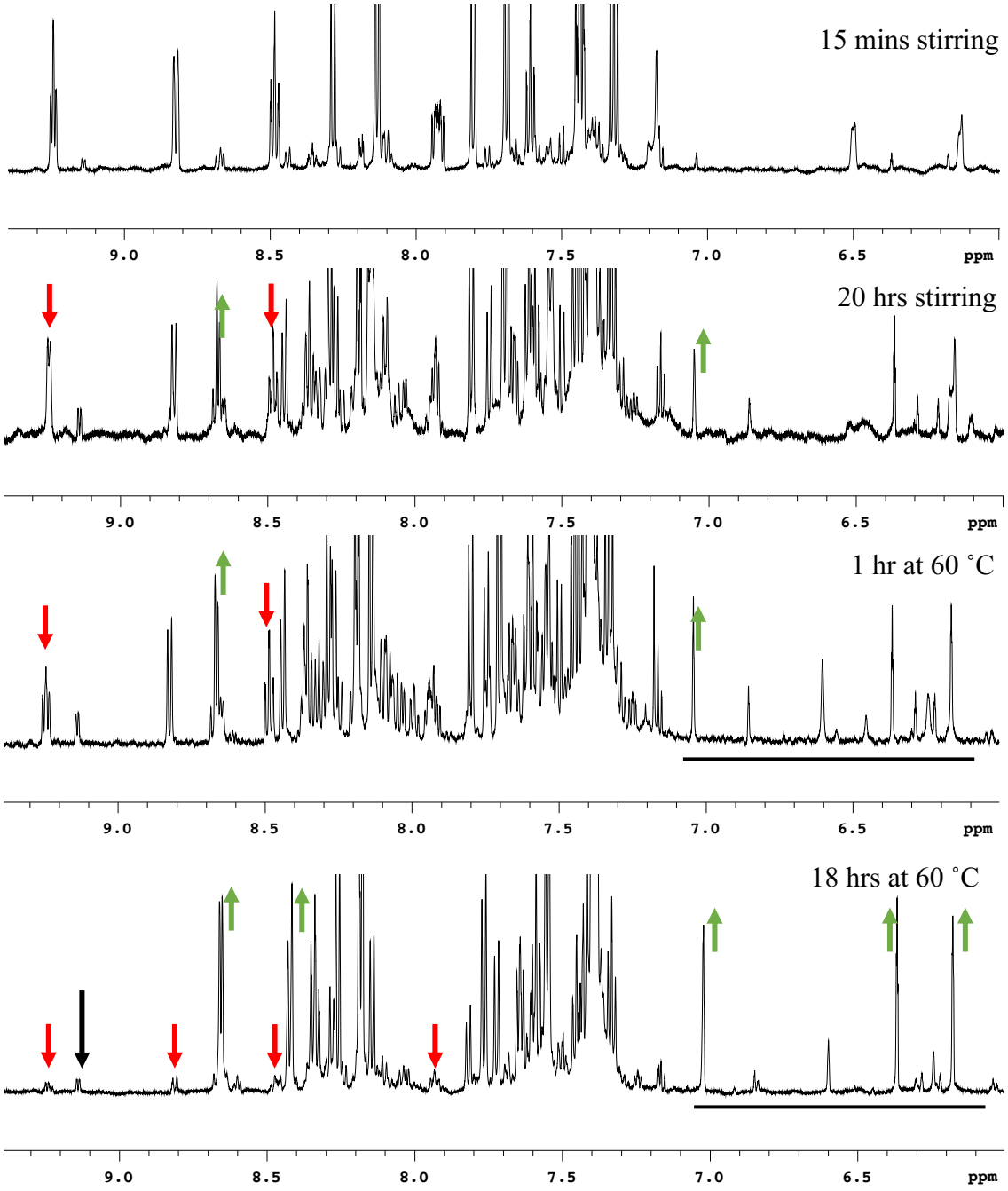

Figure 15. *^{1}H NMR of Re-**2** in d_6-acetone after stirring for 15 minutes, 20 hours then after heating the solution at 60 ˚C for 1 hour and 18 hours. Peaks corresponding to the desired product are shown by green arrows as they increase as the reaction proceeds. Peaks corresponding to the Re-acetone starting material are marked by red arrows as they react and disappear over time. The imidazole peak region is marked by a solid black line in the last two spectra, showing the convergence of rotamers into one major compound represented by the three large imidazole peaks.*

Precipitation by slow addition of diethyl ether formed a yellow solid (~ 82% yield) that exists as a mixture of rotamers of a slightly different composition as the parent solution. The

compound was characterized by ^{1}H and ^{13}C NMR spectroscopy, and HRMS. No further attempts were made to purify or characterize the rotamers. We note, however, that a control reaction between the acetone compound **5** and N-methyl imidazole went to completion and only formed one compound (*figure S40*). As expected, no rotamers were formed with N-methyl imidazole, suggesting that reactions between **5** and the 3CzIPN imidazole ligand **2** generally go to completion in high yields. Studies with ^{1}H NMR spectroscopy showed that MeCN stock solutions of the Re-dye rotamers were stable for weeks at room temperature.

In addition to the Re-**2** complex, two other Re(I)-NHC complexes were prepared by reactions between the cationic Re complex **5** and the free NHC-dye compounds **8** and **9**. These preparations proceeded with better selectivity than the reaction with the 3CzIPN imidazole dye **2**. The free NHC-dye ligands **8** and **9** were generated by deprotonation of the corresponding imidazolium compounds **3** and **4** by excess KH in d_8-THF or THF over 3 hours at 0 ˚C (*scheme 12*). KH is sufficiently basic to deprotonate the imidazolium, but not enough to react further with the free NHC, which would lead to decomposition. The reaction solution became a deep red/brown when the deprotonation was complete. *Figure 16* shows the ^{1}H NMR spectra of the free NHC-dye ligand **8** in d_8-THF. The deprotonation of the isopropyl imidazolium **4** was not carried out in d_8-THF due to the national shortage, therefore the isopropyl free NHC **9** was not characterized.

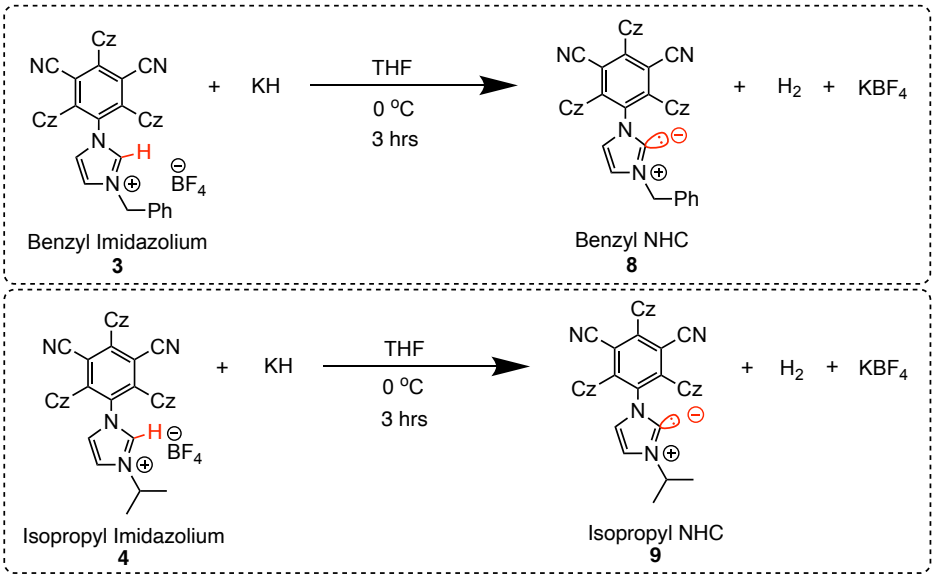

Scheme 12. *Reaction scheme of the deprotonation of* ***8*** *and* ***9*** *by KH in THF.*

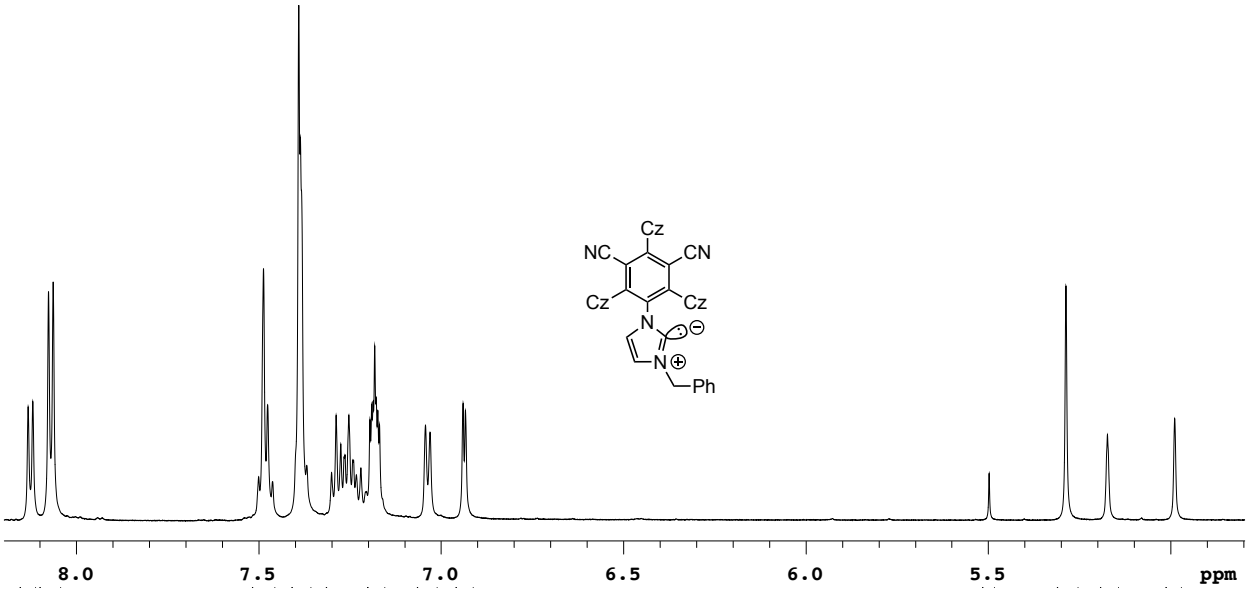

Figure 16. *^{1}H NMR spectrum of the benzyl free NHC (**8**) in d$_8$-THF.*

The deprotonation was always complete after 3 hours at 0 ˚C. It is noted that in some cases, the deprotonation was complete in less time, even after 30 minutes in one instance. It is likely that the rate of this heterogeneous deprotonation varies with factors including stir rate, KH particle size, and perhaps even the presence of KOH impurities on the KH surface. As a result, fresh and dry KH gave the best results for this reaction. The THF solution of the free NHC was decanted off

the excess KH via cannula filtration into a 0 ˚C solution of **5** (*scheme 13*). These free NHC compounds decompose slowly above 0 ˚C, requiring that the reaction with **5** be carried out at 0 ˚C. The colour of the solution quickly changed from dark red to a lighter red/orange upon mixing. ^{1}H NMR spectroscopy confirmed that the reaction was complete and the NHC groups were coordinated to Re. The reactions between the NHC-dye ligands and **5** was much faster than that with the 3CzIPN imidazole **2**, due to the higher donating ability of NHC groups over imides to metal centres. The shifts of the ^{1}H NMR signals for the benzyl NHC group and the isopropyl proton signals are all consistent with coordination to the Re metal centre. The signal corresponding to the benzyl protons was shifted downfield from 4.66 ppm to 5.29 ppm upon deprotonation by KH and the appearance of new signals corresponding to bpy confirm coordination to the Re metal centre (*figure 17*). The ^{1}H NMR signals for the isopropyl –C<u>H</u>– (C<u>H</u>$_3$)$_2$ methine and methyl groups shifted downfield from 4.73 to 3.86 ppm and from 1.42 to 0.71, respectively, upon coordination to Re (*figure 18*).

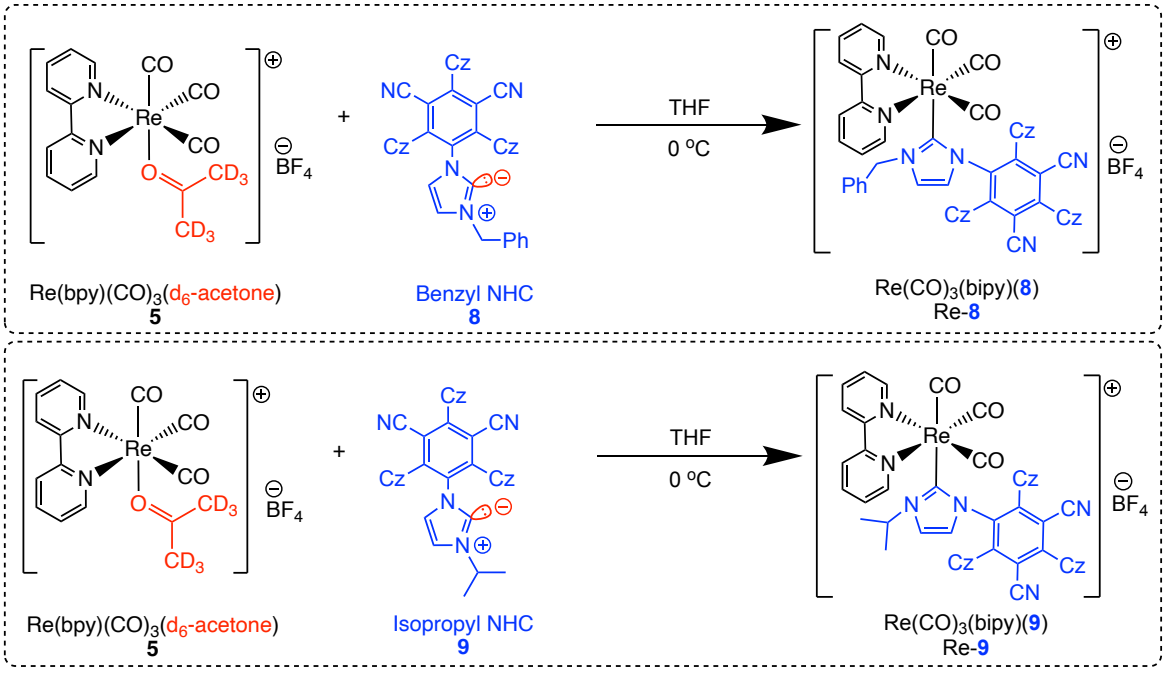

Scheme 13. *Reaction scheme of the synthesis of the Re-NHC photocatalysts by mixing the Re-acetone complex* ***5*** *with the benzyl free NHC* ***8*** *and the isopropyl free NHC* ***9****.*

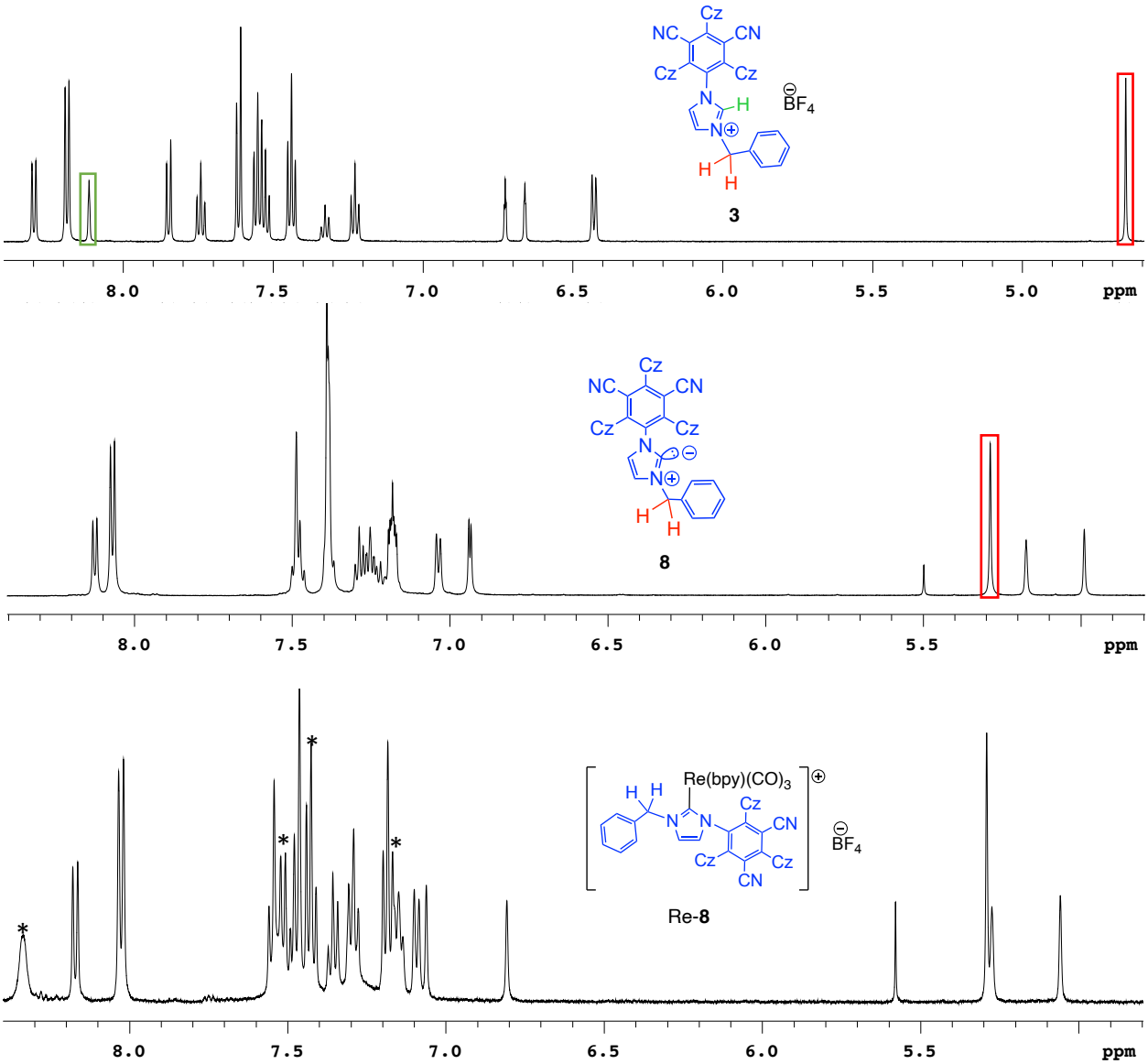

Figure 17. *^{1}H NMR spectra of the benzyl imidazolium **3** in CD_3CN (top), the benzyl free NHC dye **8** in d_8-THF (middle) and the Re-**8** complex in a d_8-THF and $(CD_3)_2CO$ mixture (bottom). The deprotonation of the imidazolium dye **3** dye was confirmed by the shift of the benzyl –CH_2– protons from 4.66 ppm to 5.29 ppm marked in red and the disappearance of the carbene proton signal marked in green. The coordination of the benzyl free NHC to the Re complex was confirmed by the appearance of bpy proton signals indicated by asterisks and the disappearance of signals corresponding to complex **5**.*

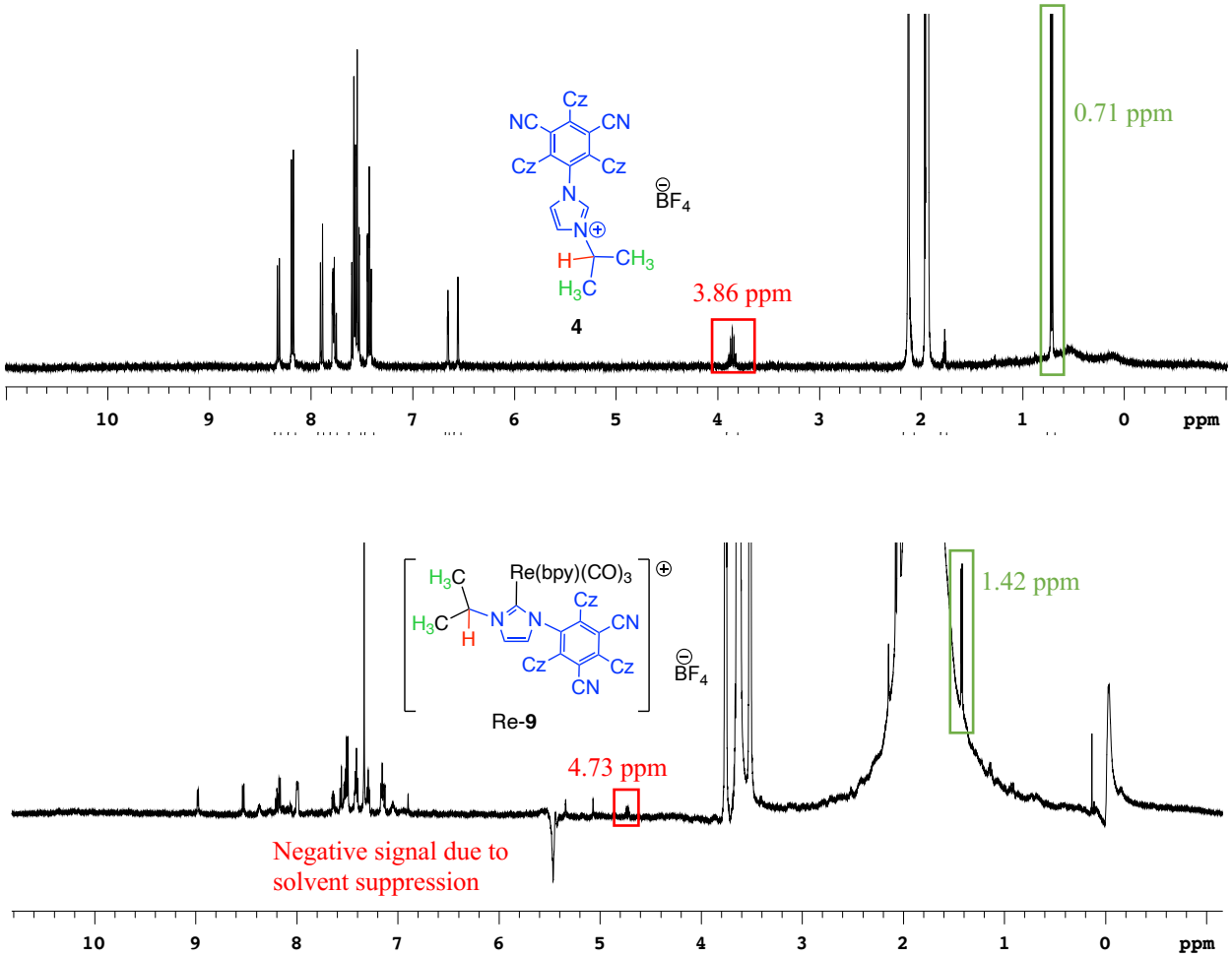

Figure 18. *^{1}H NMR spectra of the isopropyl imidazolium dye **4** in CD_3CN and the Re-**9** complex in $(CD_3)_2CO$. The coordination of the dye is confirmed by the shifting of the isopropyl –CH– (red) and $–(CH_3)_2$ (green) protons from 3.86 and 0.71 ppm to 4.73 and 1.42 ppm, respectively.*

The ^{1}H NMR spectra indicate that fewer rotamers formed upon reaction between **5** and the free NHC-dyes **8** and **9** than formed upon reaction with the imide dye **2**. This apparent greater kinetic selectivity may result from the reactions with the NHC-dyes being carried out at lower temperatures (0 ˚C) than the imide-dye, or perhaps fewer conformers exist within the NHC-dye ligands. The presence of added steric bulk in the NHC ligands hinders free rotation of the carbazole groups in the dye and forces the molecule into one specific conformation. The deprotonation of **3** to generate the free benzyl NHC **8** was carried out in *d*$_8$-THF, which allowed for characterization of the free NHC compound **8** as well as the Re-**8** complex. However, due to the national *d*$_8$-THF

shortage, the deprotonation of **4** to generate the free isopropyl NHC **9** was only achieved in regular THF. As a result, ^{1}H NMR spectroscopy with solvent suppression was required to identify and characterize both the free isopropyl NHC product **9** and the Re-**9** complex prepared upon mixing with complex **5**. Despite this limitation, the suppression of one of the THF solvent signals was sufficient to confirm successful coordination of the compounds. The main concern in the preparation of both free NHC compounds and photocatalyst complexes was their thermal instability. Both free NHC compounds and the Re-NHC photocatalysts decomposed over time, even at 0 ˚C, and attempts to isolate them proved unsuccessful. The Re-NHC solutions were used for CO_2 reduction reactions directly following preparation as they were not stable at 0 ˚C for long periods of time. Placing the solutions in the freezer for several hours resulted the formation of black solid, indicating decomposition and very low stability even at 0 ˚C. The use of the Re-NHC complexes as photocatalysts for CO_2 reduction directly after synthesis proved to be successful and will be described in more detail in the following chapter.

3.4 DISCUSSION

All three organic dyes were successfully linked to the Re metal centre to covalently link the catalyst and PS to promote increased photocatalytic activity in CO_2 reduction reactions. These complexes act as both the PS and the catalyst, so it is important that the ligand forms a strong bond with the metal centre to remain attached to the complex while promoting dissociation of the carbonyl ligands. The stronger bond with the Re catalyst results in a higher durability of the catalyst which allows for increased catalytic activity. A trans-labilizing ligand is ideal to promote the dissociation of the trans CO ligand, which then allows for the photocatalyst to interact with CO_2. The imidazole ligand **2** and the NHC ligands **8** and **9** coordinate to the metal centre in different ways (*figure 19*), with the imidazole complex **2** coordinating to the Re centre through the second imidazole nitrogen atom, a less activating σ-donor. In both NHC ligands, both imidazole nitrogen atoms are saturated due to the addition of the benzyl and isopropyl groups, so they coordinate to the Re centre through the lone pair on the carbene carbon. The carbene carbon acts as a trans-labilizing, stronger activating σ-donor ligand that forms a stronger bond with the metal centre. In addition, the free NHC compounds have added steric hindrance compared to **2** which can assist in further stabilization of the excited state of the dye, as mentioned previously. Because of this, the NHC ligands demonstrate significant advantages over the imidazole dye **2**, making them potential candidates for increased CO_2 reduction activity.

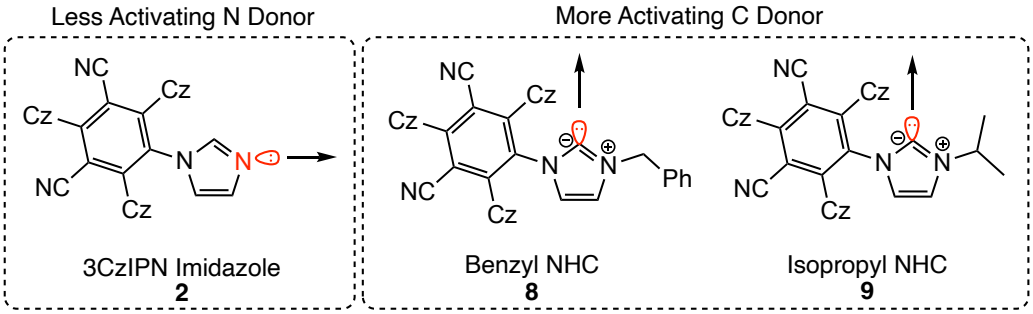

Figure 19. *Comparison of the coordination of 3CzIPN imidazole **2** and the NHC dyes **8** and **9** to the Re catalyst metal centre.*

The halide-abstraction reaction between $Re(bpy)(CO)_3Cl$ and $AgBF_4$ to generate the Re-acetone complex **5** resulted in a mixture of products. The major product identities were proposed as the aquo complex, a Re-BF_4 complex and the desired Re-acetone complex, which are all converted to the aquo complex upon addition of D_2O. A small minor product can be seen (~ 6%) in all ^1H NMR spectra and did not undergo reactions with additional $AgBF_4$ or any of the dye ligands, including a test reaction with methyl imidazole. Due to the low reactivity of this unknown product, it is postulated to be a hydroxyl complex and does not interfere in any further reactions.

Similar studies are underway in the group with manganese(I) (Mn) catalysts. The same reaction between *fac*-$Mn(bpy)(CO)_3Cl$ and $AgBF_4$ has been found to proceed significantly faster, being complete after 5 minutes of agitation. Rhenium is known to have increased stability and form stronger bonds compared to manganese, which is likely why this reaction with Re proceeds much slower in comparison.[115] Rhenium forms stronger bonds, which require more time break and react with $AgBF_4$. However, the formation of stronger bonds between the Re metal centre and the organic dyes leads to increased catalyst durability, an important factor for CO_2 reduction reactions.

The preparation of the Re(I) photocatalysts were relatively similar, with the Re-**2** complex presenting the most complications. In mixing the imidazole dye **2** and the Re-acetone complex **5**, the reaction proceeded slowly and required heating for up to 20 hours to reach completion. Additionally, many rotamers of the photocatalyst formed upon coordination of the dye, necessitating heat to convert all products into one major rotamer. Contrarily, the reaction between the free benzyl and isopropyl NHC complexes **8** and **9** and the Re-acetone complex **5** generated one major product in either case. Despite the issues with solvent suppression and inability to monitor the reactions thoroughly, the resulting photocatalyst complexes Re-**8** and Re-**9** were clean, high-yielding, and reproducible over many reactions. The synthesis of Re-**8** in d_8-THF allowed for

high quality NMR spectra to be collected of both the free benzyl NHC **8** and the photocatalyst, whereas the Re-**9** photocatalyst was only prepared in regular THF with only ^{1}H NMR spectra being collected via solvent suppression methods. The synthesis of Re-**9** must be achieved in d_8-THF to properly monitor the reaction and obtain high-quality characterization data, more specifically ^{1}H and ^{13}C spectra.

3.4 CONCLUSION

Overall, the three organic dyes were successfully coordinated to the Re catalyst in the attempt to generate more active photocatalysts for CO_2 reduction by physically linking the catalyst and PS together. The synthesis of Re-**8** and Re-**9** was more straightforward than Re-**2**, with fewer rotamers forming upon coordination and no heating required to accelerate the reaction. The coordination of the dyes was confirmed by the shift of indicative protons downfield upon linking to the Re metal centre. This is anticipated as the Re metal centre draws electrons out of the dye ligands, deshielding them and shifting the proton peaks downfield. With the successful coordination of the Re catalyst to different organic dyes, three Re(I) photocatalysts were prepared to be evaluated for their use in the photochemical reduction of CO_2 (*figure 20*).

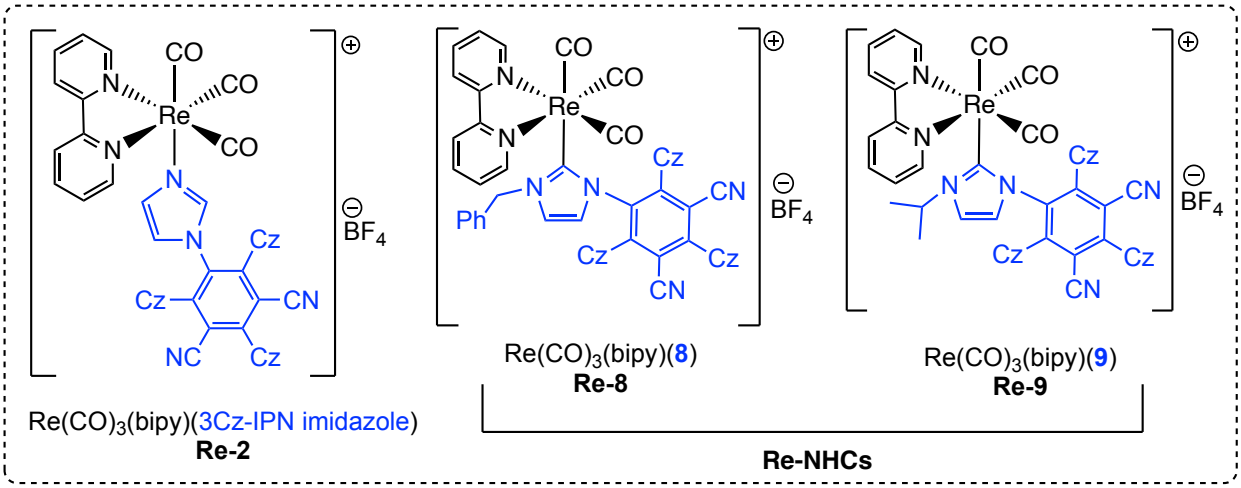

Figure 20. *Three Re(I) photocatalysts synthesized by coordinating three dye ligands,* ***2****,* ***8*** *and* ***9****, to a Re(bpy)(CO)₃Cl catalyst.*

4 – PHOTOCHEMICAL CO_2 REDUCTION

4.1 RESULTS

The three Re(I) photocatalysts were evaluated for the photochemical reduction of CO_2. As discussed previously, photochemical CO_2 reduction systems typically have three important components: the catalyst, the photosensitizer (PS) and the electron donor (D). Briefly, the excited PS initiates an electron transfer from the highest energy SOMO to the catalyst to generate a low-valent unsaturated metal complex that can interact with CO_2. The oxidized PS is then reduced by the sacrificial electron donor. Note the order of these steps may be reversed, depending upon the requirements of the reaction. Specifically, the lowest energy SOMO of the excited PS may be reduced by the sacrificial electron donor before the electron transfer from the highest energy SOMO to the catalyst. Note that the negatively charged, reduced excited state is a much stronger electron donor. In optimization studies conducted by Ellie Yao, a prior student in the group, CO_2 photoreductions were carried out with the catalyst and PS components separate in solution. Specifically, with *fac*-Re(bpy)$(CO)_3$Cl as the catalyst, **2** as the PS and BIH as the sacrificial electron donor (*scheme 14*).

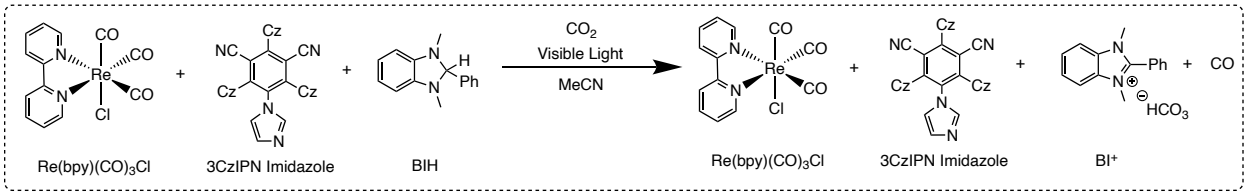

Scheme 14. *Reaction scheme for the reduction of CO_2 with a fac-Re(bpy)$(CO)_3$Cl catalyst, 3CzIPN imidazole as PS and BIH as the sacrificial electron donor. LED light source at ~ 450 nm.*

Table 4 summarizes the concentrations, additives, and the resulting TON_{CO} utilized during a conditions optimization study. All reactions were carried out in MeCN solvent at room temperature, initially under 1 atm CO_2. MeCN or DMF are the typical solvents utilized in such photocatalytic CO_2 reductions in literature.[95] MeCN was utilized for this study due to the increased

safety concerns associated with DMF. These optimization studies were carried out with blue LEDs (450 nm, 6.55 mW) with no filter as the light source. The highest TON_{CO} (233) were obtained with a 0.141 mM concentration of the catalyst, 0.127 mM for PS and a 0.1 M concentration of BIH with no additives (*table 4, exp 10 and 13*). Moving forward, the concentration of the PS was increased to 0.141 mM to match the concentration of the catalyst and promote the electron transfer process from the excited PS to the catalyst. Many reported CO_2 reduction reaction systems catalyzed by similar complexes in literature report comparable optimized conditions. Specifically, the majority of systems in the literature utilize an AM 1.5G light source (calibrated to 100 mW/cm^2), with some studies utilizing blue LEDs of known wavelength and intensity.[116–118] The reported optimum catalyst/PS concentrations are typically around 0.1 mM and [BIH] is kept around 0.1 M.[116–118] In addition to MeCN and BIH, DMF and TEOA are popular alternatives for solvent and sacrificial electron donors in literature.[116–119]

Table 4. *Summary of the optimization studies for the CO_2 reduction system by a previous student in the group. All experiments were carried out in MeCN at room temperature with 0.1 M BIH. The concentration of the catalyst and PS are indicated, as well as any additives included in the reaction solution. The absence of any additives is indicated by a blank 'Additives' column.*

Exp	[Re(bpy)(CO)$_3$Cl] (mM)	3CzIPN Imidazole **2** (mM)	Additives	Irradiation Time (h)	TON_{CO}
1	0.49	1.5	TEOA, TFE	97	3
2	0.49	1.5	TEOA	43	12
3	0.51	15	TEOA, TFE	91	0
4	0.51	15	TEOA	92	0
5	0.5	0.5	TFE	97	27
6	0.5	0.52		95	67
7	0.5	0.52	H_2O	120	21
8	0.5	0.5		116	79
9	0.26	0.25		115	153
10	**0.141**	**0.127**		**68**	**233**
11	0.141	0.242		67	83
12	0.0704	0.0691		47	151
13	**0.141**	**0.127**		**48**	**116**

TEOA proved to be a less effective sacrificial electron donor than BIH (*table 1, exp 1–4*). Trifluoroethanol (TFE) is reported to promote certain CO_2 photoreductions by acting as a source of protic hydrogen atoms.[95] Addition of TFE, however, did not promote the photoreductions carried out with the present system (*table 4, exp 1, 3, 5*), neither did addition of H_2O as a putative proton source (*table 4, exp 5*). All CO_2 reduction reactions carried out with the separate catalyst and PS complexes in solution with BIH produced CO as the only reduction product. The formation of a solid in the reaction solution was observed after 48–70 hours of irradiation for all reactions, which shut down the reaction by blocking light from entering the system.

After optimizing the reaction conditions and setup, the Re-imidazole-dye complex, Re-**2**, and the Re-NHC-dye complexes, Re-**8** and Re-**9**, were evaluated for the photocatalytic CO_2 reduction (*scheme 15*) with an AM 1.5G solar energy simulator (calibrated to 100 mW/cm^2). *Table 5* shows the results of repeated photocatalytic reductions of CO_2 catalyzed by the imidazole complex Re-**2**. The reactions proceeded quickly during the initial first stages of the photoreaction. The turnover frequencies (TOF_{CO}, TON_{CO}/h) over the initial stages of the reactions, before they slowed, were 8.5 and 9 h^{-1} (2 hrs). The reactions slowed over time, both giving ~ 60 TON_{CO} after 24 hours. In runs 1 and 3, small amounts of methane were also observed as a gaseous product. A white solid formed after the initial stages, and its formation coincided with the slowing of the reactions, perhaps because the incident light was reflected or blocked.

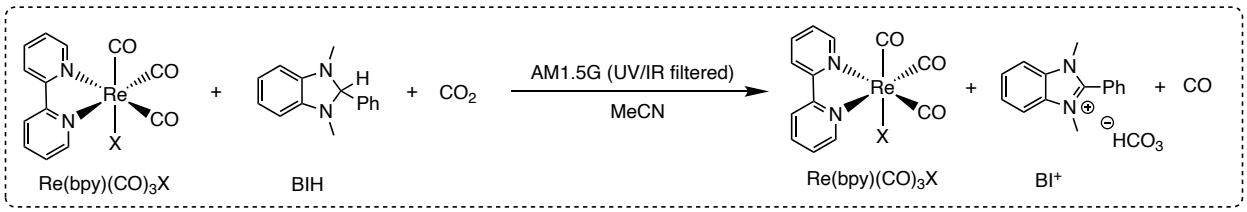

Scheme 15*. Reaction scheme for the reduction of CO_2 with a Re(bpy)(CO)$_3$X photocatalyst where X = **2** (3CzIPN imidazole), **8** (benzyl free NHC) and **9** (isopropyl free NHC) with BIH as the sacrificial electron donor. The Re-**2**, Re-**8**, and Re-**9** photocatalysts were evaluated.*

Table 5. *Summary of CO_2 reduction results for the Re-**2** photocatalyst (0.14 mM) with BIH (0.1 M) in MeCN. The TON_{CO} and TON_{CH4} was calculated with an ethane internal standard and the corresponding calibration curves.*

Run	Photocatalyst	Irradiation Time (h)	TON_{CO}	TON_{CH4}
1	Re-**2**	1	7	0
		2	17	0
		4	31	0
		24	61	0
		48	65	0
		72	66	0
2	Re-**2**	1	7	0
		2	18	0
		4	32	0
		24	59	1
		48	69	3
		72	69	6

The Re-NHC photocatalysts were evaluated for the photocatalytic reduction of CO_2 in the same conditions (*scheme 15*). All reactions were repeated, and the results were consistent between each attempt (*table 6*). *Figure 21* shows plots of TON vs time for the different catalysts. As before, the reactions proceeded quickly over the first 5–10 hours then began to slow. The initial activity of the benzyl-NHC photocatalyst, Re-**8**, was the highest by far. The TOF_{CO} during the initial stages of the reaction before any evidence of slowing was 46 and 47 h^{-1}. The TON_{CO} after 20 hours was ~ 50. Note that methane was used as the internal standard for these reactions. The activities of the Re-imidazole-dye (Re-**2**) and Re-isopropyl-NHC-dye (Re-**9**) complexes were similar during the initial stages of the reaction. The average initial TOF_{CO} was 12.5 h^{-1} for Re-**9** and 8.75 h^{-1} for Re-**2**, ~ 1/4 and 1/5 that of the benzyl-NHC complex Re-**8**, respectively. NHC ligands are strong σ-donors, and catalysts that incorporate them are often more active than the same catalyst with, for example, phosphines or related ligands.[120–122] It is likely a similar effect that results in the relatively high activity of the Re-**8** compound. Specifically, the strong σ-donation by the NHC ligand appears to increase the rate of the turnover-limiting step in the photocatalytic CO_2 reduction. The

corresponding isopropyl-NHC complex Re-**9** was less active, suggesting that steric crowding prevented the catalyst-dye complex from adopting optimum geometry for CO_2 photocatalysis. The imide-dye ligand is a weaker σ-donor than the corresponding NHC compounds, apparently resulting in activity that is lower than the benzyl-NHC ligand, but similar to the crowded isopropyl-NHC ligand. These proposed explanations must be confirmed by a detailed mechanistic analysis, which is beyond the scope of the present discovery-based study. Use of ethane as internal standard revealed that methane is formed during the photocatalytic CO_2 reductions with the isopropyl-NHC Re-**9** complex, an observation similar to the imidazole complex Re-**2**. It is rare for homogeneous photocatalysts to produce methane as a CO_2 reduction product. For this reason, the Re-**9** photocatalyst was the focus of additional experiments to investigate the origins of the methane.

Table 6. *Summary of CO_2 reduction results for the Re-**8** and Re-**9** photocatalysts (0.14 mM) with BIH (0.1 M) in MeCN. The TON for CO was calculated with either a methane or ethane internal standard and the corresponding calibration curve. The TON for CH_4 was calculated with an ethane internal standard and calibration curve. The quantification of methane produced was only achieved for reactions with an ethane internal standard.*

Run	Photocatalyst	Irradiation Time (h)	TON_{CO}	TON_{CH4}
1	Re-**8**	1	47	N/A
		1.75	62	
		19.5	53*	
		21.5	54*	
2	Re-**8**	1	46	N/A
		1.75	47	
		19.5	50*	
		22.5	51*	
1	Re-**9**	1	12	0
		1.75	24	0
		19.5	42	3
		44	43	9
2	Re-**9**	0.75	10	0
		2.5	27	0
		24	46	0
		43	49	0
		96	51	0
3	Re-**9**	1.75	30	0
		22.5	40	2
		26	40	2

		45	41	4
		96	52	4
4	Re-**9**	2.5	21	0
		24	36	0
		48	49	0
		66.5	57	0
		93	60	0

**Projected TON_{CO} values based on the CH_4 peak area in the most recent chromatogram prior to the formation of methane. The formation of methane interferes with the internal standard and quantification. In both reactions, the CH_4 peak area of the chromatogram obtained at T=1.75 h was used for quantification of TON_{CO}.*

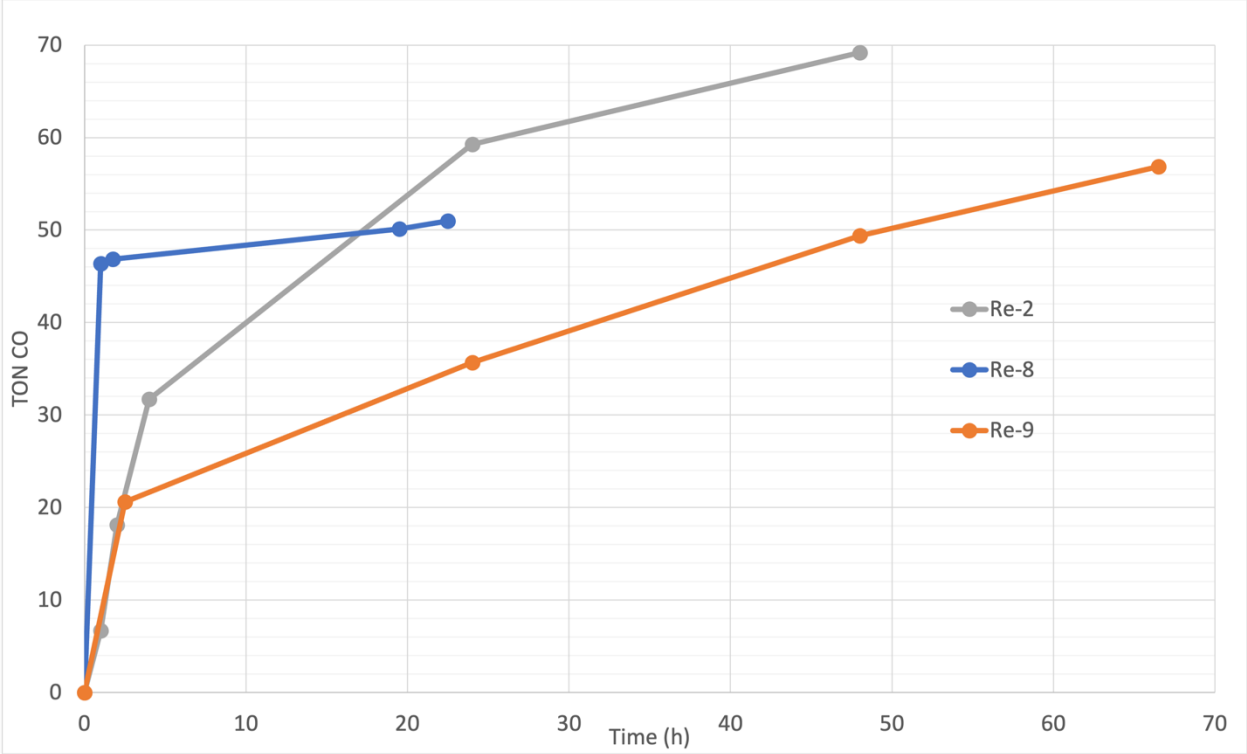

Figure 21. *TON_{CO} produced from the reduction of CO_2 with the Re-**2** (run 2, table 5), Re-**8** (run 2, table 6), and Re-**9** (run 4, table 6) photocatalysts.*

Figure 22 shows the plots of the TONs for formation of CO and CH_4 for repeated CO_2 photoreductions carried out with the isopropyl-NHC catalyst Re-**9** with ethane as internal standard (*scheme 16*). The reaction profiles are typical: an initial burst followed by a slowing. A white solid formed during all the reactions that slowed them by reflecting or blocking the incident light. The TOF_{CO} during the initial burst, before any evidence of slowing, were 13.7 and 17.1 h^{-1} for these

repeated runs. The methane formed after the reaction slowed, reaching 9 and 4 TON_{CH4} after 45 hours.

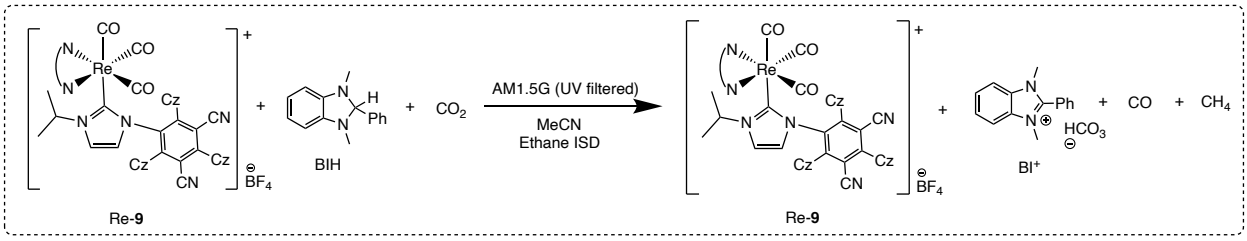

Scheme 16. *CO_2 reduction reaction with the Re-**9** photocatalyst in the presence of 0.1 M BIH in MeCN using an AM1.5G light source. Results of this reaction are plotted in figure 21.*

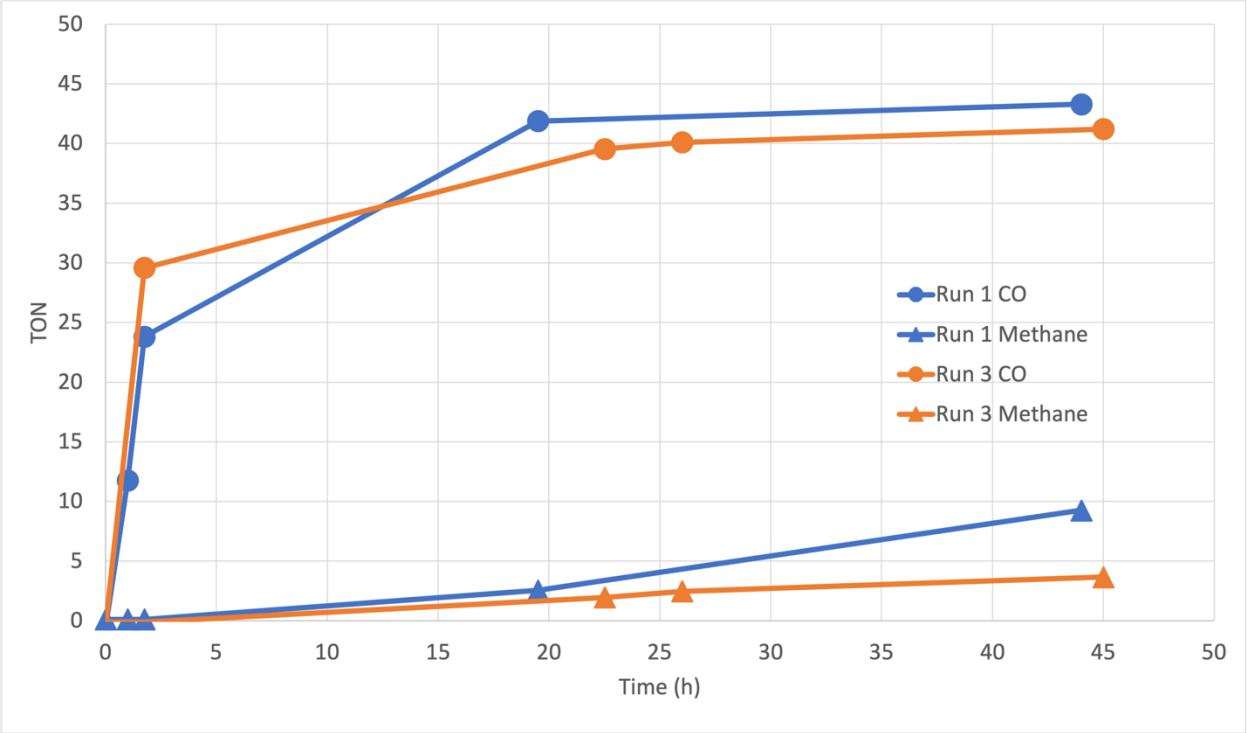

Figure 22. *TON_{CO} and TON_{CH4} of two repeat CO_2 reduction reactions, run 1 and 3 in table 6, with the Re-**9** photocatalyst.*

A white solid precipitated from all these photocatalytic CO_2 reductions, usually after ~ 40–60 TON_{CO}, but the time and TON_{CO} before precipitate formation varied among the reactions. The formation of the solid blocks and reflects much of the incident light, effectively shutting down the reactions slowed dramatically after the solid forms. The solid was characterized as a mixture of the oxidized and deprotonated BIH (BI^+), specifically 1,3-dimethyl-2-phenylbenzimidazolium

bicarbonate [BI^+] [HCO_3^-], via ^1H NMR spectroscopy and HRMS, and a substantial number of unidentified species. The BI^+ was identified by comparing the ^1H NMR and mass spectra (*m/z* 223.1235, *figure S41*) to those reported in literature. The anion was qualitatively identified as bicarbonate, HCO_3^-, via an acid test.[123] Specifically, bubbling was observed upon addition of dilute HCl (1.2 M), confirming the presence of HCO_3^- (or CO_3^{2-}) in solution (*scheme 17*). The resulting [BI^+] [Cl^-] complex was treated with silver nitrate ($AgNO_3$), resulting in the formation of an AgCl precipitate in the solution that turned grey upon exposure to light (*scheme 17*). The identities of the unknown aromatic compounds were not determined, but they are presumably the products of unknown reactions undergone by the BIH or BI^+. The ^1H NMR spectrum was also recorded of the reaction solvent diluted in d_6-acetone. Solvent suppression was required to reduce interference from the MeCN reaction solvent. The reaction mixture mainly contained BIH, some BI^+, and small unidentified signals in the aromatic region. Notably, the peak at 5.45 ppm, assigned to the hydrogen at C_2 of the remaining BIH, in the ^1H NMR spectrum is absent in the spectrum of BI^+ (*figure 23*). There were no definitive peaks in the solution ^1H NMR spectrum from MeOH, formic acid, or other soluble products from CO_2 reduction.

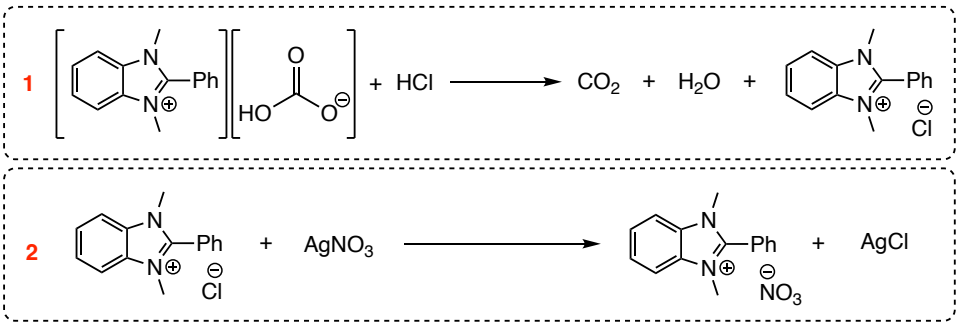

Scheme 17. *Scheme of the two reactions that were used to confirm the identity of the bicarbonate anion in the [BI^+] [HCO_3^-] complex. The precipitate was first treated with a dilute acid to release CO_2 and form the chloride anion. The [BI^+] [Cl^-] complex was then mixed with silver nitrate which resulted in the formation of an AgCl precipitate.*

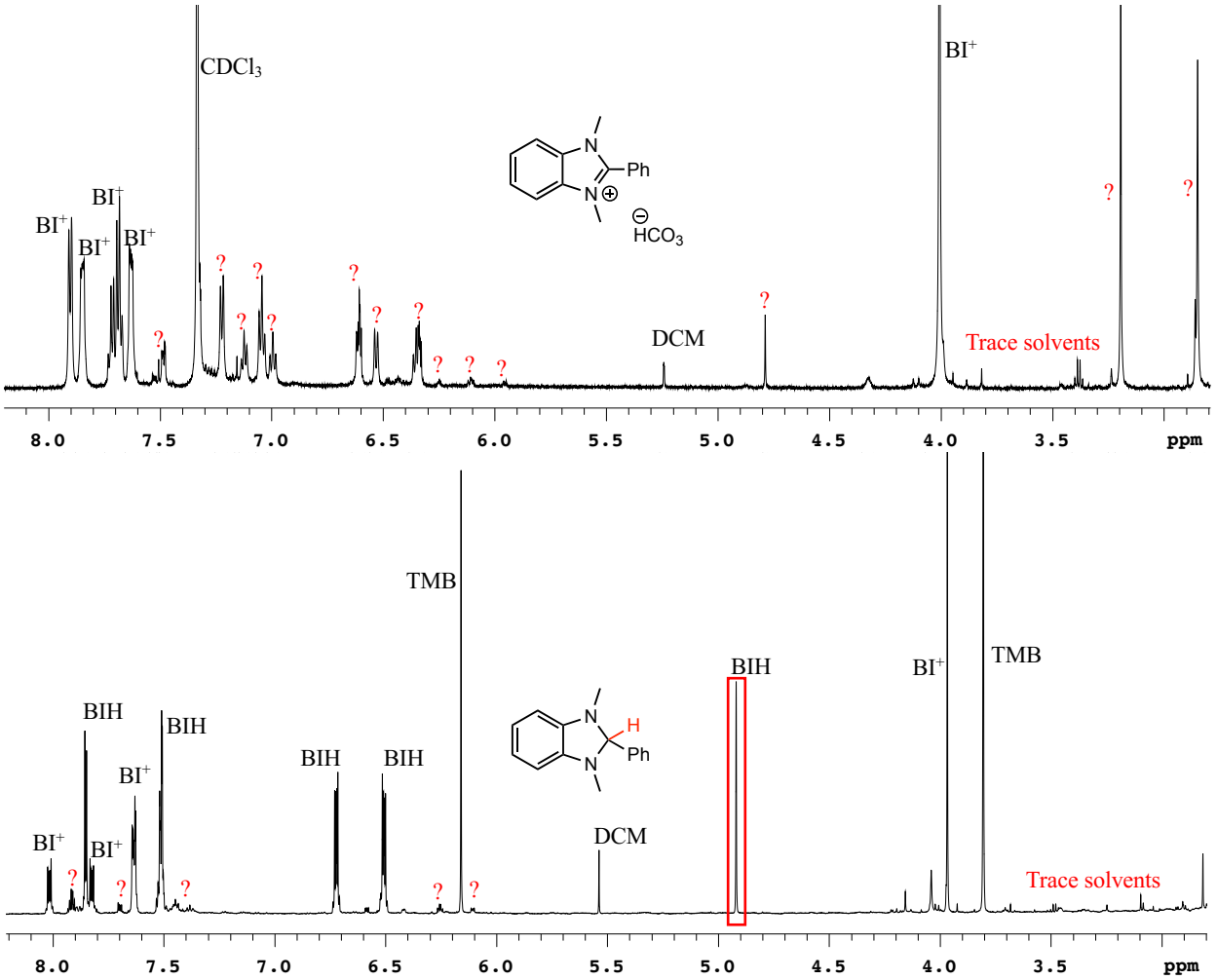

Figure 23. *^{1}H NMR spectrum of the [BI$^+$] [HCO$_3^-$] precipitate in CDCl$_3$/d$_6$-acetone (top) and the reaction solvent in d$_6$-acetone (bottom) following CO$_2$ reduction with Re-**2**. The oxidation and deprotonation of BIH to BI$^+$ is seen by the disappearance of the peak at 5.45 ppm indicated by the red box. All identifiable peaks were labelled, and unknown product signals are indicated.*

The gaseous CO_2 reduction products were identified and quantified by GC-TCD. The gases were identified in the chromatograms based on comparison of retention times to authentic samples. In some cases, the identities were confirmed with GC-MS, *vide infra*. *Table 7* summarizes all gaseous compounds and products present along with their corresponding retention times. Out of these compounds, only CO and CH_4 make up the reaction products with the remaining compounds being part of the reagents or reaction conditions, such as O_2, N_2, CO_2, C_2H_6 and MeCN. The gas

products were quantified with the internal standard and corresponding calibration curves made with authentic samples.

Table 7. *Compounds identified on a standard GC-TCD chromatogram used to monitor the progress of a photochemical CO_2 reduction reaction and their corresponding retention times. The retention times can vary by several seconds based on injection technique. No complications were encountered in identifying the peaks on chromatograms.*

Compound	Retention Time (min)	Source
N_2	2.77	Injection
O_2	3.02	Injection
CO*	3.87	**Reaction product**
CH_4*	6.51	**Reaction product**/Internal standard
CO_2	8.64	Reagent
C_2H_6	12.98	Internal standard
MeCN	22.45	Reaction solvent

*Compounds that are produced throughout the reaction. All other compounds are present in the T=0 chromatograms obtained prior to start of the CO_2 reduction reactions.

In addition to the gaseous products, the amounts of [BI^+] [HCO_3^-] formed and of BIH consumed were quantified by the addition of the NMR standard, 1,3,5-trimethoxybenzene (TMB), after the reaction was complete. The peaks in the ^1H NMR spectrum of TMB do not interfere with those of BI^+ or BIH (*figure 24*). *Table 8* summarizes the amount of BI^+ formed and BIH consumed in different CO_2 reduction reactions with different photocatalysts compared to the quantity of methane produced. As mentioned previously, the Re-**9** photocatalyst was carried forward over the Re-**8** photocatalyst for additional experiments so the amounts of BI^+ and BIH were only quantified for reactions with the Re-**2** and Re-**9** photocatalysts.

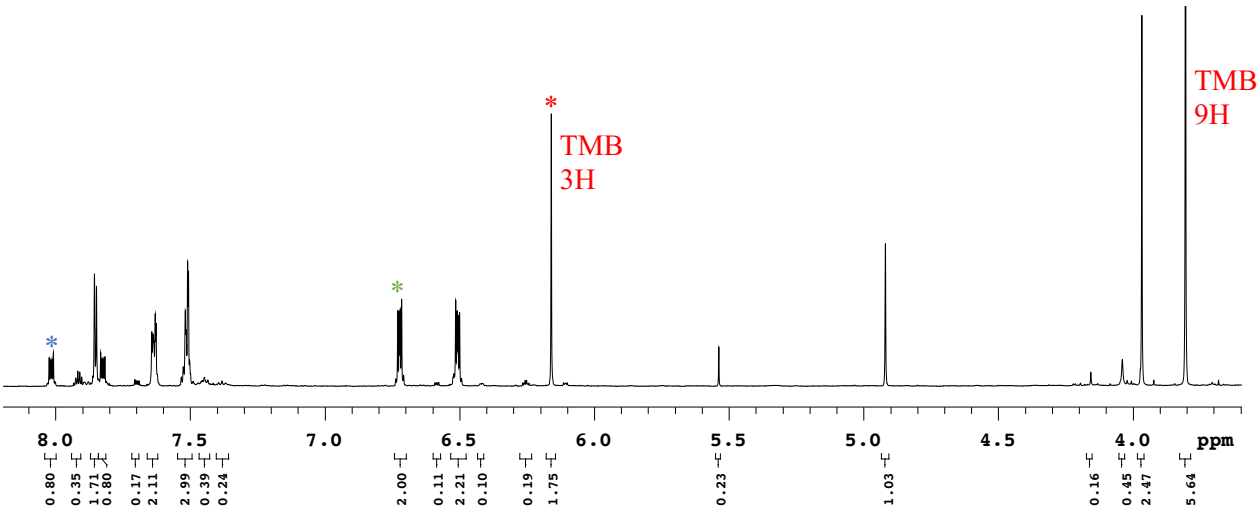

Figure 24. *^{1}H NMR spectrum of the CO_2 reduction products in the solvent following experiment 1 in table 4 (4-1). The reaction solvent was cannulated to a test tube containing the internal standard, TMB, and the NMR spectrum was obtained in d_6-acetone via solvent suppression of the MeCN solvent peak. Peaks corresponding to the standard and the reaction solvent are labelled. The standard peak used for quantification is indicated by a red asterisk. The peak used for quantification of BIH is indicated by a green asterisk and the peak used for BI^+ is indicated by a blue asterisk.*

Table 8. *Quantification of BIH and BI^+ following CO_2 reduction by the addition of 1,3,5-trimethoxybene as an internal standard for ^{1}H NMR. Amounts were calculated based on the peak integration ratios of BIH and BI^+ protons compared to that of the standard added.*

Exp	TMB Added (mmol)	BIH (mmol)	BI^+ (mmol)	BIH Consumed (mmol)	CO Produced (mmol)	CH_4 Produced (mmol)
4-1	0.0654	0.112	0.144*	0.188	0.016 (189h)	0.007
4-2	0.316	0.121	0.154♦	0.179	0.030 (144h)	0

*Amounts of $[BI^+]$ $[HCO_3^-]$ were measured by removing the solvent via cannula filtration, then washing with MeCN, drying under vacuum, and obtaining the weight.

♦Amounts of $[BI^+]$ $[HCO_3^-]$ were obtained by transferring the reaction solvent to flask containing the TMB standard then removing the solvent under vacuum. Resulting dried products were dissolved in d_6-acetone and quantified via ^{1}H NMR.

As of today, no Re(I) photocatalysts have been reported to produce methane as a CO_2 reduction product in photochemical reactions in literature. A detailed analysis showed that the methane formed largely after the reaction had slowed, presumably due to the build-up of solid $[BI^+]$ $[HCO_3^-]$ in the reaction mixture. Several control experiments were carried out to determine whether the methane produced throughout the reactions originated from CO_2 or from a side reaction involving BIH. The production of methane from the cleavage of one of the methyl groups

on BIH is plausible in these reaction conditions. BIH deuterated at the C_2 position, 1,3-dimethyl-2-phenyl-2,3-dihydro-2-^{2}H-benzo[d]imidazole (**10**, D-BIH), was prepared from 2-phenylbenzimidazole as outlined in *scheme 18* and was used as an isotopically labelled electron donor in a CO_2 reduction reaction.

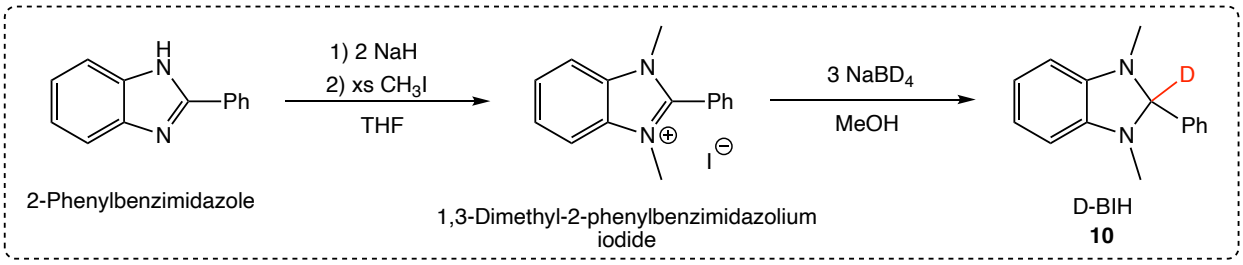

Scheme 18. *Reaction scheme for the synthesis of the deuterated form of D-BIH* ***10*** *from 2-phenylbenzimidazole for isotopic labelling experiments.*

Table 9. *Results from CO_2 reduction reactions with 0.14 mM Re-**9** photocatalyst and 0.1 M BIH or D-BIH in MeCN. Both reactions were quantified with an ethane internal standard and produced CO and CH_4 as reduction products.*

Run	Photocatalyst	BIH/D-BIH	Irradiation Time (h)	TON_{CO}	TON_{CH4}
3-i	Re-**9**	BIH	1.75	30	0
			22.5	40	2
			26	40	2
			45	41	4
			96	52	4
3-i-D	Re-**9**	D-BIH	1.75	22	0
			22.5	28	5
			26	28	5
			45	29	6
			96	36	6

Table 9 summarizes the results from the photocatalytic CO_2 reduction with D-BIH utilizing the isopropyl-NHC catalyst Re-**9**. GC-MS was utilized to determine the extent of deuterium substitution in the d_n-methane product. In theory, if the methane production originated from the reduction of CO_2, it would mostly consist of CD_4 with the deuterium being supplied by the de-deuteronation of the C_2 position of D-BIH (**10**). However, if the methane results from the cleavage of a methyl group on BIH, then CH_3D would be the major form of methane produced. Two

identical CO_2 reduction reactions were run at the same time, one with BIH and another with the D-BIH at the same concentrations. GC-TCD was used to monitor the progress of the reaction and quantify the reduction products. Both CO and methane were obtained, and GC-MS was used to analyze the methane produced (*figure 25*). The EI-MS spectrum of the methane produced by the CO_2 photoreduction with BIH shows that, as expected, CH_4 is the major isotopomer, as confirmed by injecting an authentic sample. In comparison, the CO_2 reduction reaction with D-BIH yielded an array of CH_nD_{4-n} isotopomers, with the major being CH_3D. Very little CD_4, if any, was detected in the product methane. The exact ratios of the isotopomers were not determined because control mixtures of the isotopomers were unavailable. The lack of higher isotopomers in the methane product during the photocatalytic CO_2 reduction with D-BIH is a strong indicator that the methane is not produced by reduction of CO_2.

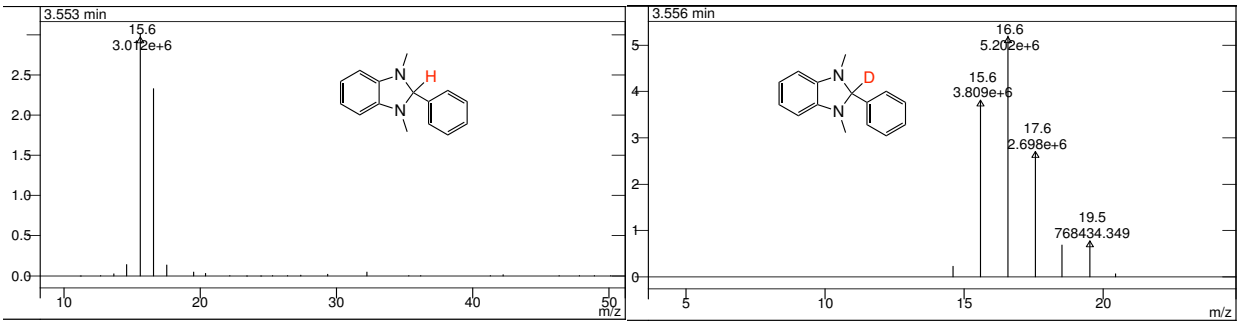

Figure 25. *Comparison of the GC-MS spectrum of the CH_4 gas produced by the CO_2 reduction reaction with the Re-**9** photocatalyst with BIH (left) and D-BIH (right). The y-axis units are mega counts per second (MCps) for both spectra. The GC-MS of CH_4 was confirmed by comparison to an authentic sample.*

$^{13}CO_2$ labelling experiments are applied often in literature to confirm the origin of CO_2 reduction products. A major downside of these isotope experiments is the very high cost associated with $^{13}CO_2$. At Sigma Aldrich, a lecture cylinder of 99% $^{13}CO_2$ containing 1 litre of gas costs $460 CAD at the time of this writing. A photocatalytic $^{13}CO_2$ reduction was carried out with the Re-**9** photocatalyst by first flushing the reaction solution with CO_2 as usual then with $^{13}CO_2$ for 10 minutes (*table 10*). The reaction was monitored with GC-TCD to observe the distribution of

reaction products. This reaction produced a surprisingly small amount of CO and a relatively large amount of methane, a result that differed from all identical reactions carried out under the same conditions with $^{12}CO_2$. The reasons for the difference in behaviour were not determined, but likely involve catalyst decomposition by adventitious water, air, or some other contaminant in the $^{13}CO_2$. It is noteworthy, however, that GC-MS analysis showed that little, if any, $^{13}CH_4$ was formed by the reaction (*figure 26*), demonstrating that there is another pathway to methane formation.

Table 10. *Results from the $^{13}CO_2$ reduction reaction with 0.14 mM Re-**9** photocatalyst and 0.1 M BIH in MeCN. The TON_{CO} and TON_{CH4} were quantified with an ethane internal standard.*

Exp	Photocatalyst	Irradiation Time (h)	TON_{CO}	TON_{CH4}
8-3	Re-**9**	1	0	0
		2	0	0
		27	0	31
		43	22	35

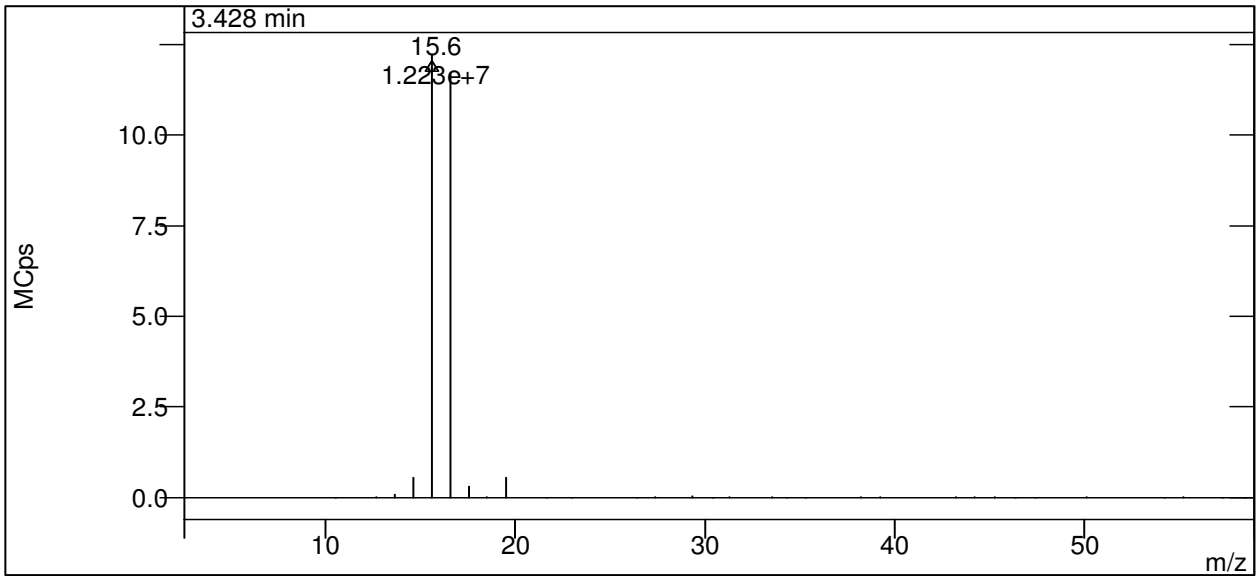

Figure 26. *GC-MS spectrum of the CH_4 gas produced by the $^{13}CO_2$ reduction reaction with the Re-**9** photocatalyst and BIH as sacrificial electron donor.*

In a final attempt to confirm that the methane is produced from the cleavage of a methyl group on BIH, the demethylated form of BI^+ was synthesized. 1-Methyl-2-benzimidazole (**12**) was prepared and analyzed via NMR to potentially identify the same compound in the CO_2 reduction solvent following a reaction that produces methane (*figure 27*). While the product was synthesized

successfully, its purification was challenging due to the presence of starting material, 2-phenylbenzimidazole. The starting material peaks were easy to identify and disregard so the purification of the desired product was not prioritized. A major drawback in attempting to identify 1-methyl-2-phenylbenzimidazole in the NMR spectrum of the reaction solvent is that it is present in very minor quantities. The de-methylated BI^+ would be present in the solution in amounts proportional to the quantity of methane produced, compared to BIH which is present is significantly larger quantities. For example, the largest volume of methane produced in a CO_2 reduction reaction with Re-**9** was 3.88×10^{-6} mol of CH_4, giving 9 TON_{CH4}. If the methane is originating from the cleavage of a methyl group on BIH, then the resulting 1-methyl-2-phenylbenzimidazole product would also be in the solution in the same amount, 3.88×10^{-6} mol. Compared to the much higher quantities of BI^+ and BIH in solution, it was extremely challenging to identify protons peaks associated with this compound in solution. While there were extremely minor peaks that could potentially be attributed to this compound in solution, the results from this analysis remain inconclusive. Combined, the results from the D-BIH experiments and the $^{13}CO_2$ reduction are coherent and, taken together, indicate somewhat conclusively that the methane produced from these reaction does not result from the reduction of CO_2.

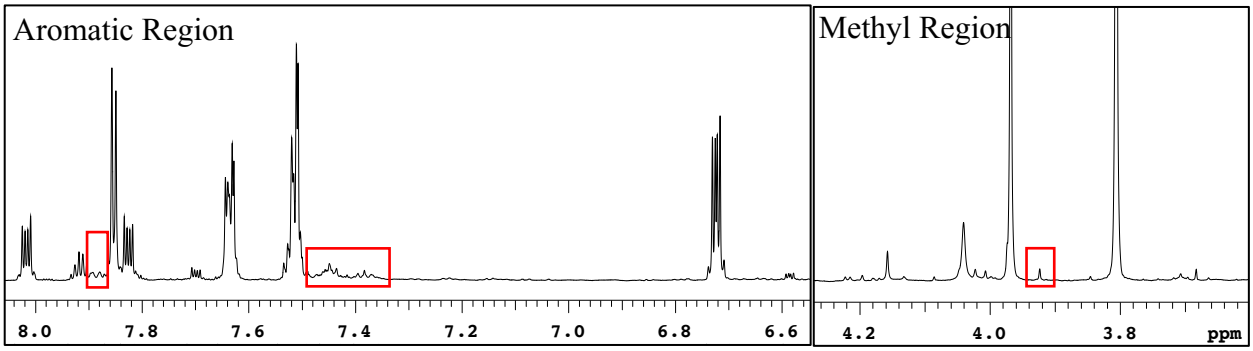

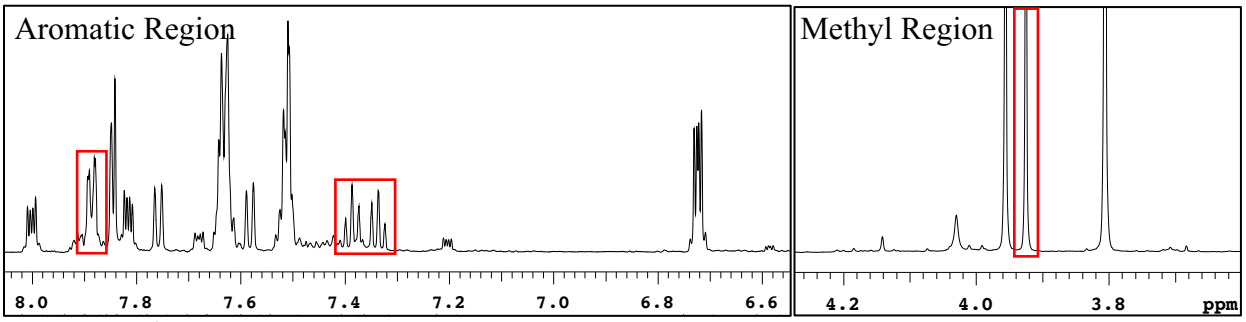

Figure 27. *^{1}H NMR spectrum of the reaction solvent following CO_2 reduction reaction containing the TMB internal standard alone (top) and with 1-methyl-2-phenylbenzimidazole added (bottom) in d_6-acetone. Potential peaks corresponding to the de-methylated BI^+ product in the CO_2 reduction solvent are indicated by red boxes.*

Photoluminescence data were collected to gain insight into the photochemical properties of Re-**2** and Re-**9**. Stern-Volmer (SV) plots were constructed by measuring the maximum emission intensity for the photocatalysts in the presence of varying BIH concentrations. *Figure 28A* and *figure 28B* show the SV plots for Re-**2** and Re-**9**, respectively. In these systems, BIH acts as the sacrificial electron donor that quenches the T_1 excited state of the organic dye that is physically linked to the catalyst. Identical trends were observed for both photocatalysts, with higher [BIH] resulting in increased quenching of the excited state represented by the decrease in intensity. Both Stern-Volmer plots demonstrated a linear relationship between [BIH] and I_0/I of the emission spectrum, where I_0 is the emission intensity in the absence of BIH, and I is the emission intensity of the sample (*figure 29*). Both photocatalysts showed linear relationships as [BIH] increased with the Re-**2** plot having a slope approximately 5x larger than the Re-**9** photocatalyst (0.1758 vs 0.0354).

The Stokes shifts for Re-**2** and Re-**9** were measured by comparing the excitation and emission spectra in MeCN and DCM (*table 11*). The Stokes shift for the imidazole-dye complex Re-**2** complex was 170 nm in MeCN and 110 nm in DCM (*figure 30A*). The increase in Stokes shift is interpreted as the stability of the charge-separated excited state being high in more solvent,

such as MeCN. The difference in Stokes shift of the isopropyl-NHC-dye complex Re-**9** behaved similarly, being 190 nm in MeCN and 170 nm in DCM (*figure 30B*).

Table 11. *Summary of the photoluminescence data collected for the Re-**2** and Re-**9** photocatalysts, and their calculated Stokes shifts compared to the corresponding free dyes.*

	DCM			MeCN		
	Excitation (nm)	Emission (nm)	Stokes shift (nm)	Excitation (nm)	Emission (nm)	Stokes shift (nm)
Re-**2**	440	550	110	400	570	170
2	400	545	145	400	570	170
Re-**9**	400	570	170	400	590	190
4	400	570	170	400	590	190

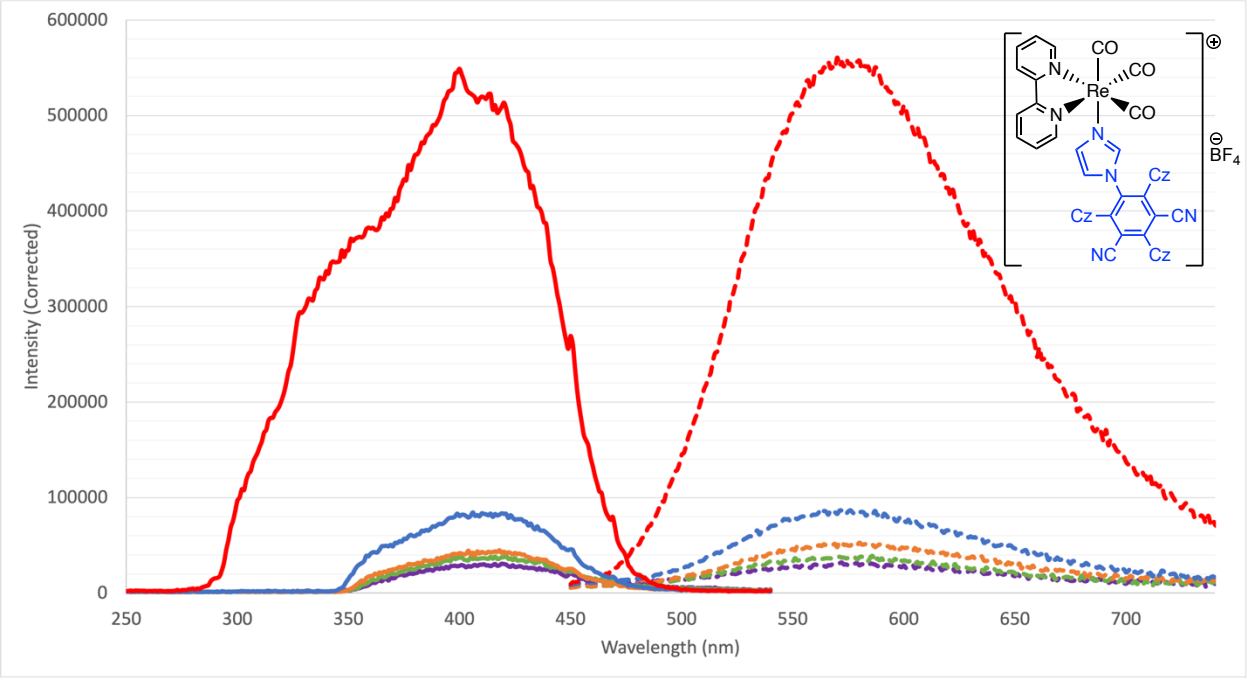

Figure 28A. *Excitation and emission spectrum of Re-**2** with varying amounts of BIH. Excitation data is marked by solid lines on the left and emission data is indicated by dashed lines on the right. The concentrations of BIH are: 0 mM (red), 25 mM (blue), 50 mM (orange), 75 mM (green) and 100 mM (purple).*

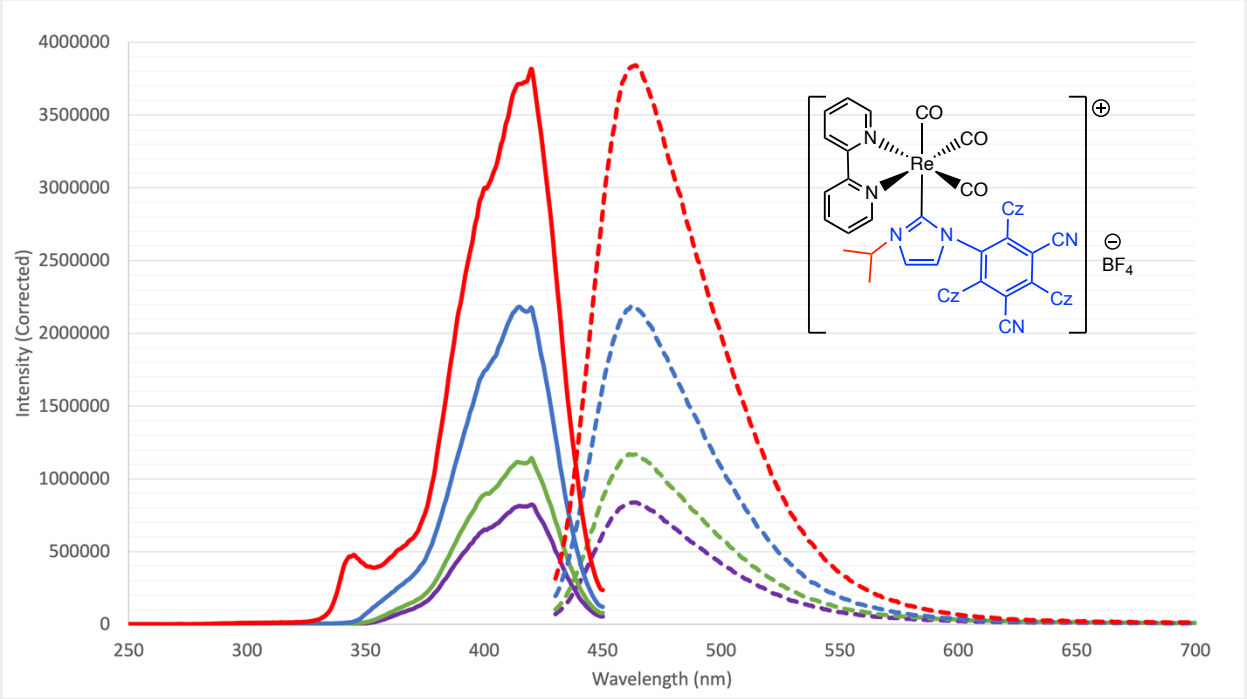

Figure 28B. *Excitation and emission spectrum of Re-**9** with varying amounts of BIH. Excitation data is marked by solid lines on the left and emission data is indicated by dashed lines on the right. The concentrations of BIH are: 0 mM (red), 25 mM (blue), 75 mM (green) and 100 mM (purple).*

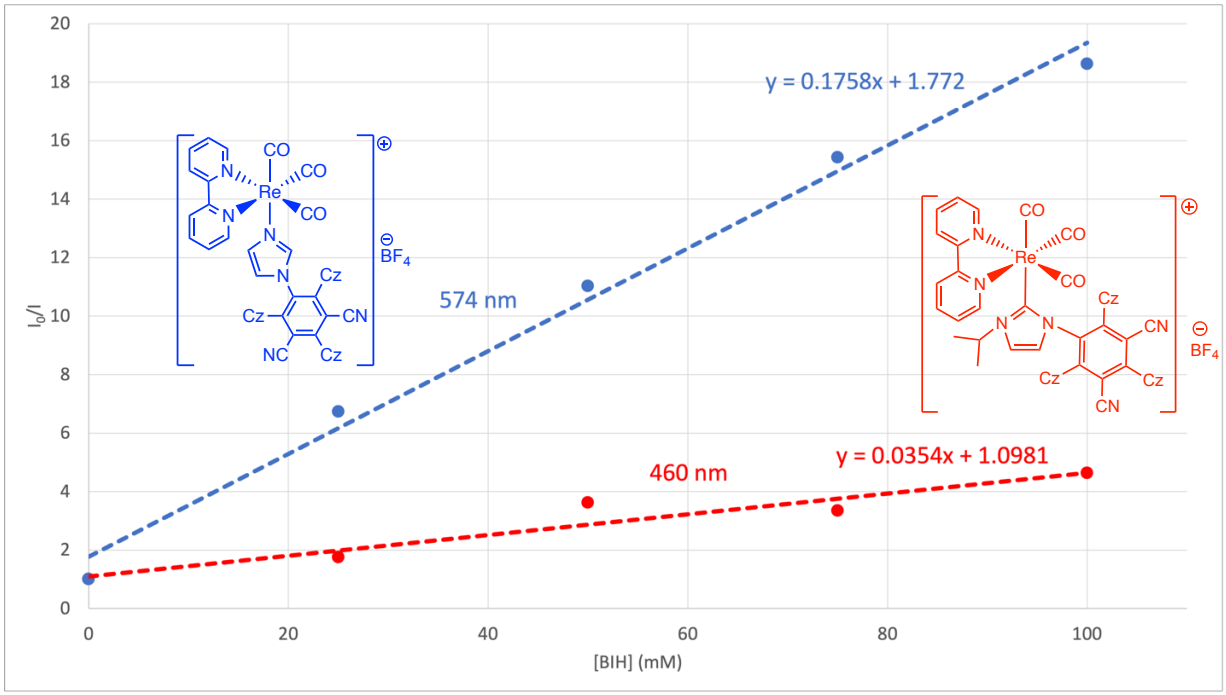

Figure 29. *Stern-Volmer plot depicting I_0/I of Re-**2** (blue) and Re-**9** (red) with varying [BIH] (mM). The y-values were calculated by dividing the emission intensity at 574 and 460 nm, respectively, of all five samples by the emission intensity of the 0 mM [BIH] sample. The concentrations of BIH included are: 0, 25, 50, 75 and 100 mM. The resulting SV plots demonstrate a linear relationship marked by the dotted trendlines.*

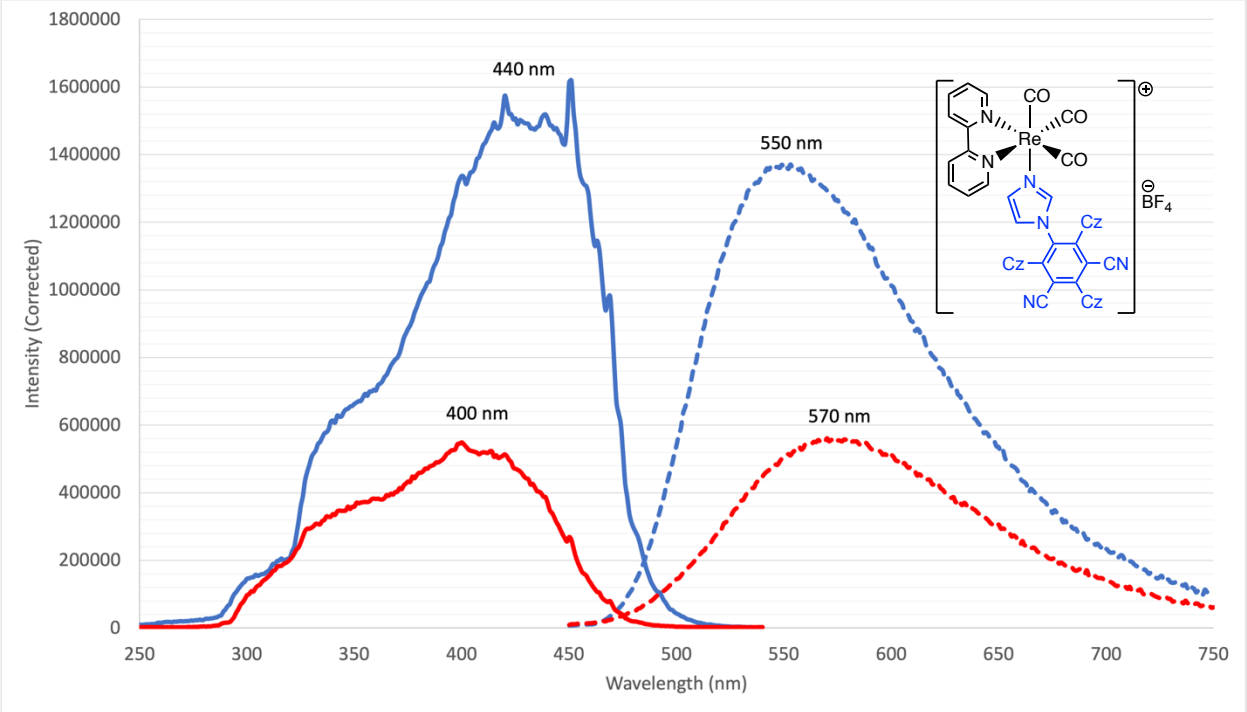

Figure 30A. *Excitation and emission spectra of the Re-**2** photocatalyst in MeCN (red) and DCM (blue) depicting the Stokes shift of the complex. Excitation data is marked by solid lines on the left and emission data is indicated by dashed lines on the right.*

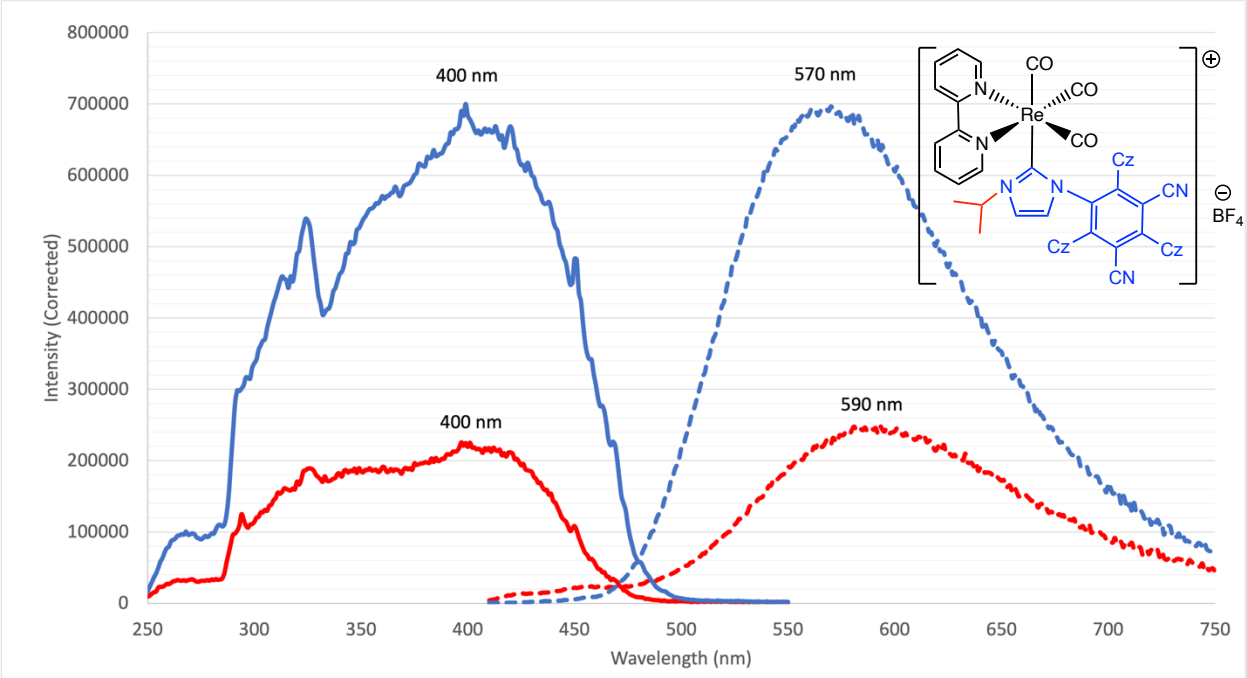

Figure 30B. *Excitation and emission spectra of the Re-**9** photocatalyst with 0.1 M BIH in MeCN (red) and DCM (blue) depicting the Stokes shift of the complex. Excitation data is marked by solid lines on the left and emission data is indicated by dashed lines on the right.*

4.2 DISCUSSION

The principal objective of this project was to covalently link various organic dyes to a Re(I) catalyst and evaluate the resulting photocatalysts in the photochemical reduction of CO_2. Physically linking the organic dye PS to the *fac*-Re(bpy)$(CO)_3$Cl catalyst allows intramolecular electron transfer that reduces the catalyst upon excitation of the PS. Intramolecular electron transfer can occur through the bridging imidazole group or perhaps through non-bonding interactions between the dicyanobenzene-carbazole ring and the Re moiety. Solar energy is an ecologically clean and abundant energy source that is approximately 40% visible light in composition.[124] For this reason, the development of CO_2 photoreduction systems that are driven by entirely visible light is desirable and one of the main objectives of this work. Accordingly, an AM 1.5G solar light simulator with both UV and IR light filters was utilized for the CO_2 reduction reactions with the Re(I) photocatalysts in this study.

As mentioned previously, all three photocatalysts reproducibly carried out the photocatalytic reduction of CO_2 with BIH as sacrificial electron donor. All the CO_2 photoreduction reactions proceeded with an initial burst of reaction followed by a slowdown. A white solid formed that consisted of a mixture containing $[BI^+]$ $[HCO_3^-]$ and unknown aromatic compounds. It appears that the solid slowed the reaction by blocking or reflecting the incident light. The average TOF_{CO} during the initial burst stage of the photoreduction, before any appreciable slowdown, were 8.75 h^{-1} for the imidazole-dye complex Re-**2**, 46.5 h^{-1} for the benzyl-NHC-dye complex Re-**8**, and 14 h^{-1} for the isopropyl-NHC-dye complex Re-**9**. The benzyl-NHC complex Re-**9** was by far the most active, likely because of the strong σ-donating ability of the NHC ligand moiety, and steric hindrance that matched the requirements of the photocatalytic CO_2 photoreduction. The initial

TOF_{CO} of the imidazole-dye photocatalyst Re-**2** and the isopropyl-NHC-dye photocatalyst Re-**9** were similar.

In addition to CO, small amounts of methane formed after the CO_2 photoreduction slowed. The production of methane was unexpected as no Re(I) photocatalysts have been reported to produce methane from the reduction of CO_2. Methane was also not observed in any photoreductions carried out with the catalyst and PS separate in solution in early screening reactions, suggesting that covalently bonding the catalyst and dye changed their activities.

While the gaseous CO_2 reduction products were quantified and monitored throughout the reaction, the solution-phase and solid products were quantified by ^{1}H NMR spectroscopy with an added internal standard after the photoreduction was complete. These experiments were carried out with the isopropyl-NHC-dye complex Re-**9**. Surprisingly, the amount of BIH consumed should be, in theory, stoichiometrically equivalent to the amount of CO produced, indicating the presence of additional reactions in the system (*scheme 19*). The amounts of BI^+ formed were less (~ 76%) than the amount of BIH consumed. Further, there were substantial amounts of unidentified aromatic molecules present in the solid that precipitated out of the reaction. Finally, definitive peaks for soluble CO_2 reduction products including methanol, formaldehyde (paraformaldehyde), methyl formate and formic acid could not be found in the ^{1}H NMR spectra of the reaction mixture recorded with solvent suppression after the photocatalytic reduction of CO_2 was complete. Although small amounts of methane formed after the CO_2 photoreduction slowed, the amounts were too small to account for the large excess of BIH consumed and BI^+ formed. Taken together, these results show that BIH, BI^+ or perhaps some intermediate undergoes substantive amounts of unidentified reactions to form new aromatic species. While these species were not identified, it is quite evident that BIH is not simply acting as a 2-electron, 1-proton sacrificial donor. The system

is more complex than this simplistic assertation. There are no reports of the quantification of BIH/BI^+ in literature at the time of this writing. The presence of additional side reactions involving BIH shows that the amount of CO produced is the lower limit of the Re(I) photocatalysts, as there was competition with the side reactions of BIH. No further effort was expanded on determining the nature of the side reactions of the sacrificial electron donor because ultimately it is a dead-end. The ultimate source of electrons for CO_2 photoreduction must come from the oxygen evolution reaction (*scheme 20*) that will be discussed further in the future direction section.

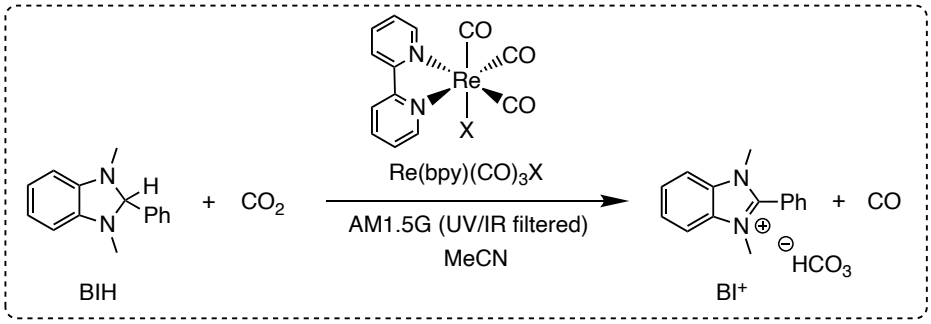

Scheme 19. *Reaction scheme for the reduction of CO_2 to CO by the Re(bpy)(CO)$_3$X photocatalysts. The quantity of BIH consumed, BI^+ formed and CO formed are all stoichiometrically equivalent.*

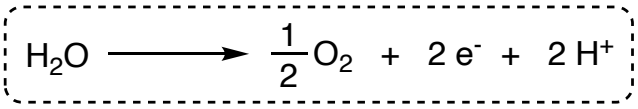

Scheme 20. *Water oxidation half-reaction.*

Several experiments were carried out to investigate the origin(s) of methane in these reactions. The utilization of $^{13}CO_2$ in a trial reaction did not generate appreciable amounts of CO, likely because of adventitious O_2, H_2O, or some other contaminant. The reaction did, however, produce significant amounts of methane (35 TON_{CH4}). GC-MS showed little, if any, ^{13}C was present in the methane, indicating that a pathway besides CO_2 reduction can generate methane in this system. This observation strongly suggests that the production of CO is unrelated to the production of methane under these conditions. Another labelling experiment utilizing D-BIH produced CH_3D and CH_2D_2 as major methane isotopomers with little, if any, CD_4. Any formation

of methane from reduction of CO_2 would involve protons from BIH (*scheme 21*). The absence of higher D-labelled isotopomers of methane is strong evidence that the methane is generated as a side reaction of BIH chemistry.

A recent paper by Wang et al.[125] that studied fluorosulfonylating methods via radical reaction pathways of sulfonyl fluoride imidazolium salts supports the proposed mechanism for the production of methane via cleavage of a methyl group originally in BIH in a radical-chain process outlined in *scheme 21.* Oxidation with deprotonation of BIH generates BI^+, which accumulates in solution as the reduction of CO_2 to CO proceeds. Once a certain [BI^+] is reached, BI^+ begins to compete with CO_2 for electrons from the excited PS on the photocatalyst. A one-electron reduction of BI^+ forms the neutral radical **11** that then undergoes homolytic cleavage of a N-methyl bond to generate the methyl radical and 1-methyl-2-phenylbenzimidazole (**12**). Abstraction of a hydrogen atom from another molecule of BIH in solution forms methane and regenerates the neutral radical **11**, and so on. With this mechanism, the formation of methane and de-methylation of BI^+ molecules depend initially on the formation of CO until BI^+ accumulates in solution. This explains the delay in methane production until at least 20 hours following the start of the reaction when CO has been produced sufficiently. This side reaction is likely completely unrelated to the CO_2 reduction and commences after enough BI^+ is formed. As a result, the TON_{CO} and TON_{CH4} are unrelated in this process which was observed in a majority of the CO_2 reduction reactions carried out. The radical chain nature of the proposed mechanism predicts that only a few events of electron transfer from the excited PS to BI^+ are required to initiate the chain reactions.

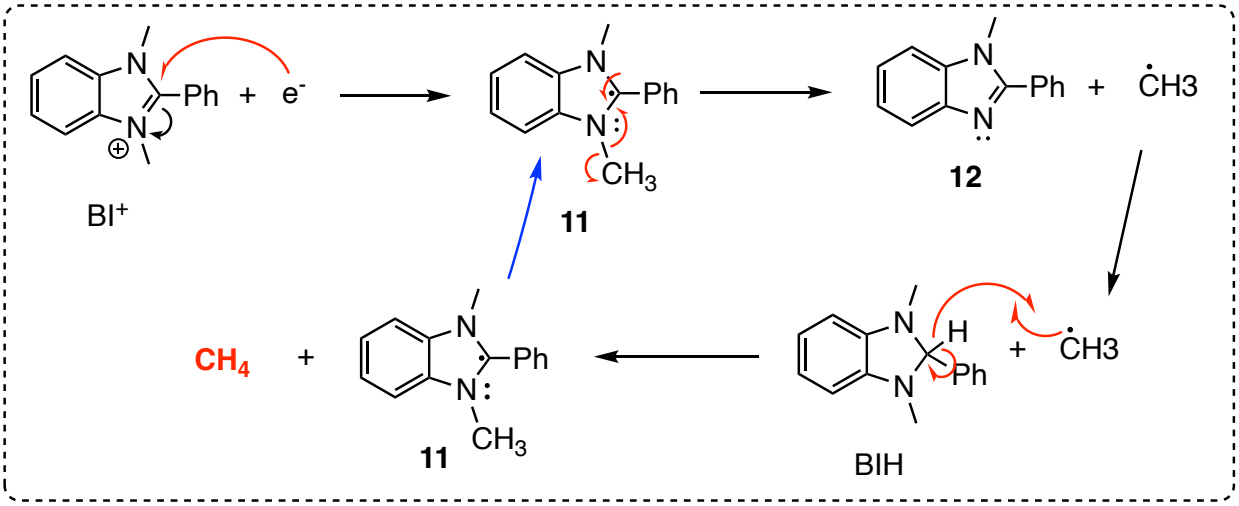

Scheme 21. *Overview of the radical reaction process that yields CH_4 under CO_2 reduction reaction by cleavage of a methyl group on BIH. BI^+ first accepts an electron from the excited PS to generate a radical $BI^\bullet$ species **11** that can undergo a radical reaction to generate 1-methyl-2-phenylbenzimidazole **12** and a methyl radical. The reaction between the methyl radical and another BIH molecule in solution generates a new $BI^\bullet$ species **11** that can continue the reaction chain (shown by the blue arrow).*

The cleavage of a N–Me bond by this process would eventually yield 1-methyl-2-phenylbenzimidazole (**12**, *scheme 21*). Unfortunately, since only small amounts of methane are produced during the photocatalytic reduction of CO_2, **12** could not be conclusively identified in the NMR spectra of the reaction mixture because of significant overlap with the other compounds in solution, even upon the addition of 1-methyl-2-phenylbenzimidazole, which was independently synthesized for this study. Some small peaks in the ^{1}H NMR spectrum of the reaction mixture overlapped with those for the added 1-methyl-2-phenylbenzimidazole (**12**), but the number of overlapping peaks was not sufficient to conclusively identify **12** as a side product of methane formation (*figure 27*).

The production of methane via this process was observed for all three Re(I) photocatalysts, whereas no methane was produced in CO_2 reduction reactions with the separated components. The observation of methane has also not been reported in the literature during photocatalytic reactions with BIH as a sacrificial electron donor. This observation suggests that Re complexes of the

imidazole-, and especially the NHC-derivatives have lower redox potentials (are more reducing) than the other systems. Further investigations regarding the nature of this process and the electron-donating ability of these complexes must be carried out to investigate these propositions.

The construction of Stern-Volmer (SV) plots for both the Re-**2** and Re-**9** photocatalysts revealed information regarding the quenching process that occurs throughout the CO_2 reduction reaction. Both photocatalysts demonstrated a linear relationship between I_0/I and [BIH], indicating that collisional quenching is likely occurring. A linear SV plot is indicative of a collisional quenching in which the quencher, BIH, diffuses to the photocatalyst during the lifetime of the excited state and returns the photocatalyst to ground state without emission of a photon upon contact.[126] The linear SV plot could also indicate static quenching between BIH and the photocatalyst in which a non-fluorescent ground state complex is formed between the photocatalyst and the quencher.[126] However, due to the mechanism and nature of these complexes, it is likely collisional quenching that is occurring. The SV equation (*equation 1*) was used to determine the SV constant K_{SV} for both photocatalysts from their respective SV plot. In this case, K_{SV} is equivalent to the slope of the linear trendline which is 0.1758 and 0.0354 mol^{-1} L for Re-**2** and Re-**9**, respectively. The value of K_{SV} is indicative of the availability of the quencher to the excited molecule/fluorophore, therefore an increase in value corresponds to a reduction of the distance between the two components.[127] The K_{SV} of the Re-**2** photocatalyst is about 5x higher than the K_{SV} of Re-**9**, meaning BIH is closer in location to Re-**2**.

$$\frac{I_f^\circ}{I_f} = 1 + K_q\tau_0[Q] \qquad \text{where } K_q\tau_0 = K_{SV}$$

$$\frac{I_f^\circ}{I_f} = 1 + K_{SV}[Q] \qquad (\textit{Equation 1})$$

The rate of diffusion in the two systems should be similar as both SV plots were derived under similar conditions, with the same quencher and solvent mixture. The large difference in K_{SV}

between the photocatalysts indicates that the quenching process may be unrelated to the rate of diffusion and linked with intrinsic electron transfer processes between the compounds. Many calculations would be required for a thorough analysis of these processes; however, we can conclude that the quenching mechanism is not diffusion limited for these systems.

Both the Re-**2** and Re-**9** complexes demonstrated a larger Stokes shift in MeCN compared to DCM. As mentioned previously, polar solvents result in increased Stokes shifts due to solvent stabilization and relaxation, explaining these observations. Additionally, the Stokes shift of the photocatalysts were similar to that of the corresponding free dyes, with only the Re-**2** in DCM solution (110 nm) demonstrating a smaller value compared to the DCM solution of compound **2** (145 nm). The other values were identical in the free dye and the photocatalyst.

The mechanism of the reduction of CO_2 with Re(I) catalysts has been debated in literature. The Re(I) photocatalyst is first exposed to visible light where an electron transfer excitation process is initiated (*scheme 22*). The PS moiety absorbs a photon and gets promoted to its excited state where an electron is transferred from the nitrogen atom on a carbazole group into the dicyanobenzene ring. The presence of the dicyano groups on the benzene ring help to stabilize the excited state, allowing for electron transfer reactions to occur. The electron is then transferred to the Re metal centre, generating a Re(0) species. The excited PS moiety then receives an electron from BIH, the electron donor, in the reductive quenching process (*scheme 23*), returning it back to ground state. This process is repeated once again to transfer a second electron to the Re metal centre, generating a Re(–1) species. Both electrons transferred to the catalyst are placed in the antibonding orbitals which contribute to weakening the Re-CO bond and promote the dissociation of the CO ligand. The dissociation of CO generates a low-valent, unsaturated metal complex that can interact with CO_2 in the reaction atmosphere and reduce it to CO. The order of the steps are

heavily debated in literature with some arguing that the Re(0) complex first interacts with CO_2 then accepts a second electron from BIH to then reduce it to CO.

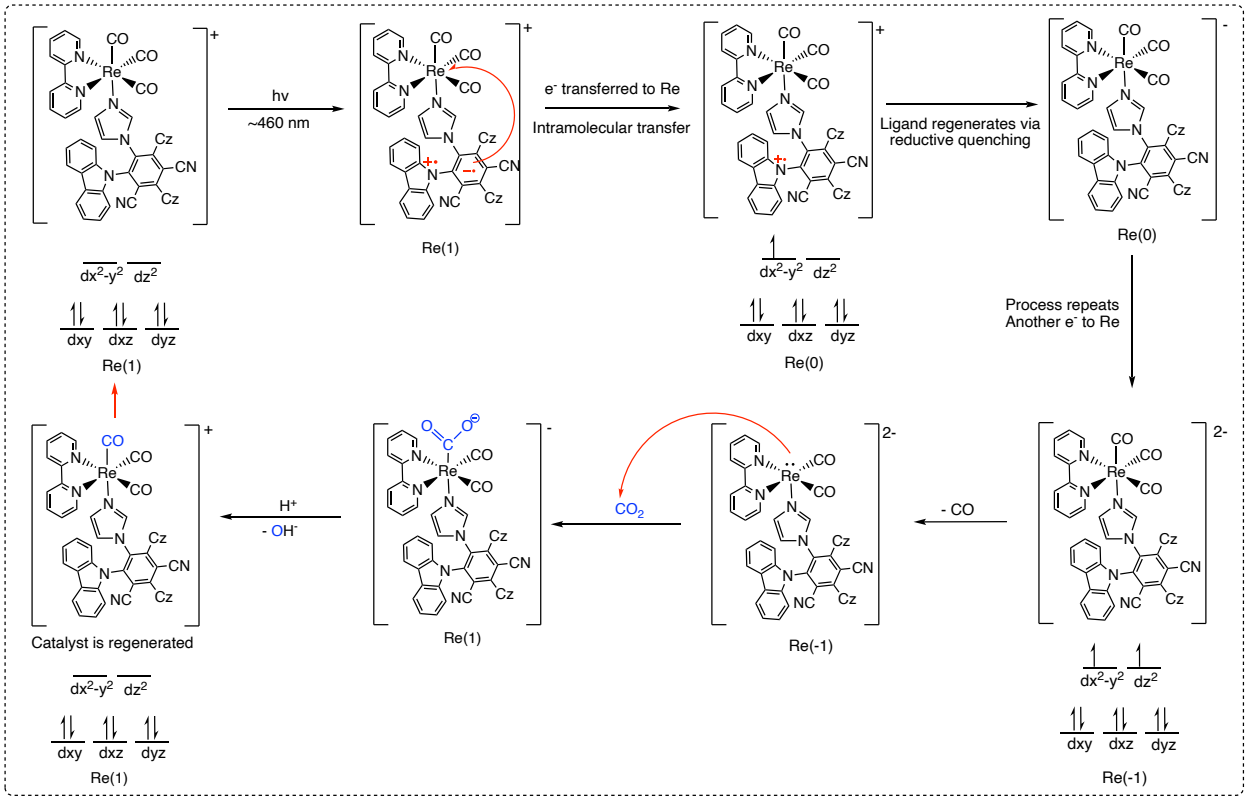

Scheme 22. *Postulated mechanism for the CO_2 reduction to CO catalyzed by the Re-**2** photocatalyst. The same mechanism applies to the Re-NHC photocatalysts. The Re(I) photocatalyst is regenerated in the final step and can re-enter the catalytic cycle, as indicated by the red arrow.*

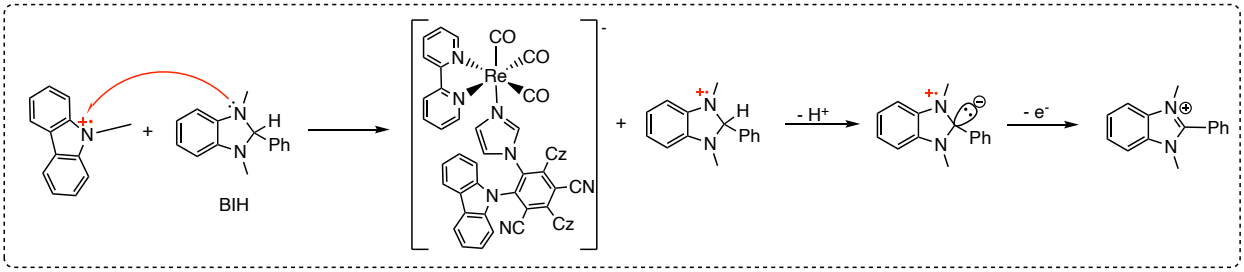

Scheme 23. *Reductive quenching of the excited photocatalyst by BIH following the electron transfer to the Re metal centre.*

4.3 CONCLUSION

In sum, all three photocatalysts were successful for the reduction of CO_2 to CO driven by visible light. The unexpected presence of methane in these reactions was studied and found to originate from the cleavage of a methyl group on BIH via isotopic labelling studies. The SV plots for the Re-**2** and Re-**9** were obtained and revealed information regarding the quenching mechanism throughout the reaction. Finally, the mechanism through which these photocatalysts catalyze the reduction of CO_2 was hypothesized. Additional experiments with the Re-**8** photocatalyst should be carried out, specifically photoluminescence experiments, and the synthesis of Re-**9** in d_8-THF to obtain high-quality characterization data such as ^1H and ^{13}C NMR spectra should also be achieved. The radical reaction pathway that generates methane should also be explored in further detail, including the amount of BI^+ required to initiate the reaction chain, the competition between BI^+ and the photocatalyst for accepting electrons from the excited PS moiety and the impact of this process on the catalytic cycle of the reduction of CO_2 to CO.

5 – FUTURE DIRECTIONS

Over the course of this project, three novel CDCB-based organic dyes were successfully prepared and linked to a *fac*-Re(bpy)$(CO)_3Cl$ catalyst to generate Re(I) photocatalysts for the photochemical reduction of CO_2 to CO. These photocatalysts operated under purely visible light with BIH as the sacrificial electron donor in solution. The development of these photochemical systems remains relatively incomplete and there are several experiments that must be completed. The Re-**9** photocatalyst should be prepared in d_8-THF to obtain high quality ^1H and ^{13}C NMR spectra and photoluminescence data must be collected for Re-**8**. Both Re-NHC photocatalysts have yet to be isolated and require further characterization, such as MS and NMR correlation experiments. Improvements to the preparation of the Re-NHC photocatalysts must also be achieved to successfully isolate these complexes. The $^{13}CO_2$ reduction experiment should be repeated with the each photocatalyst to successfully identify ^{13}CO and $^{12}CH_4$ in the reaction and undeniably confirm the theories proposed in this dissertation. Additionally, the CO_2 reduction reactions should be attempted with a different sacrificial electron donor. The absence of BIH would likely prevent the radical side reaction that leads to methane production, as well as the accumulation of BI^+ in solution that contributes to shutting the reaction down. Without these elements present in the reaction, a higher production of CO could occur and the effect on the TON_{CO} could be examined. Finally, the oxidizing potential of both the Re photocatalysts and BI^+ under these conditions should be investigated to evaluate whether BI^+ accepts electrons from the excited PS over the Re metal centre which leads to the radical cleavage of a methyl group.

Long-term objectives for this work include the development of Mn(I) photocatalysts based on these Re(I) photocatalysts and the application of these systems towards heterogeneous electrochemical CO_2 reduction with visible light. The Mn analogs of these photocatalysts, Mn-**2**,

Mn-**8**, and Mn-**9**, have begun developing within the group and show similar activity towards the photochemical reduction of CO_2 to CO. Manganese is an earth-abundant metal and is significantly less costly than rhenium. Rhenium is one of the rarest elements on Earth, with an abundance of less than 1 part-per-billion (ppb) in the continental crust according to the United States Geological Survey (USGS).[128] On the contrary, manganese is the 5th most abundant metal in the Earth's crust making it significantly cheaper.[129] On Sigma Aldrich, 5 g of Re powder (99.995% trace metals basis) is available for $546 CAD compared to 25 g of Mn powder (99.9% trace metals basis) available for $124 CAD. As a result, the conversion of Re-based systems to Mn-based systems is extremely desirable due to the economic and sustainability advantages. Exploratory electrochemical experiments have begun within the group to directly translate the homogeneous results to heterogeneous systems. The organic dyes have been shown to easily polymerize on ITO and carbon via electropolymerization of the carbazole groups on the dicyanobenzene ring. The polymerization of both the Re(I) and Mn(I) photocatalysts on ITO and carbon via this process would allow for the direct translation of these systems to heterogeneous applications. A new project within the group involves the direct electropolymerization of the analogous Mn(I) photocatalysts onto carbon and ITO electrodes for the electrochemical reduction of CO_2 with visible light (*scheme 23*). In electrochemical CO_2 reduction systems, the electrons are supplied to the catalyst by the electrodes which results in a faster electron injection rate. As well, this allows for the complete elimination of the sacrificial electron donor, BIH, and its perplexing nature. The elimination of BIH could potentially lead to increased activity due to the absence of any side reactions or the formation of products that decrease activity and the faster injection speed.

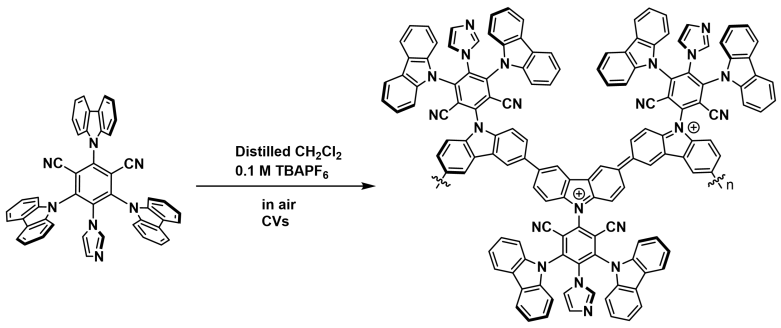

Scheme 23. *Electropolymerization of 3CzIPN imidazole (**2**) in air. This figure was taken from a recently published paper by another member of the group.*[130]

The ultimate goal of this work is to develop a fuel cell that reduces CO_2 and oxidizes H_2 to produce energy in a closed system (*figure 31*). H_2-CO_2 fuel cells are promising technologies that help promote the use of CCS strategies to reduce atmospheric CO_2 levels on the planet. In these technologies, H_2 produced by HER is oxidized to H^+ ions that can reduce CO_2 to CH_4. This work has focused specifically on the reduction of CO_2 while other areas within the group are focused on H_2 evolution catalysts. Some groups have successfully used this technology for the development of CO_2/H_2 fuel cells that can reduce CO_2 while also generating electricity.[131,132] Technologies that are capable of reduction of atmospheric CO_2 while also producing useable electricity present numerous attractive features that could help solve the current global environmental crisis resulting from the excess build-up of CO_2 in the Earth's atmosphere.

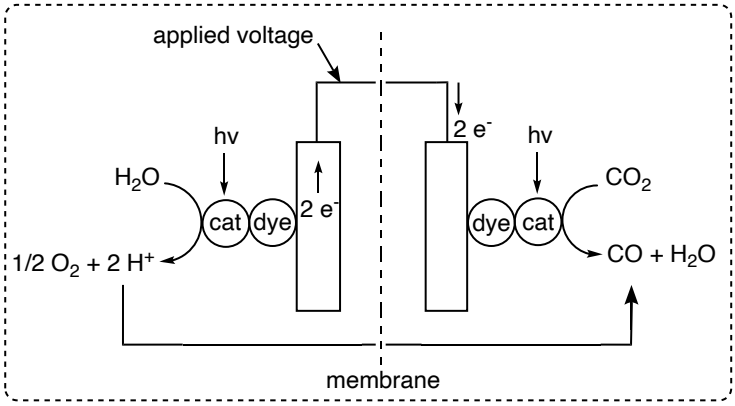

Figure 31. *Schematic depiction of the photocatalytic/electrocatalytic cell involving the reduction of CO_2 and oxidation of water. The absence of an applied voltage renders the system photocatalytic whereas the presence of an applied voltage renders it electrocatalytic.*

6 – EXPERIMENTAL

6.1 MATERIALS.

Chemicals were used without any further treatment unless mentioned otherwise. All solvents were distilled for air and moisture sensitive reactions. The following chemicals were obtained from Sigma Aldrich: carbazole (≥ 95 %), sodium hydride (60 % oil suspension, THF washed, dried), potassium tert-butoxide (95 %), potassium hydride (from 60% oil suspension, THF washed, dried), silver tetrafluoroborate (99 %), sodium borodeuteride (98% atom D, 90% CP), cesium carbonate (99 %), 2-phenylbenzimidazole (97 %), 2-iodopropane (with copper stabilizer, 99 %), 1,3,5-trimethoxybenzene (99 %), benzyl bromide (98 %), iodomethane (with copper stabilizer, 99 %), $^{13}CO_2$ (99 %), pentacarbonylchlororhenium(I) (98%). The following chemicals were obtained from Fischer Chemical: anhydrous ethyl ether (ACS reagent), sodium chloride (ACS reagent, crystalline), ammonium chloride (ACS reagent, crystalline), hexanes (ACS reagent), acetonitrile (HPLC grade, ≥ 99.9 %), dichloromethane (ACS reagent, ≥ 99.5 %), ethyl acetate (ACS reagent), methanol (ACS reagent), toluene (ACS reagent), acetone (HPLC grade), tetrahydrofuran (ACS reagent, ≥ 99.0 %), potassium dichromate (ACS reagent, crystalline), anhydrous magnesium sulfate. Tetrafluoroisophthalonitrile (> 98.0%) was purchased from TCI Chemicals. Imidazole was purchased from Baker. 2,2'-Dipyridyl was obtained from Terochem Laboratories. 1,3-Dimethyl-2-phenyl-2,3-dihydro-1H-benzimidazole (97%) was purchased from Ambeed. The following compressed gases were purchased from Linde Canada: CO_2, ethane (99%), methane. Acetone-d_6 was obtained from Cambridge Isotope Laboratories (D 99.9%).

6.2 INSTRUMENTATION.

^{1}H NMR spectra were collected using 400, 500, 600 and 700 MHz Agilent Inova spectrometers. ^{13}C NMR spectra were collected using 500 and 700 MHz Agilent Inova spectrometers. Photoluminescence spectra were collected using a Horiba-PTI QM-8075-11 Fluorescence System. Gas chromatography was carried out with an HP 6890 series GC system equipped with a thermal conductivity detector (TCD) and a Restek micropacked shincarbon column (st, 2m x 1mm, 1/16' OD,100/120 mesh, RK19809). HRMS data were collected on Agilent Technologies 6220 orthogonal acceleration TOF (oaTOF) instrument. FTIR data were collected on a Thermo Nicolet 8700 FTIR spectrometer. Isotopic labelling studies were carried out on a Bruker Scion 456-GC-TQ GC-MS instrument equipped with an Agilent fused silica capillary column (HP-Plot/Q, 30 m x 0.32 mm i.d., 0.2 μm film thickness). The MS spectrometer was operated in electron-impact (EI) mode.

6.3 CALIBRATION CURVES

Methane-CO calibration curve. Acetonitrile (3.000 mL, 57.44 mmol) was transferred to small test tube (15 x 125 mm) equipped with a stir bar and rubber septum with a 5 mL syringe and needle. The solution was bubbled with CO_2 for 10 minutes with an ice bath followed by 5 minutes at room temperature. Methane gas (20 µL) was added to the test tube with a 50 µL syringe after purging the syringe 4 times. Carbon monoxide gas was added to the test tube in varying amounts (0–500 µL) with a 50 µL syringe after purging the syringe 4 times. Gases were allowed to equilibrate for 15 minutes prior to injecting 100 µL of the test tube headspace into the GC-TCD. The peak area ratios were calculated by manual integration to develop a calibration curve. Duplicate injections were carried out for each volume of CO and the average peak area ratio was used for the curve. The average peak area ratio was plotted as a function of CO volume in Excel and the equation of the resulting linear trendline was determined.

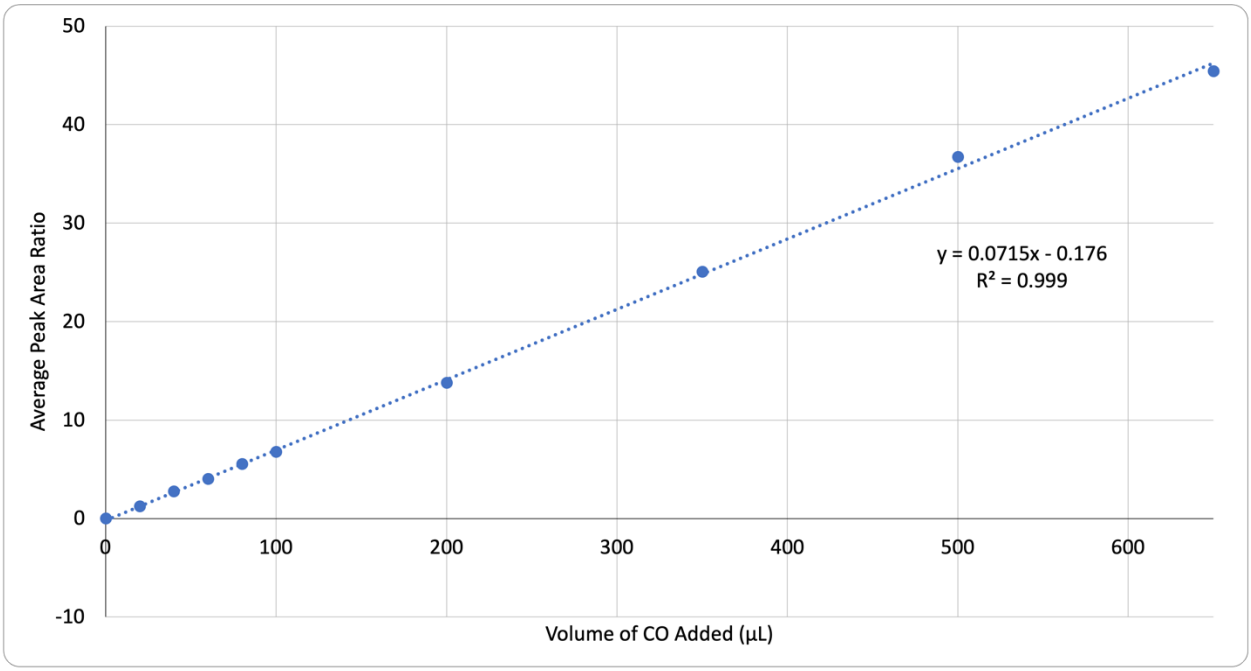

Ethane-CO calibration curve. The ethane-CO calibration curve was developed by another member in the research group using the same method described in the methane-CO calibration curve procedure.

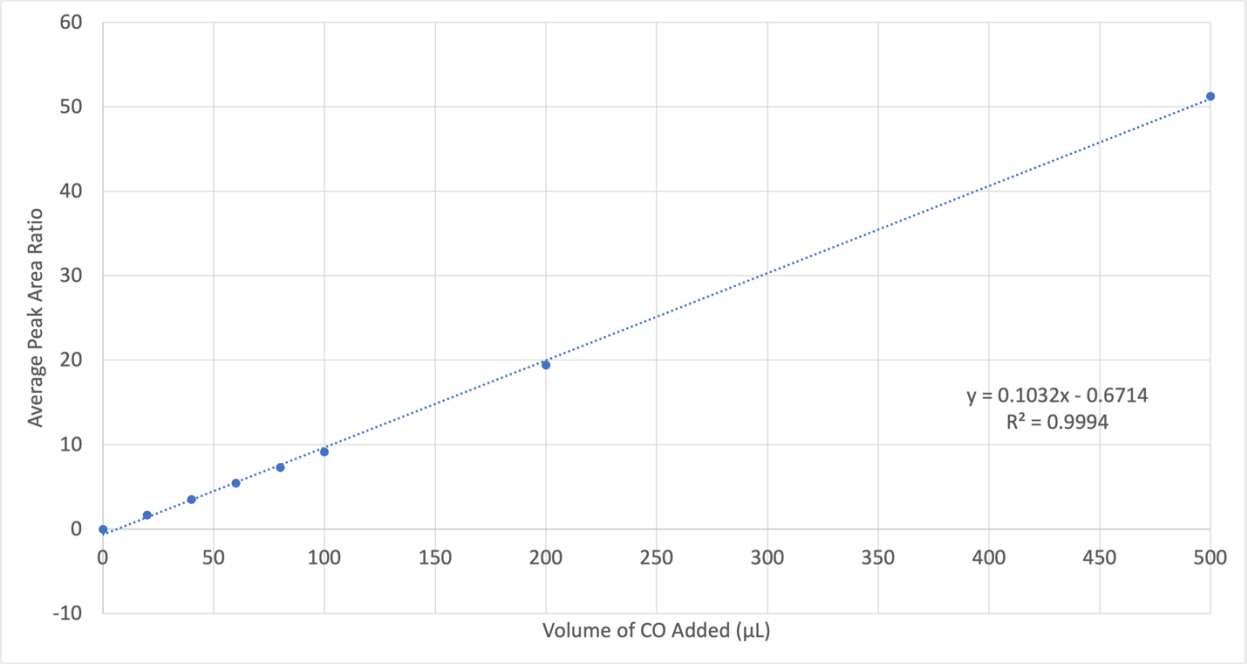

Ethane-methane calibration curve. Acetonitrile (3.000 mL, 57.44 mmol) was transferred to small test tube equipped with a stir bar and rubber septum with a 5 mL syringe and needle. The solution was bubbled with CO_2 for 10 minutes with an ice bath followed 5 minutes at room temperature. Ethane gas (20 µL) was added to the test tube with a 50 µL syringe after purging the syringe 4 times. Methane gas was added to the test tube in varying amounts (0–200 µL) with a 50 µL syringe after purging the syringe 4 times. Gases were allowed to equilibrate for 15 minutes prior to injecting 100 µL of the test tube headspace into the GC-TCD. The peak area ratios were determined to develop a calibration curve. Duplicate injections were carried out for each volume of methane and the average peak area ratio was used for the curve. The average peak area ratio was plotted as a function of methane volume in Excel and the equation of the resulting linear trendline was determined.

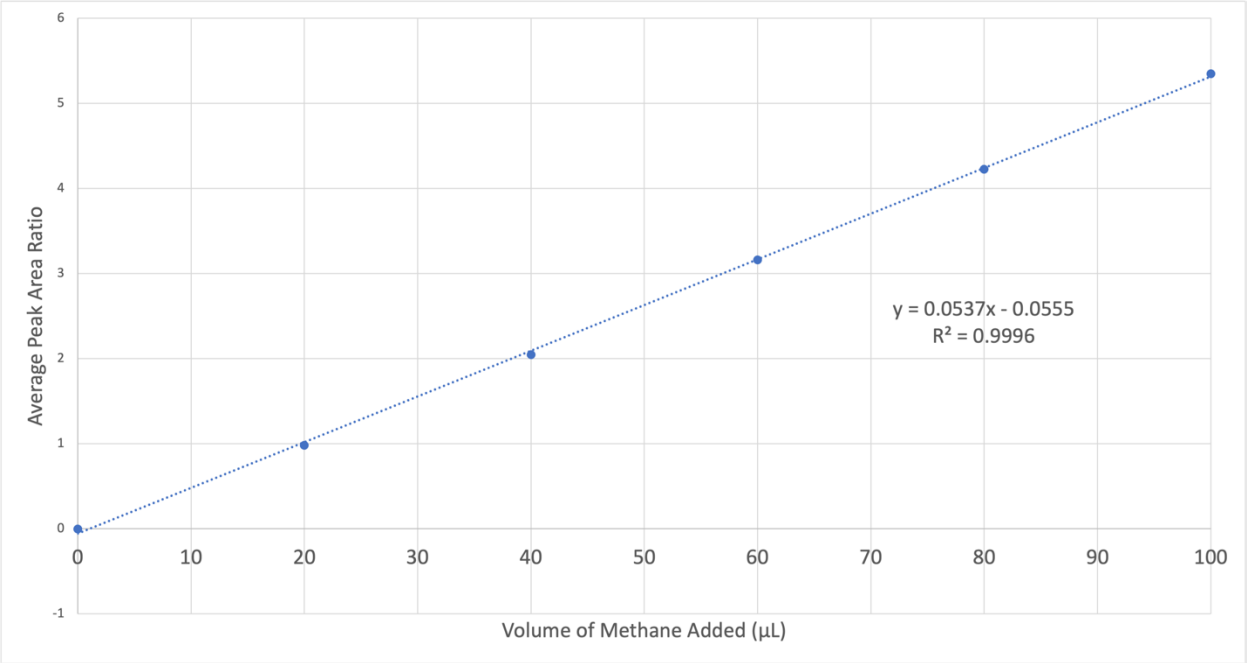
Average Peak Area Ratio
Volume of Methane Added (µL)
y = 0.0537x - 0.0555
R² = 0.9996
6
5
4
3
2
1
0
-1
0
10
20
30
40
50
60
70
80
90
100

6.4 SYNTHETIC AND EXPERIMENTAL PROCEDURES

Synthesis of 5-fluoro-2,4,6-tri(9H-carbazol-9-yl)benzene-1,3-dicarbonitrile (1, 3CzFIPN).

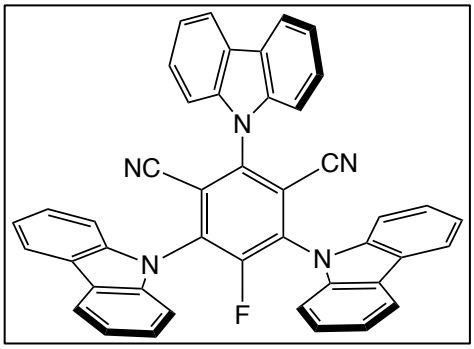

Tetrafluoroisophthalonitrile (1.104 g, 5.516 mmol) was weighed into a Schlenk flask equipped with a stir bar and rubber septum then purged under nitrogen. Distilled THF (30.00 mL) was cannula transferred to the Schlenk flask to dissolve the compound. Sodium hydride (60% oil suspension, 0.883 g, 36.79 mmol) was weighed into a separate Schlenk flask equipped with a stir bar and rubber septum. The NaH oil suspension was washed with distilled THF (2 x 15.00 mL) then suspended in 30.00 mL THF. Carbazole (1.845 g, 11.03 mmol) was weighed into a third Schlenk flask and dissolved in THF (50.00 mL) under inert atmosphere. The carbazole solution was slowly cannulated to the NaH solution while stirring at 0 ˚C, releasing gas and forming a slightly yellow solution. The ice bath was removed once the solution stopped bubbling and the reaction mixture was stirred for 1 hour at room temperature. The dissolved tetrafluoroisophthalonitrile was cooled to −196 ˚C in a $N_{2(l)}$ bath and the deprotonated carbazole solution was cooled to −78 ˚C in a dry ice bath. The carbazole solution was cannulated dropwise to tetrafluoroisophthalonitrile solution over 10 minutes, resulting in a yellow precipitate forming on the side of the flask. The reaction solution was then stirred for 3 hours at −78 ˚C then allowed to warm up to room temperature. The solution was quenched by dropwise addition of a saturated $NH_4Cl_{(aq)}$ solution (approximately 2.00 mL). The reaction mixture was filtered in air and washed with excess THF. The solvent was removed under vacuum, dissolved in 250.0 mL DCM then extracted with water (2 x 30.00 mL) then brine (1 x 30.00 mL). The organic layer was dried over $MgSO_4$ for 40 minutes then filtered. The solvent was removed under vacuum, yielding a yellow

solid (2.837 g, 4.421 mmol, 80%). **^{1}H NMR** ($CDCl_3$, 600 MHz, 27.0 ˚C): δ 8.19 (2 H, d, *J* = 7.8 Hz), 8.15 (4 H, d, *J* = 7.8 Hz), 7.61 (2 H, td, *J* = 7.8, 1.2 Hz), 7.56 (4 H, td, *J* = 8.4, 1.2 Hz), 7.46–7.39 (8 H, m), 7.35 (4 H, d, *J* = 7.8 Hz). **^{13}C{^{1}H} NMR** (180 MHz, $CDCl_3$, 27.0 ˚C): δ 142.6, 140.2, 139.4, 135.3 (d, *J* = 13.8 Hz), 127.1, 127.0, 125.0, 124.9, 123.7, 122.7, 122.5, 121.5, 121.3, 115.5, 113.9, 111.0, 110.0, 109.3. **^{19}F NMR** ($CDCl_3$, 380 MHz, ambient temp): δ −111.0 (1 F, s). **HRMS** (ESI-TOF): *m/z* $[M+Na]^+$ calc for $C_{44}H_{24}FN_5$ 641.2016, found 641.2017.

Synthesis of 1-(2,4,6-tri(9H-carbazol-9-yl)benzene-1,3-dicarbonitrile)imidazole (2, 3CzIPN Imidazole).

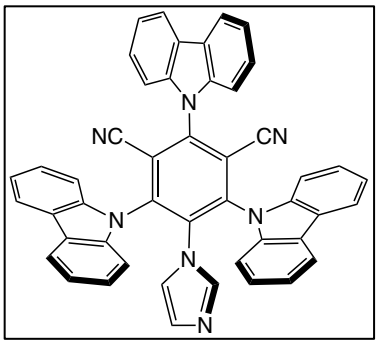

Imidazole (0.0800 g, 1.18 mmol) and cesium carbonate (1.14 g, 3.51 mmol) were weighed into a Schlenk flask equipped with a stir bar and rubber septum. The flask was purged with argon for 5 minutes. Distilled acetonitrile (30.00 mL) was transferred to the flask while stirring under inert atmosphere via cannula. The reaction mixture was equipped with a condenser and heated at 50 ˚C while stirring under argon for 30 minutes. The reaction flask was removed from the oil bath and allowed to cool to room temperature. **1** (0.750 g, 1.17 mmol) was weighed into a second Schlenk flask equipped with a stir bar and rubber septum and flushed with argon for 15 minutes. Distilled acetonitrile (10.00 mL) was transferred to the Schlenk flask containing 3CzF-IPN via cannula while stirring. The dissolved 3CzF-IPN was cannula transferred to the Schlenk flask containing the cesium carbonate and imidazole mixture while stirring and rinsed with excess acetonitrile. The resulting mixture was heated at 65 ˚C while stirring under argon for 3 hours, yielding a dark red/brown solution. The flask was removed from heat and allowed to cool to room temperature. The reaction solution was filtered in air and the solvent was removed under vacuum, resulting in a dark red product. The product was dissolved in 100 mL of DCM and extracted with water (3 x 40 mL) and brine (3 x 10 mL). The organic layer was dried over $MgSO_4$ while stirring for 30 minutes and filtered. The solution was removed under vacuum to yield the crude product (0.750 g, 92.6%) that was recrystallized in acetone/ether (1:5), yielding pure 3Cz-IPN imidazole (0.338 g, 41.7%). **^{1}H NMR** ($CDCl_3$, 600 MHz, 27.0 ˚C): δ 8.19 (2 H, d, *J* = 7.6 Hz), 8.07 (4 H, d, *J* = 7.2 Hz), 7.64 (2 H, td, *J* = 7.2, 1.2 Hz), 7.50–4.41 (8 H, m), 7.35 (4 H, td, *J* = 6.4, 1.2 Hz), 7.15 (4 H, d, *J* = 8.4 Hz), 6.54

(1 H, s), 6.15 (1 H, s), 5.87 (1 H, dd, J = 1.2, 1.2 Hz). **^{13}C{^{1}H} NMR** ($CDCl_3$, 180 MHz, 27.0 ˚C): δ 144.9, 142.3, 139.6, 139.0, 135.9, 135.0, 130.3, 127.0, 127.0, 125.0, 124.6, 122.6, 122.6, 121.4, 121.4, 117.7, 117.1, 110.8, 109.4, 108.5. **HRMS** (ESI-TOF): *m/z* $[M+H]^+$ calc for $C_{47}H_{28}N_7$ 689.2328, found 690.2401.

Synthesis of 1-(2,4,6-tri(9H-carbazol-9-yl)benzene-1,3-dicarbonitrile)-3-benzyl imidazolium bromide.

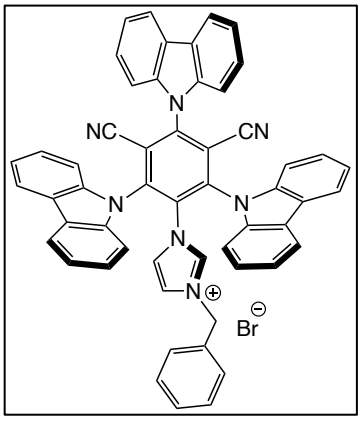

Compound **2** (400 mg, 0.58 mmol) was weighed into a side-arm flask then evacuated and purged with argon 3 times. Distilled benzyl bromide (2.88 g, 16.84 mmol) was added with a syringe and the flask was heated at 120 ˚C under argon for 2 hours. The solid dissolved upon heating and a yellow precipitate formed. The solvent was removed by cannula filtration and the resulting yellow solid was washed with ether (2 x 25.0 mL) to give the imidazolium bromide in 95% yield. **^{1}H NMR** (700 MHz, $CDCl_3$, 27.0 ˚C): δ 8.90 (1 H, s), 8.16 (2 H, d, *J* = 7.7 Hz), 8.01 (4 H, d, *J* = 7.7 Hz), 7.66 (2 H, dd, *J* = 7.7, 7.0 Hz), 7.62 (2 H, d, *J* = 8.4 Hz), 7.51 (4 H, br s), 7.46 (2 H, td, *J* = 7.0, 0.7 Hz), 7.37 (4 H, t, *J* = 7.7 Hz), 7.19 (2 H, t, *J* = 7.7 Hz), 6.45 (2 H, d, *J* = 7.0 Hz), 6.19 (1 H, dd, *J* = 2.1, 1.4 Hz), 6.19 (1 H, dd, *J* = 2.1, 1.4 Hz), 4.64 (2 H, s). **^{13}C{^{1}H} NMR** (130 MHz, DMSO, 27.0 ˚C): δ 154.2, 152.1, 147.5, 143.7, 139.3, 138.7, 138.5, 135.1, 133.3, 128.7, 128.4, 126.9, 126.6, 123.8, 123.6, 123.3, 122.4, 121.3, 121.1, 120.8, 116.8, 111.4, 110.7, 107.8, 65.9. **HRMS** (ESI-TOF): *m/z* [M^+] calc for $C_{54}H_{34}N_7$ 780.2876, found 780.2870.

Synthesis of 1-(2,4,6-tri(9*H*-carbazol-9-yl)benzene-1,3-dicarbonitrile)-3-benzyl-imidazolium tetrafluoroborate (3).

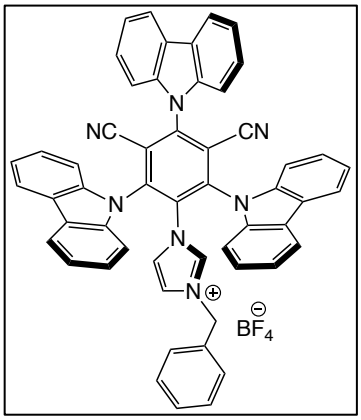

The imidazolium bromide salt (0.4000 g, 0.4647 mmol) was weighed into a side-arm flask that was evacuated and filled with argon 3 times. Distilled acetonitrile (10.00 mL) was transferred to the flask via syringe to suspend the dye. Silver tetrafluoroborate (0.1099 g, 0.5645 mmol) was weighed into a Schlenk flask in the glovebox. Distilled acetonitrile (3.000 mL) was transferred to the $AgBF_4$ via syringe under inert atmosphere. The dissolved $AgBF_4$ was transferred to the flask containing the imidazolium bromide and extra acetonitrile (2.000 mL) was used to rinse the flask. The reaction mixture was stirred at room temperature for 1 hour. The solution was filtered through a celite plug and the solvent was removed under vacuum. The resulting yellow solid was washed with ether (2 x 25.00 mL) to yield the imidazolium tetrafluoroborate (0.4029 g, 99.93%). **^{1}H NMR** (700 MHz, CD_3CN, 27.0 ˚C): δ 10.50 (1 H, s), 8.15 (2 H, d, *J* = 7.7 Hz), 8.01 (4 H, d, *J* = 7.7 Hz), 7.83 (4 H, br s), 7.63 (2 H, t, *J* = 7.7 Hz), 7.55 (4 H, t, *J* = 7.7 Hz), 7.43 (2 H, dd, *J* = 7.7, 7.0 Hz), 7.35 (4 H, t, *J* = 7.7 Hz), 7.29 (1 H, dd, *J* = 7.7, 7.0 Hz), 7.18 (2 H, dd, *J* = 8.4, 7.7 Hz), 6.44 (2 H, d, *J* = 7 Hz), 6.26 (1 H, s), 6.10 (1 H, s), 4.77 (2 H, s). **^{13}C{^{1}H} NMR** (180 MHz, CD_3CN, 27.0 ˚C): δ 149.2, 144.9, 140.4, 139.8, 136.4, 133.4, 132.9, 130.2, 128.6, 128.3, 128.2, 125.5, 125.3, 124.4, 124.1, 123.9, 123.8, 122.2, 122.2, 118.6, 112.3, 111.7, 111.3, 53.8, 16.2. **HRMS** (ESI-TOF): *m/z* [M*$^+$] calc for $C_{54}H_{34}N_7$ 780.2876. Found: 780.2862.

Synthesis of 1-(2,4,6-tri(9*H*-carbazol-9-yl)benzene-1,3-dicarbonitrile)-3-isopropyl-imidazolium tetrafluoroborate (4).

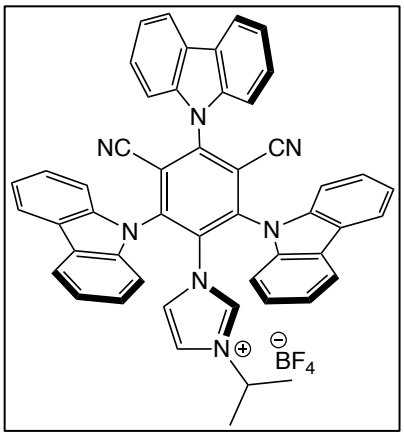

Excess iodopropane (1.50 mL, 15.9 mmol) was added to a flask containing 3Cz-IPN imidazole (0.125 g, 0.182 mmol) with a micropipette. The Schlenk flask was equipped with a condenser and the reaction mixture was heated at 110 ˚C in an oil bath while stirring under inert atmosphere for 3.5 hours. A yellow solid was formed, and NMR indicated the reaction was complete. The yellow product was washed with distilled ether (5 x 10.0 mL, 3 x 20.0 mL). The reaction flask was heated to 60 ˚C under reduced pressure to remove any remaining iodopropane or ether, yielding a bright yellow solid. Acetonitrile (10.0 mL) was transferred to the flask containing the yellow product then the flask was heated to 60 ˚C under inert atmosphere. $AgBF_4$ (0.0390 g, 0.200 mmol) was dissolved in distilled MeCN (1.00 mL) then transferred to flask containing the isopropyl NHC product while stirring. The flask was equipped with a condenser and the reaction mixture was stirred for 45 minutes under inert atmosphere. The oil bath was removed, and the solution was cooled to room temperature, revealing a yellow solution with a white AgI precipitate. The reaction mixture was passed through a celite column via cannula filtration into a new Schlenk flask under inert atmosphere. The solvent was evaporated under reduced pressure, yielding the final product, a yellow powder (0.120 g, 0.147 mmol, 80.0%). **^{1}H NMR** (CD_3CN, 400 MHz, 27.0 ˚C): δ 8.32 (2 H, d, *J* = 8.0 Hz), 8.19 ppm (4 H, d, *J* = 7.6 Hz), 7.90 (2 H, d, *J* = 8.4 Hz), 7.79–7.75 (3 H, comp m), 7.60–7.53 (10 H, m), 7.43 (4 H, td, *J* = 8.0, 1.2 Hz), 6.66 (1 H, t, *J* = 2.0 Hz), 6.56 (1 H, t, *J* = 2.0 Hz), 3.86 (1 H, septet, *J* = 6.4 Hz), 0.72 (6 H, d, *J* = 6.4 Hz). **^{13}C{^{1}H} NMR** (CD_3CN, 130 MHz, 27.0 ˚C): δ 145.6, 144.8, 140.5, 139.7, 137.9, 134.7, 128.4, 128.3, 125.5, 125.3, 124.0, 123.9,

123.7, 122.5, 122.2, 122.1, 120.4, 112.6, 111.7, 111.5, 55.2, 22.0. **HRMS** (ESI-TOF): *m/z* [M^+] calc for $C_{50}H_{34}N_7$ 732.2876, found 732.2869.

Synthesis of *fac*-Re(bpy)(CO)$_3$Cl.

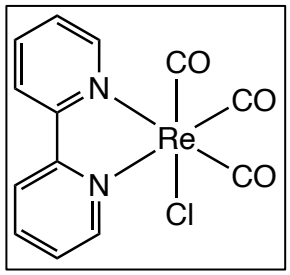

Pentacarbonylchlororhenium(I) (0.3011 g, 0.8324 mmol) and 2,2'-bipyridine (0.1296 g, 0.8297 mmol) were dissolved in toluene (30.00 mL) under inert atmosphere in a Schlenk flask equipped with a condenser. The solution was heated to 115 ˚C in an oil bath with stirring under inert atmosphere. After 2.5 hours, a yellow solid was observed in the flask and the solution was removed from the oil bath to cool to room temperature. The toluene was removed from the flask via cannula filtration and the yellow precipitate was washed with hexanes (3 x 20.00 mL) followed by ether (3 x 20.00 mL). Any remaining solvent was removed under vacuum overnight to yield a bright yellow solid (0.3572 g, 0.7734 mmol, 92.95%). **^{1}H NMR** (CD_3CN, 600 MHz, 27.0 ˚C): δ 9.02 (2 H, d, *J* = 5.4 Hz), 8.42 (2 H, d, *J* = 7.8 Hz), 8.20 (2 H, dt, *J* = 7.8, 1.8 Hz), 7.63 (2 H, dt, *J* = 6, 1.2 Hz). **^{13}C{^{1}H} NMR** ($CD_3C(O)CD_3$, 180 MHz, 27.0 ˚C): δ 156.7, 153.9, 140.8, 128.5, 124.9. **HRMS** (ESI-TOF): *m/z* [M*+] calc for $C_{14}H_8N_2O_4$[Re] 455.0042, found 455.0036.

Synthesis of *fac*-Re(bpy)(CO)$_3$(acetone) (5).

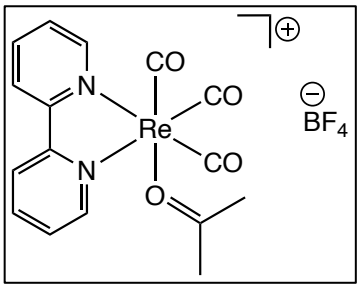

Distilled d_6-acetone (0.3 mL) was transferred to an NMR tube equipped with a rubber septum containing Re(CO)$_3$(bpy)Cl (0.0100 g, 0.021 mmol) and a second NMR tube equipped with a rubber septum containing $AgBF_4$ (0.0051 g, 0.026 mmol) both under inert atmosphere. The $AgBF_4$ solution was transferred to the Re(CO)$_3$(bpy)Cl solution via cannula and the reaction mixture was sonicated for 1.5 hrs. The AgCl precipitate formed at the bottom of the test tube and NMR revealed complete replacement of the Cl ligand by the solvent. The solution was used further for other experiments. **^{1}H NMR** (CD_3COCD_3, 400 MHz, 27.0 ˚C): δ 9.23 (2 H, dd, J = 5.6, 4.8 Hz), 8.84 ppm (2 H, d, J = 8.0 Hz), 8.49 (2 H, td, J = 8.0, 1.6 Hz), 7.92 (2 H, ddd, J = 7.6, 5.6, 1.2 Hz). **^{13}C{^{1}H} NMR** (180 MHz, CD_3COCD_3, 27.0 ˚C): δ 157.2, 155.0, 155.0, 142.5, 129.3, 129.3, 125.5, 125.5.

Synthesis of Re(bpy)(CO)$_3$(3CzIPN Imidazole) (Re-2).

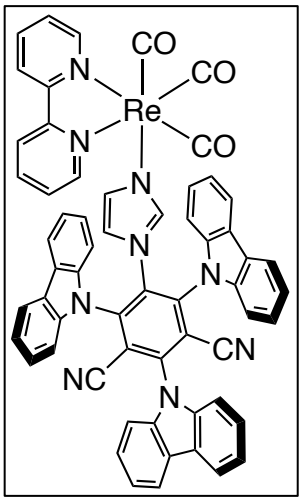

Re(bpy)(CO)$_3$Cl (0.0500 g, 0.108 mmol) and $AgBF_4$ (0.0300 g, 0.154 mmol), were weighed into a small Schlenk tube equipped with a greased stopcock, stir bar and rubber septum in the glovebox. Distilled acetone (5.00 mL) was transferred to the Schlenk flask while stirring under inert atmosphere. The solution was sonicated for 1.5 hrs. The AgCl precipitate formed at the bottom of the test tube and NMR revealed complete replacement of the Cl ligand by the solvent. The Re(bpy)(CO)$_3$(acetone) solution was filtered through a celite plug via cannula transfer under inert atmosphere into a flask containing 3Cz-IPN imidazole (0.0749 g, 0.109 mmol). The celite plug was rinsed with an additional 5.00 mL of distilled acetone to remove any remaining compound. The reaction flask containing both compounds was equipped with a condenser and the solution was heated at 50 ˚C in an oil bath under inert atmosphere overnight. The solution was removed from heat and allowed to cool to room temperature. NMR revealed the complete reaction of the Re-acetone complex. Excess ether was bubbled with nitrogen for 10 minutes. Ether was slowly cannulated into reaction mixture, adding 5 drops at a time, while stirring under inert atmosphere until a brown solid began to precipitate out of solution. The flask was placed in the freezer overnight to allow more precipitate to form. The solvent was removed via cannula filtration to yield a yellow powder (0.0999 g, 0.0887 mmol, 82.1 %) and NMR was obtained. A 0.840 mM stock solution in distilled MeCN (20.0 mL) was prepared to use in future reactions. **^{1}H NMR** ($(CD_3)_2CO$, 600 MHz, 27.0 ˚C): δ 8.68 (2 H, d, *J* = 4.8 Hz), 8.46 (2 H, d, *J* = 7.8 Hz), 8.38 (2 H, dd, *J* = 7.8, 7.2 Hz), 8.28 (2 H, d, *J* = 7.8 Hz), 8.20 (4 H, d, *J* = 7.8 Hz), 7.72 (2 H, d, *J* = 8.4 Hz), 7.68 (2 H, dd, *J* = 13.2, 8.4 Hz), 7.59 (2 H, t, *J* = 7.8 Hz), 7.53 (2 H, d, *J* = 7.8 Hz), 7.47-7.38 (8 H, comp m), 7.34 (2 H, t, *J* =

7.8 Hz), 7.09 (1 H, s), 6.37 (1 H, s), 6.14 (1 H, s). **^{13}C{^{1}H} NMR** ($CD_3C(O)CD_3$, 180 MHz, 27.0 ˚C): δ 156.7, 153.9, 140.8, 128.5, 124.9. **HRMS** (ESI-TOF): *m/z* [M*+] calc for $C_{60}H_{35}N_9O_3$[Re] 1116.242, found 1116.2415.

Synthesis of 1-(2,4,6-tri(9*H*-carbazol-9-yl)benzene-1,3-dicarbonitrile)-3-benzyl-1,3-dihydro-2H-imidazol-2-ylidene (**8**).

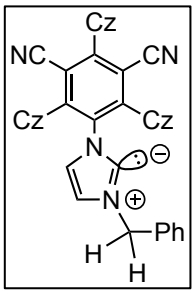

Compound **3** (30 mg, 0.035 mmol) and KH (13.9 mg, 0.035 mmol, 10 equiv.) were weighed into a Schlenk flask and sealed with septa inside a glove box. The Schlenk flask was then moved to a Schlenk line and placed into an ice-water bath. Freshly distilled d_8-THF (~ 1 mL) was added into the Schlenk flask under inert atmosphere. The suspension was stirred for 3 hours at 0 ºC, under bubbler pressure. The original yellow suspension became a brown solution, indicating a complete reaction. The ^{1}H NMR spectrum showed that the carbene was the only product present. **^{1}H NMR** (600 MHz, d_8-THF, 27.0 °C): δ 8.13 (2 H, d, *J* = 7.8 Hz), 8.07 (2 H, *J* = 7.8 Hz), 7.48 (4 H, dd, *J* = 15.0, 7.8 Hz), 7.39–7.37 (8 H, m), 7.30–7.22 (5 H, comp m), 7.20–7.17 (2 H, m), 7.04 (2 H, d, *J* = 7.2 Hz), 6.94 (2 H, s, *J* = 4.2 Hz), 5.29 (2 H, s), 5.17 (1 H, s), 4.99 (1 H, s). **^{13}C NMR** (180 MHz, d_8-THF, 27.0 °C): δ 138.4, 137.3, 136.2, 134.0, 131.4, 130.5, 125.2, 124.4, 124.1, 123.0, 122.7, 122.3, 120.1, 118.2, 116.8, 116.7, 116.6, 116.2, 114.0, 113.1, 109.5, 107.0, 106.0, 46.1, 18.6.

Synthesis of Re(bpy)(CO)$_3$(8) (Re-8).

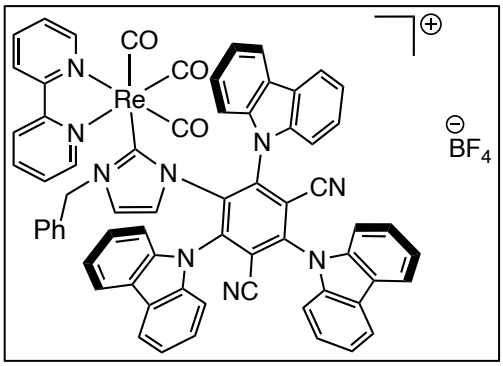

3Cz-IPN benzyl NHC (0.018 g, 0.022 mmol) and KH (0.0043 g, 0.11 mmol) were weighed into a Schlenk flask under inert atmosphere and cooled to 0 ˚C in an ice bath. Cold distilled THF (4.0 mL) was transferred to the flask containing the reagents via cannula while stirring under inert atmosphere. The yellow solution was stirred for 3 hours at 0 ˚C and became dark red after 2.5 hours indicating the deprotonation of the NHC was complete. The Re(bpy)(CO)$_3$(*d*$_6$-acetone) solution was cooled to 0 ˚C and transferred to the flask containing the deprotonated NHC solution while stirring without disturbing the layer of settled AgCl precipitate. The resulting solution was cannula filtered to a new Schlenk flask under inert atmosphere to remove any excess KH or solid particles and an NMR spectrum was obtained with solvent suppression. **^{1}H NMR** (*d*$_8$-THF, 500 MHz, 27.0 ˚C): δ 8.34 (2 H, br s), 8.17 (2 H, d, *J* = 8.0 Hz), 8.03 (4 H, d, *J* = 8.0 Hz), 7.56–7.41 (14 H, comp m), 7.36 (2 H, dd, *J* = 7.5, 7.0 Hz), 7.29–7.28 (3 H, m), 7.20–7.14 (6 H, comp m), 7.09 (2 H, d, *J* = 7.0 Hz), 7.06 (1 H, s), 6.81 (1 H, s), 5.29 (1 H, s), 5.28 (2 H, d, *J* = 8.0 Hz), 5.06 (1 H, s). **^{13}C NMR** (*d*$_8$-THF, 180 MHz, 27.0 ˚C): δ 140.1, 139.4, 138.4, 137.2, 136.2, 134.0, 132.9, 131.4, 130.5, 125.2, 124.7, 124.4, 124.1, 123.1, 133.7, 122.3, 120.1, 118.1, 116.8, 116.7, 116.6, 116.2, 114.0, 113.1, 112.7, 111.2, 109.5, 108.1, 107.0, 106.0, 56.9, 46.7.

Synthesis of Re(bpy)(CO)$_3$(9) (Re-9).

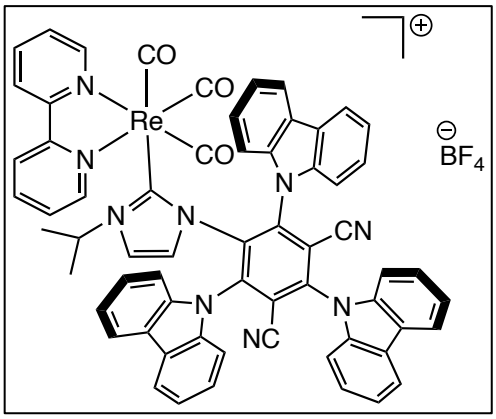

3Cz-IPN isopropyl NHC (0.018 g, 0.022 mmol) and KH (0.0043 g, 0.11 mmol) were weighed into a Schlenk flask under inert atmosphere and cooled to 0 ˚C in an ice bath. Cold distilled THF (4.0 mL) was transferred to the flask containing the reagents via cannula while stirring under inert atmosphere. The bright solution was stirred for 3 hours at 0 ˚C and became dark orange-brown after 1.5 hours indicating the deprotonation of the NHC was complete. The Re(bpy)(CO)$_3$(*d*$_6$-acetone) solution was cooled to 0 ˚C and transferred to the flask containing the deprotonated NHC solution while stirring without disturbing the layer of settled AgCl precipitate. The resulting solution was cannula filtered to a new Schlenk flask under inert atmosphere to remove any excess KH or solid particles and an NMR spectrum was obtained with solvent suppression. **^{1}H NMR** ((CD$_3$)$_2$CO, 600 MHz, 27.0 ˚C): δ 8.98 (2 H, d, *J* = 4.8 Hz), 8.53 (2 H, d, *J* = 8.4 Hz), 8.20 (2 H, td, *J* = 8.4, 1.8 Hz), 8.17 (2 H, d, *J* = 7.8 Hz), 8.00 (4 H, d, *J* = 7.8 Hz), 7.64 (2 H, dd, *J* = 6.6, 6.0 Hz), 7.56 (2 H, d, *J* = 7.8 Hz), 7.53 (2 H, t, *J* = 8.4 Hz), 7.50 (2 H, d, *J* = 8.4 Hz), 7.41 (4 H, t, *J* = 7.8 Hz), 7.29 (2 H, t, *J* = 7.8 Hz), 7.16 (4 H, t, *J* = 7.2 Hz), 6.90 (1 H, s), 5.34 (1 H, s), 5.07 (1 H, s), 4.73 (1 H, septet, *J* = 6.6 Hz), 1.42 (6 H, d, *J* = 6.6 Hz). **FTIR** (cast film, THF): 3517, 3050, 2972, 2928, 2859, 2225, 2018, 2000, 1887, 1689, 1601, 1559, 1491, 1470, 1455, 1394, 1334, 1314, 1226, 1153, 1120, 1054, 1030, 816, 751, 723 cm^{-1}.

Preparation of CO_2 reduction solution with Re-8 and Re-9 complexes.

The Re-NHC complexes were prepared in a solution of THF and *d_6*-acetone in known amounts. The desired catalyst concentration was achieved by calculating the amount of the Re-NHC photocatalyst in solution then determining the volume to add to the reaction flask. This volume was typically around 100 μL and was added to 2.9 mL MeCN for a total volume of 3 mL to achieve the desired 0.14 mM catalyst concentration (*sample calculation 1*). BIH was maintained at 0.1 M in this solution.

Sample Calculation 1. *Calculating the volume of Re-NHC solution to add to the CO_2 reduction flask to achieve the desired 0.14 mM concentration.*

$$n_{\text{cat in solution}} = 0.00002165 \text{ mol}$$

$$n_{\text{cat desired}} = 0.000141 \frac{\text{mol}}{\text{L}} \times 0.003 \text{ L} = 0.00000042 \text{ mol}$$

$$\text{ratio} = \frac{0.00002165 \text{ mol}}{0.00000042 \text{ mol}} = 51.55 \text{ eq in solution}$$

$$V_{\text{reaction total}} = 4 \text{ mL THF} + 1.31 \text{ mL } d_6\text{acetone} = 5.31 \text{ mL}$$

$$V_{\text{CO2 reaction}} = \frac{5.31 \text{ mL}}{51.55} = 0.103 \text{ mL} = 103 \text{ μL}$$

$$V_{\text{CO2 reaction total}} = 3 \text{ mL} - 0.103 \text{ mL} = 2.897 \text{ mL} = 2.90 \text{ mL MeCN}$$

Photochemical reduction of CO_2.

1,3-Dimethyl-2-phenyl-2,3-dihydro-1H-benzimidazole (0.0673 g, 0.300 mmol) was weighed into a small test tube equipped with a stir bar and a rubber septum under inert atmosphere. Distilled acetonitrile (3.00 mL) was transferred to the test tube with a 5 mL syringe while stirring. The catalyst (0.0004200 mmol) was added to the reaction mixture via syringe (amount varied depending on catalyst). The resulting solution was bubbled with CO_2 or $^{13}CO_2$ for 10 minutes with an ice bath followed by 5 minutes at room temperature. The internal standard, methane (20.0 μL) or ethane gas (20.0 μL) was added to the test tube with a 50 μL syringe. A T=0 GC injection was done prior to starting the reaction to ensure the internal standard was successfully added to the reaction test tube. An AM1.5G solar light simulator was calibrated to 100 mW/cm^2 and a UV filter or K_2CrO_7 solution was applied to exclude UV light. The test tube was placed in the solar light simulator with stirring and a fan to prevent any heating from the light source. The extent of CO_2 reduction was monitored in the gas phase by periodic samplings and injections into GC-TCD utilizing methane (CH_4) or ethane (C_2H_6) gas as internal standard. All GC quantifications were determined from control calibration curves. A precipitate formed and was analyzed via NMR.

Synthesis of 1,3-Dimethyl-2-phenylbenzimidazolium iodide.

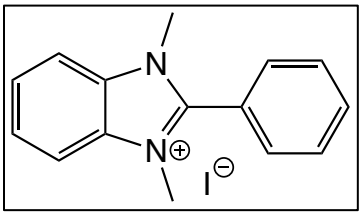

2-Phenylbenzimidazole (5.000 g, 25.74 mmol) was dissolved in distilled THF (70.00 mL, 861.6 mmol) in a Schlenk flask while stirring under inert atmosphere. NaH (1.235 g, 51.48 mmol) was washed with THF (3 x 10.00 mL) under inert atmosphere and suspended in THF (30.00 mL). The NaH solution was slowly transferred to the flask containing the 2-phenylbenzimidazole solution via cannula while stirring at 0 ˚C under inert atmosphere. The ice bath was removed and warmed to room temperature, then allowed to stir for 1 hour. Iodomethane (4.258 g, 30.00 mmol) was added to the flask with a syringe and needle while stirring. The reaction mixture was stirred for 4 hours under inert atmosphere then the solvent was removed under reduced pressure. Excess iodomethane (10.96 g, 77.22 mmol) was added to the flask with a needle and syringe while stirring. The flask was equipped with a condenser and was heated at reflux for 6 hours under inert atmosphere, yielding a pink solid. The product was washed with excess acetone, vacuum filtered in air and recrystallized in hot ethanol to yield pink needle crystals (. **^{1}H NMR** (CD_3CN, 400 MHz, 27.0 ˚C): δ 7.91 (2 H, m), 7.85 (1 H, tt, *J* = 7.0, 1.4 Hz), 7.79–7.73 (6 H, comp m), 6.44 (2 H, m), 3.86 (6 H, s). **^{13}C{^{1}H} NMR** (180 MHz, CD_3CN, 27.0 ˚C): δ 134.2, 133.0, 131.5, 130.7, 128.0, 121.9, 114.1, 110.8, 109.4, 33.8. **HRMS** (ESI-TOF): *m/z* [M*+] calc for $C_{15}H_{15}N_2$ 223.1235, found 223.1229.

Synthesis of 1,3-Dimethyl-2-phenyl-2,3-dihydro-1D-benzimidazole (10).

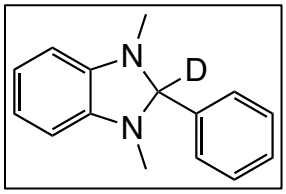

1,3-Dimethyl-2-phenylbenzimidazolium iodide (0.8002 g, 2.285 mmol) was dissolved in distilled methanol (5.000 mL, 123.6 mmol) in a Schlenk flask under inert atmosphere. $NaBD_4$ (0.2869 g, 6.855 mmol) was dissolved in distilled methanol (5.000 mL, 123.6 mmol) in a second Schlenk flask under inert atmosphere. The $NaBD_4$ solution was slowly transferred to other flask via cannula transfer and rinsed with approximately 1.000 mL of methanol. The reaction mixture was stirred for 30 minutes under bubbler pressure then the solvent was removed under reduced pressure, yielding a pink solid. The product was recrystallized in ethanol and vacuum filtered, resulting in pink needle crystals (0.2315 g, 1.024 mmol, 44.80%). **^{1}H NMR** (CD_3CN, 600 MHz, 27.0 C): δ 7.57–7.55 (2 H, comp m), 7.46–7.43 (3 H, comp m), 6.67–6.65 (2 H, m), 6.45–6.43 (2 H, m), 2.51 (6 H, s). **^{13}C{^{1}H} NMR** (CD_3CN, 180 MHz, 27.0 ˚C): δ 143.3, 140.2, 130.3, 129.7, 129.4, 120.2, 109.3, 106.7, 94.7, 33.6. **HRMS** (ESI-TOF): *m/z* $[M+H]^+$ calc for $C_{15}H_{15}DN_2$ 225.1376, found 226.1453. Tentative, to be repeated/examined further.

Synthesis of 1-Methyl-2-phenylbenzimidazole (12).

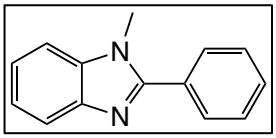

2-Phenylbenzimidazole (0.7004 g, 3.606 mmol) and potassium *tert*-butoxide (0.4207 g, 3.749 mmol) were weighed into a Schlenk flask equipped with a stir bar and a rubber septum in the glovebox. Distilled THF (40.00 mL) was cannula transferred to the reaction flask while stirring under inert atmosphere. Iodomethane (0.5700 g, 4.016 mmol) was added the solution with a micropipette. The rubber septum was replaced, and the solution was stirred overnight under argon. The solvent was removed under vacuum, yielding a light pink crude product. The crude product was dissolved in DCM and extracted with water (3 x 10.00 mL), then dried over $MgSO_4$ and gravity filtered into a round-bottom flask. The solvent was removed under vacuum, yielding a pink solid. (0.4828 g, 2.318 mmol, 64.21%). **^{1}H NMR** (CD_3CN, 700 MHz, 27.0 ˚C): δ 7.87 (2 H, dd, *J* = 8.4, 1.5 Hz), 7.68 (1 H, d, *J* = 7.8 Hz), 7.58−7.51 (4 H, m), 7.29 (1 H, td, *J* = 7.2, 1.2 Hz), 7.24 (1 H, td, *J* = 7.8, 1.2 Hz), 3.92 (3 H, s). **^{13}C{^{1}H} NMR** (CD_3CN, 180 MHz, 27.5 ˚C): δ 154.7, 144.0, 137.9, 131.7, 130.5, 130.4, 129.6, 123.4, 122.9, 120.1, 119.2, 111.2, 32.4. **HRMS** (ESI-TOF): *m/z* $[M+H]^+$ calc for $C_{14}H_{13}N_2$ 208.0997, found 209.1073. Tentative, to be repeated/examined further.

Construction of a Stern-Volmer plot.

$Re(CO)_3$(bpy)(3Cz-IPN isopropyl NHC) catalyst was synthesized by procedures previously stated. Five varying quantities of 1,3-Dimethyl-2-phenyl-2,3-dihydro-1H-benzimidazole (BIH) were weighed into separate small test tubes equipped with rubber septa to achieve different concentrations. The five concentrations were: 100 mM (0.0673 g, 0.300 mmol), 75 mM (0.0505 g, 0.225 mmol), 50 mM (0.0336 g, 0.150 mmol), 25 mM (0.0168 g, 0.0749 mmol) and 0 mM. Distilled acetonitrile (2.900 mL) was added to each test tube via syringe to dissolve the BIH. $Re(CO)_3$(bpy)(3Cz-IPN isopropyl NHC) in THF (0.100 mL, 0.000420 mmol) was added to each test tube via 100 μL syringe. A cuvette equipped with a rubber septum secured by copper wire was flushed under argon and filled with each solution via cannula transfer. The excitation spectrum of each solution was measured from 250 nm to 450 nm with a fixed emission wavelength of 460 nm. The emission spectrum of each solution was measured from 430 nm to 700 nm with a fixed excitation wavelength of 420 nm. The Stern-Volmer plot was derived by plotting I_0/I as a function of [BIH] where I_0 is the fluorescence intensity of the excitation spectrum at 420 nm of the 0 mM BIH solution, and I is the fluorescence intensity of the excitation spectrum at 420 nm of the other solutions. The resulting plot demonstrated a linear relationship.

6.5 CALCULATIONS

Blue LED wavelength and intensity.

Figure S5 in a previous publication[86] outlines the measurement of the wavelength (λ_{max}) and light intensity of the blue LED light source. The average intensity was 5.96×10^{-1} mW cm^{-2}. The height of the exposed reaction solution was 2.50 cm. The radius of the exposed reaction solution was 0.70 cm. The intensity of incident light was calculated by multiplying the surface area of the reaction solution ($2\pi rl = 2 \times 3.14 \times 2.50 \times 0.70 = 10.996$ cm^2 = 11 cm^2) by the average power density (5.96×10^{-1} mW cm^{-2}) to give 6.55 mW.

Calculation of TOF for the photocatalysts.

The TOF_{CO} of the photocatalysts were calculated with the TON_{CO} values summarized in the following table. Initial activities of the photocatalysts within the first 3 hours of the reaction were used for this calculation with the following equation.

$$TOF_{CO} = \frac{TON_{CO}}{time\ (h)}$$

Table S1. *Calculated average TOF_{CO} for each Re(I) photocatalyst.*

Photocatalyst	Run	TON_{CO}	Time (h)	TOF_{CO} (h^{-1})	Average TOF_{CO} (h^{-1})
Re-**2**	1	17	2	8.5	8.75
	2	18	2	9	
Re-**8**	1	47	1	47	46.5
	2	46	1	46	
Re-**9**	1	24	1.75	13.7	12.5
	2	27	2.5	10.8	
	3	30	1.75	17.1	
	4	21	2.5	8.4	

Quantification of BIH and BI^+.

A known amount of TMB was added to the reaction solution following the CO_2 reduction reaction. Using the integration values of peaks belonging to BIH, BI^+ and the standard, the amount of moles of BIH and BI^+ in solution were calculated according to *sample calculation 2* below.

Sample calculation 2. *Quantification of BIH remaining in a reaction with a 1,3,5-trimethoxybenzene (TMB) internal standard (exp 6–1). The same process was used for the quantification of* BI^+.

$$TMB = \frac{1.75}{3H} = 0.583$$

$$BIH = \frac{2.00}{2H} = 1$$

$$ratio = \frac{1}{0.583} = 1.714$$

$$n_{BIH} = ratio \times n_{TMB\ added} = 1.714 \times 0.0654\ mmol = 0.112\ mmol\ BIH\ remaining$$

7 – SUPPLEMENTARY FIGURES

Figure S1. ^{1}H NMR spectrum of 5-fluro-2,4,6-tri(9H-carbazol-9-yl)benzene-1,3-dicarbonitrile (**1**, 3CzFIPN) in $CDCl_3$.

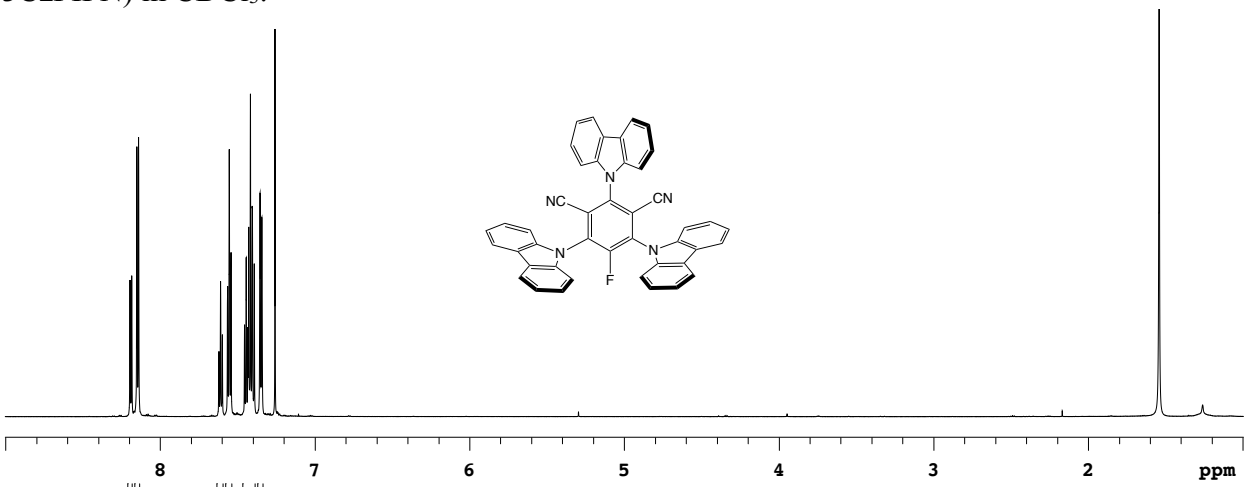

Figure S2. $^{13}C\{^{1}H\}$ NMR spectrum of 5-fluro-2,4,6-tri(9H-carbazol-9-yl)benzene-1,3-dicarbonitrile (**1**, 3CzFIPN) in $CDCl_3$.

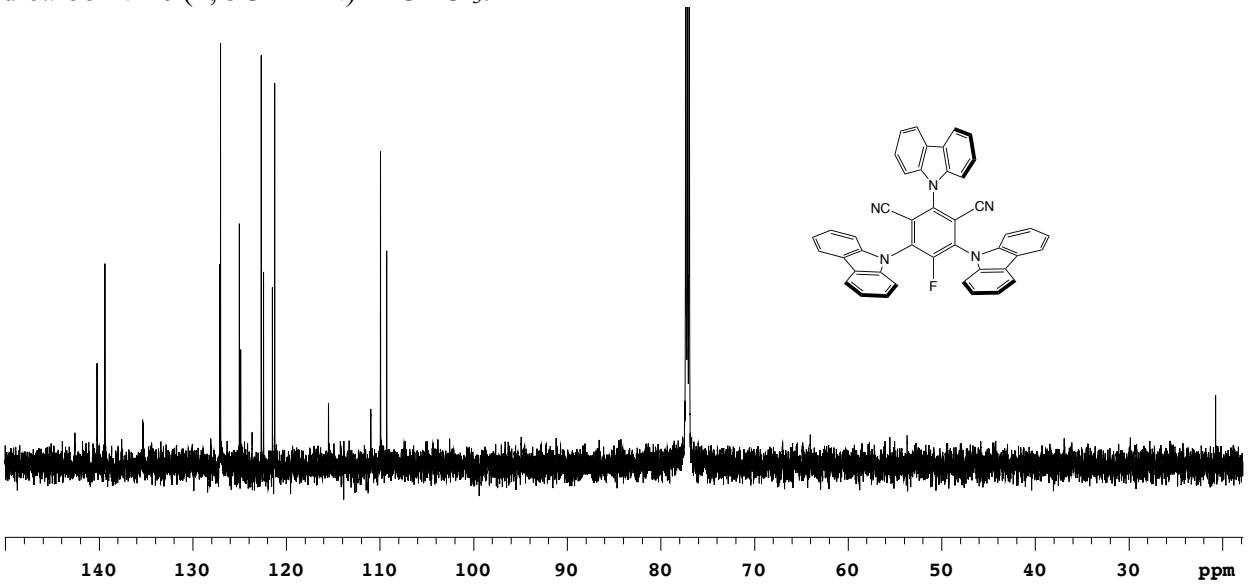

Figure S3. ^{19}F NMR spectrum of 5-fluro-2,4,6-tri(9H-carbazol-9-yl)benzene-1,3-dicarbonitrile (**1**, 3CzFIPN) in $CDCl_3$.

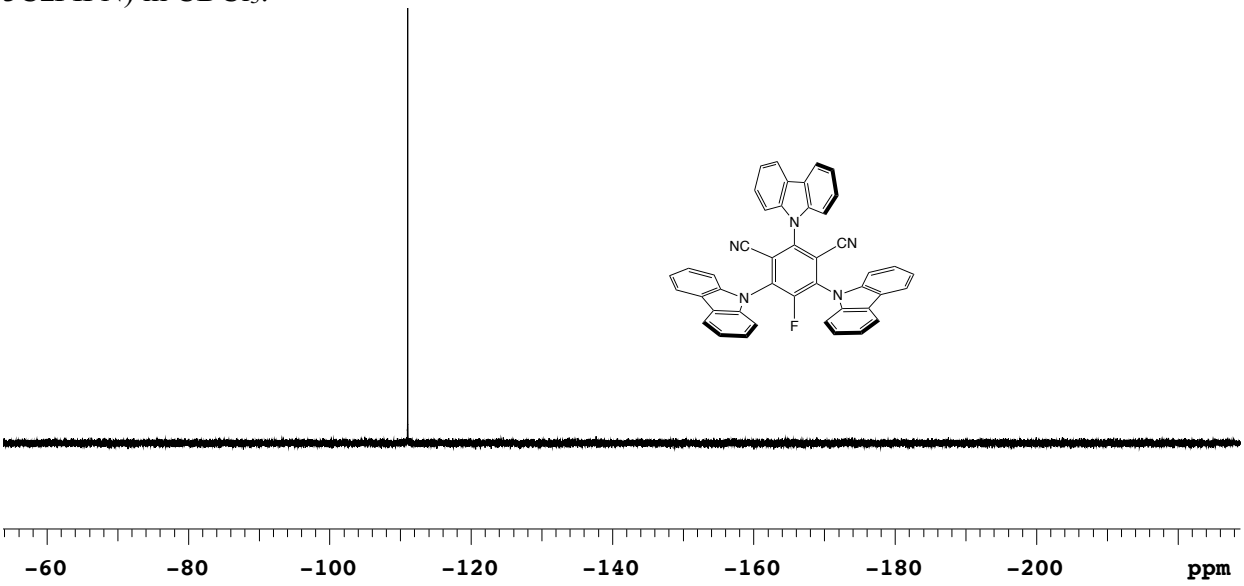

Figure S4. HRMS-ESI spectrum of 5-fluro-2,4,6-tri(9H-carbazol-9-yl)benzene-1,3-dicarbonitrile (**1**, 3CzFIPN).

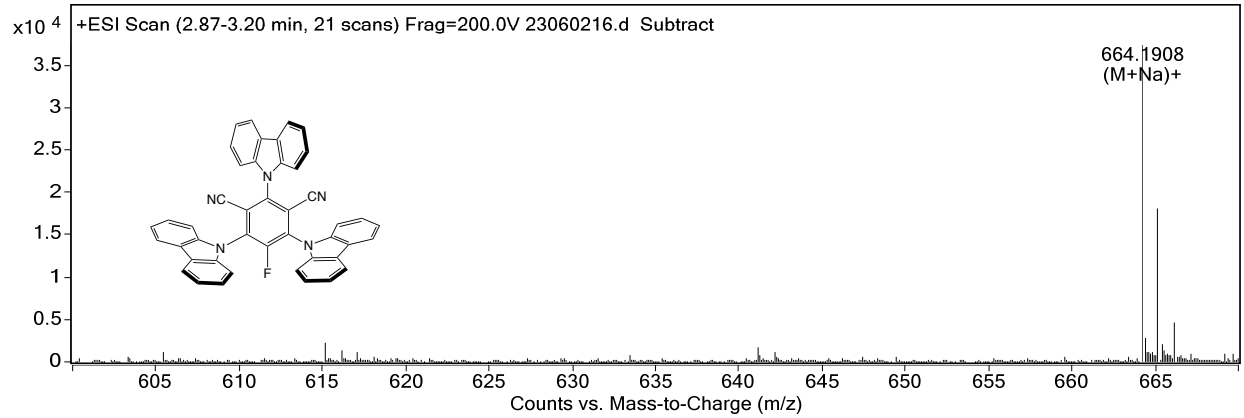

Figure S5. ^{1}H NMR spectrum of 1-(2,4,6-tri(9*H*-carbazol-9-yl)benzene-1,3-dicarbonitrile)imidazole (**2**, 3CzIPN imidazole) in $CDCl_3$.

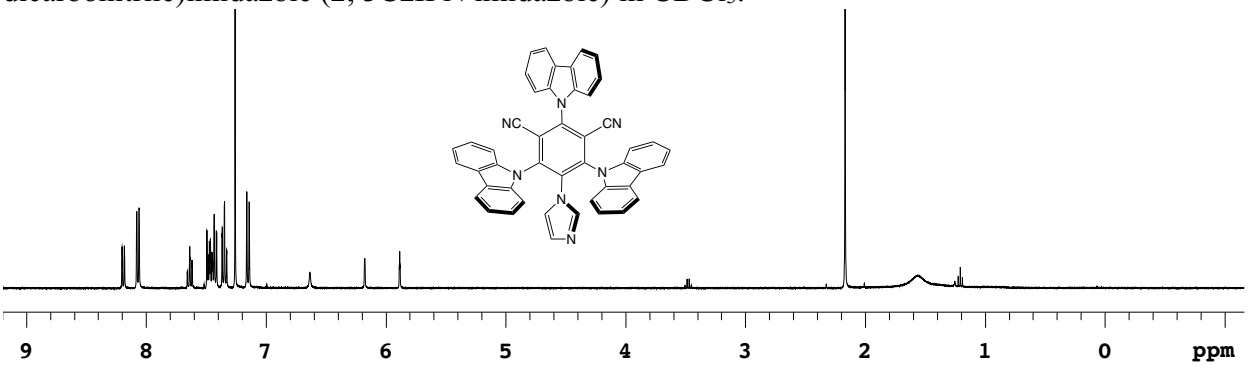

Figure S6. $^{13}C\{^{1}H\}$ NMR spectrum of 1-(2,4,6-tri(9*H*-carbazol-9-yl)benzene-1,3-dicarbonitrile)imidazole (**2**, 3CzIPN imidazole) in $CDCl_3$.

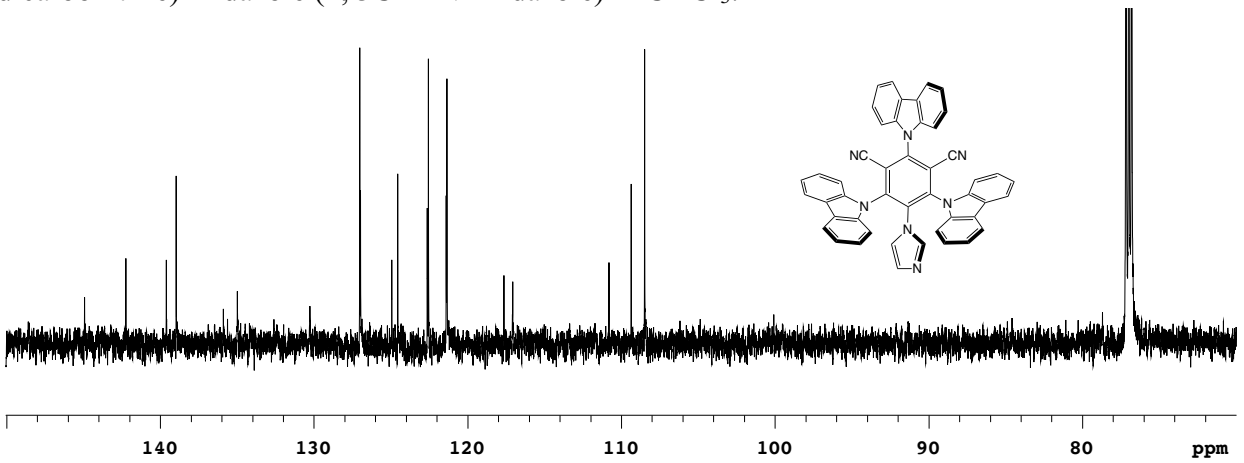

Figure S7. HRMS-ESI spectrum of 1-(2,4,6-tri(9*H*-carbazol-9-yl)benzene-1,3-dicarbonitrile)imidazole (**2**, 3CzIPN imidazole).

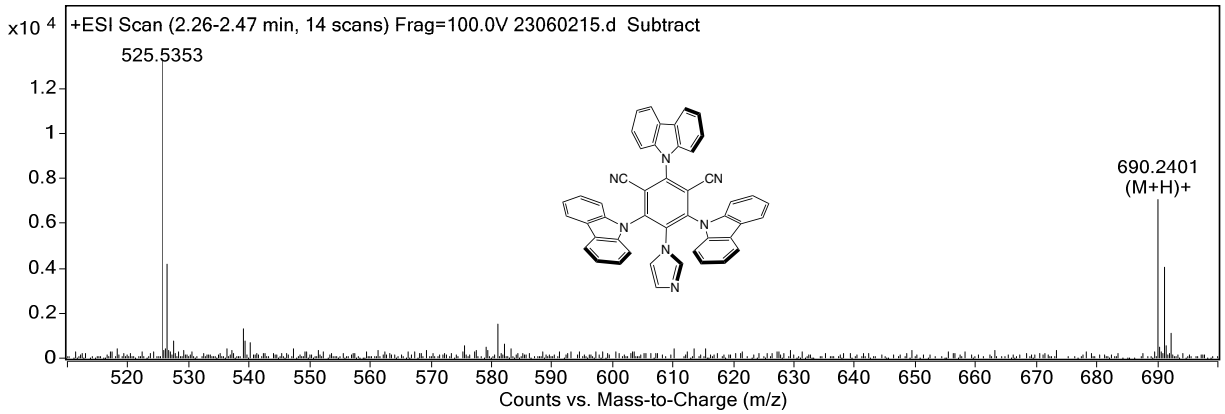

Figure S8. ^{1}H NMR spectrum of 1-(2,4,6-tri(9H-carbazol-9-yl)benzene-1,3-dicarbonitrile)-3-benzyl imidazolium bromide in $CDCl_3$.

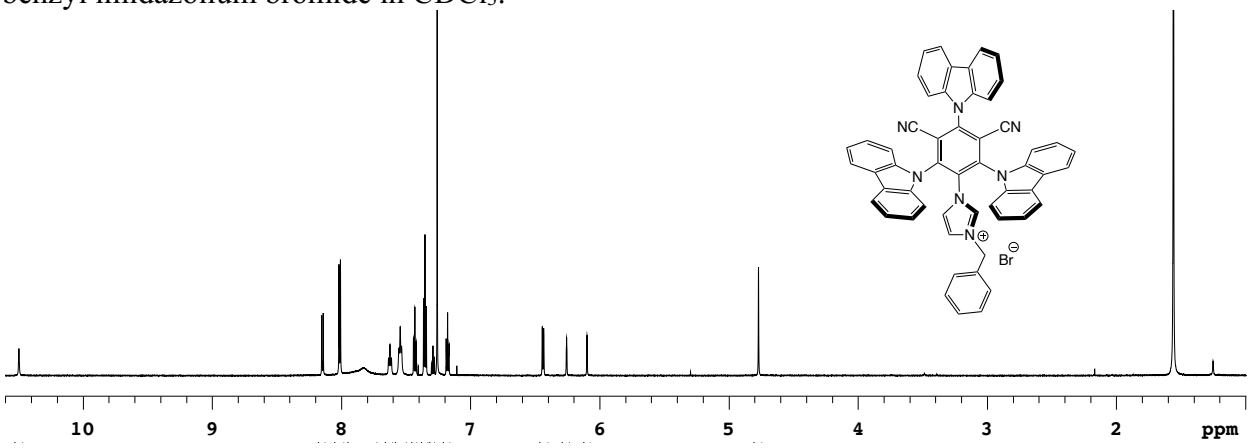

Figure S9. $^{13}C\{^{1}H\}$ NMR spectrum of 1-(2,4,6-tri(9H-carbazol-9-yl)benzene-1,3-dicarbonitrile)-3-benzyl imidazolium bromide in DMSO.

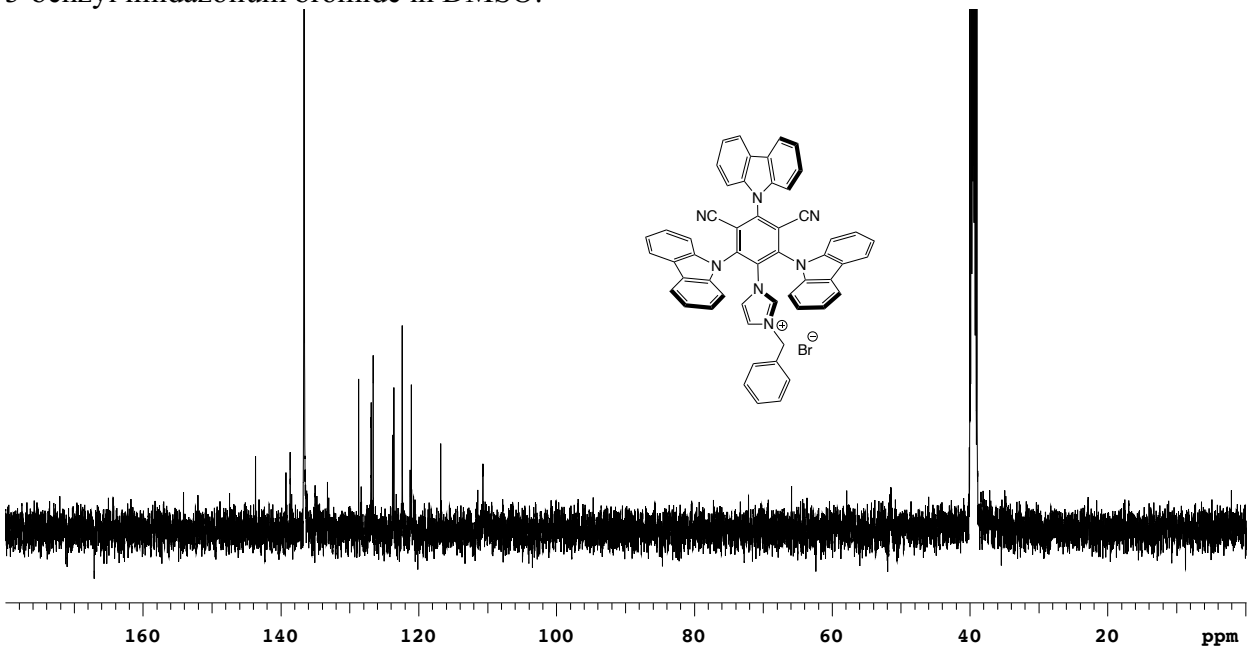

Figure S10. HRMS-ESI spectrum of 1-(2,4,6-tri(9H-carbazol-9-yl)benzene-1,3-dicarbonitrile)-3-benzyl imidazolium bromide.

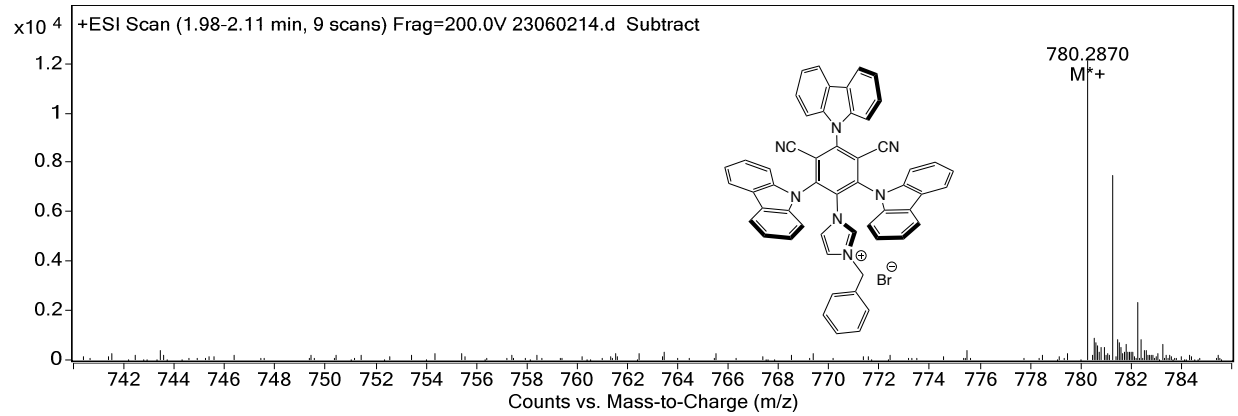

Figure S11. ^{1}H NMR spectrum of 1-(2,4,6-tri(9H-carbazol-9-yl)benzene-1,3-dicarbonitrile)-3-benzyl imidazolium tetrafluoroborate (**3**) in $CDCl_3$.

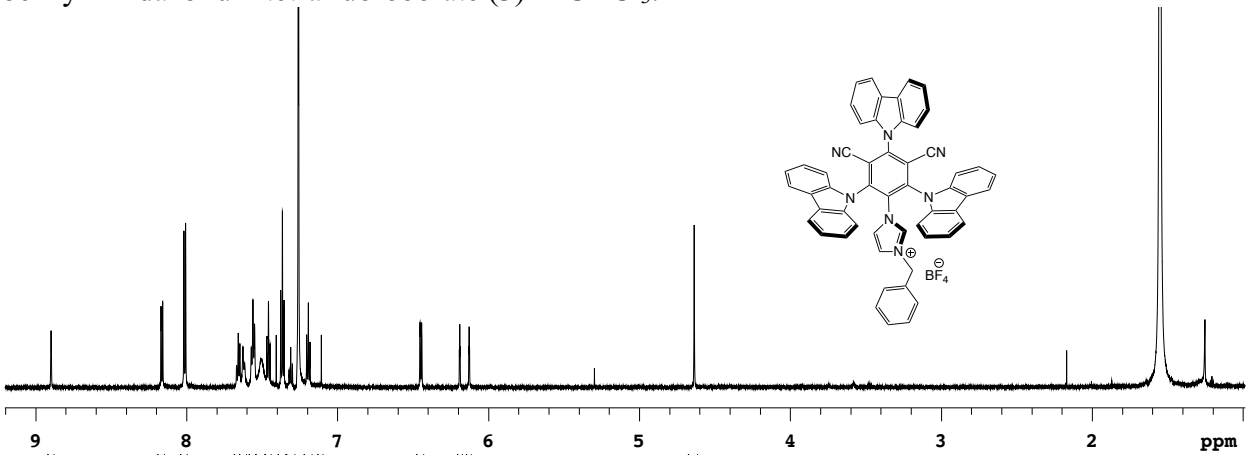

Figure S12. $^{13}C\{^{1}H\}$ NMR spectrum of 1-(2,4,6-tri(9H-carbazol-9-yl)benzene-1,3-dicarbonitrile)-3-benzyl imidazolium tetrafluoroborate (**3**) in $CDCl_3$.

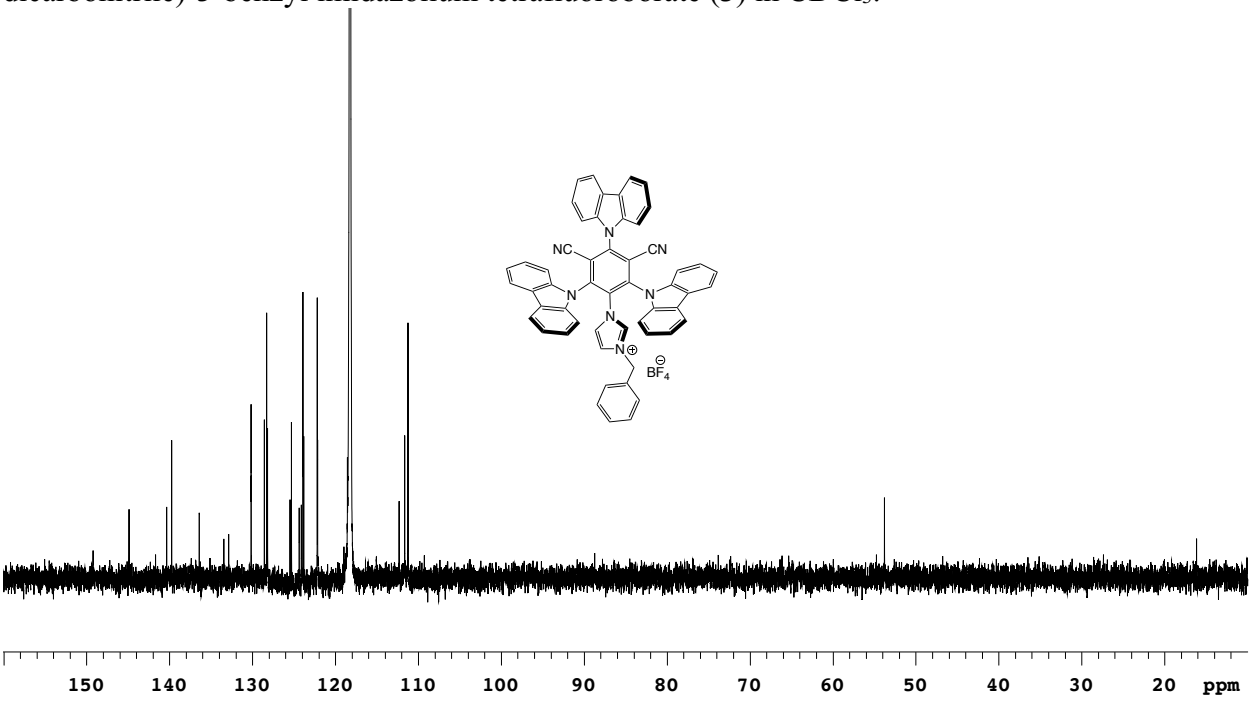

Figure S13. HRMS-ESI spectrum of 1-(2,4,6-tri(9H-carbazol-9-yl)benzene-1,3-dicarbonitrile)-3-benzyl imidazolium tetrafluoroborate (**3**).

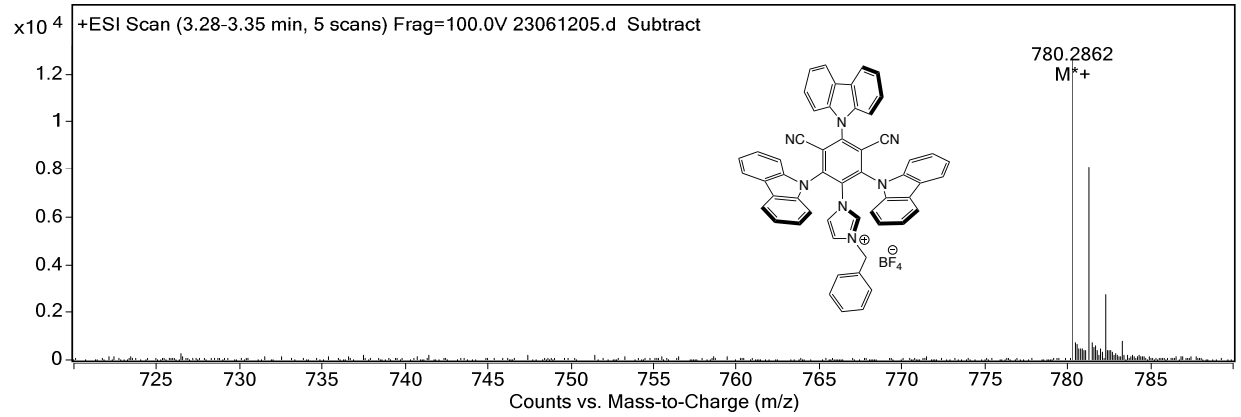

Figure S14. ^{1}H NMR spectrum of 1-(2,4,6-tri(9*H*-carbazol-9-yl)benzene-1,3-dicarbonitrile)-3-isopropyl-imidazolium tetrafluoroborate (**4**) in $CDCl_3$.

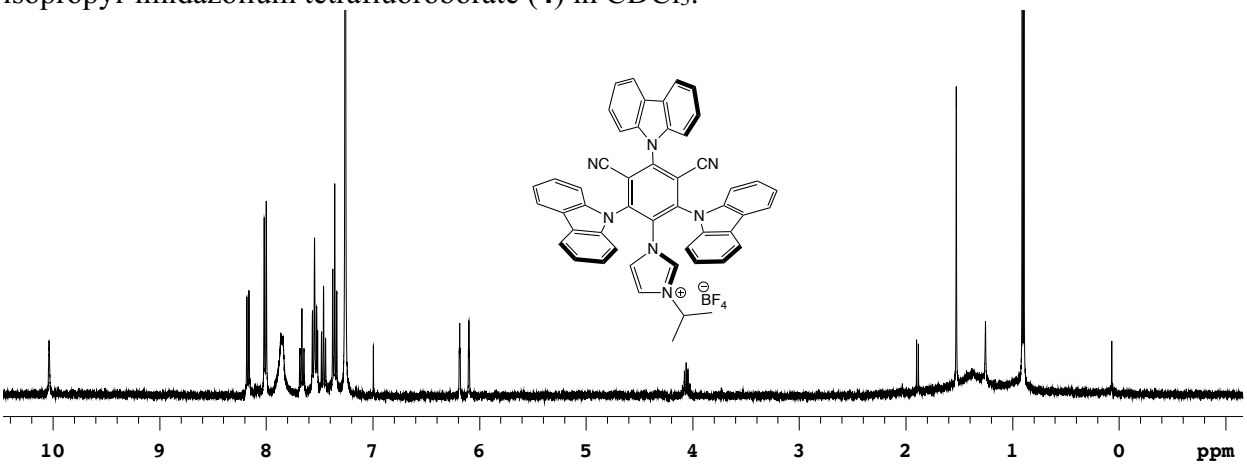

Figure S15. $^{13}C\{^{1}H\}$ NMR spectrum of 1-(2,4,6-tri(9*H*-carbazol-9-yl)benzene-1,3-dicarbonitrile)-3-isopropyl-imidazolium tetrafluoroborate (**4**) in CD_3CN.

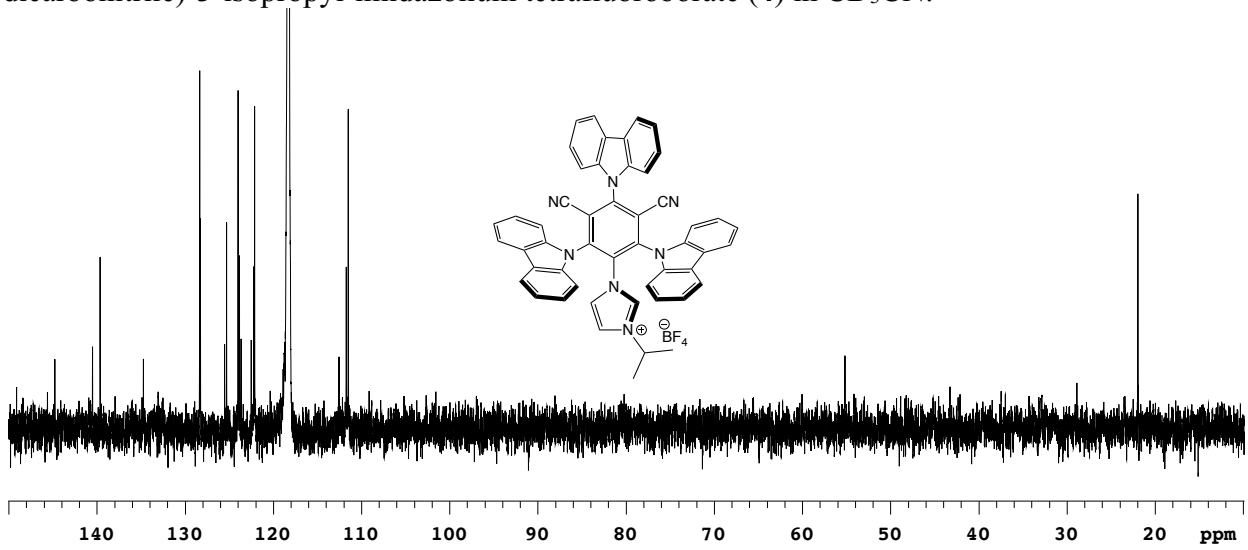

Figure S16. HRMS-ESI spectrum of 1-(2,4,6-tri(9*H*-carbazol-9-yl)benzene-1,3-dicarbonitrile)-3-isopropyl-imidazolium tetrafluoroborate (**4**).

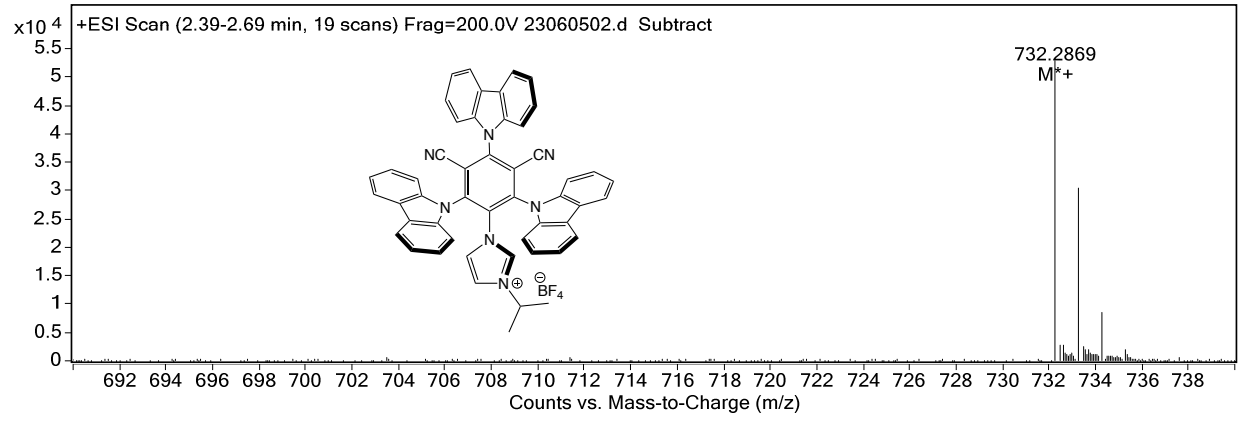

Figure S17. ^{1}H NMR spectrum of $Re(bpy)(CO)_3Cl$ in $(CD_3)_2CO$.

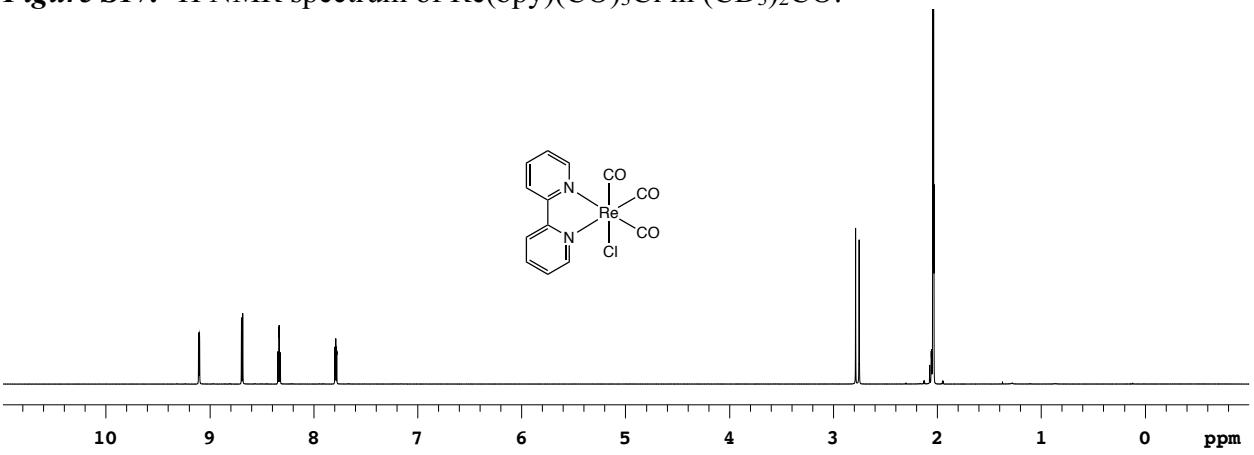

Figure S18. $^{13}C\{^{1}H\}$ NMR spectrum of $Re(bpy)(CO)_3Cl$ in $(CD_3)_2CO$.

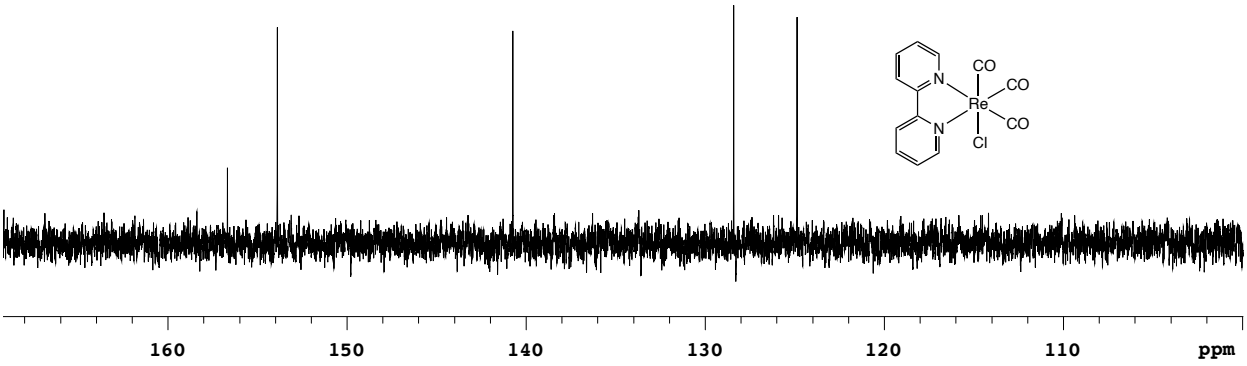

Figure S19. HRMS-ESI spectrum of $Re(bpy)(CO)_3Cl$.

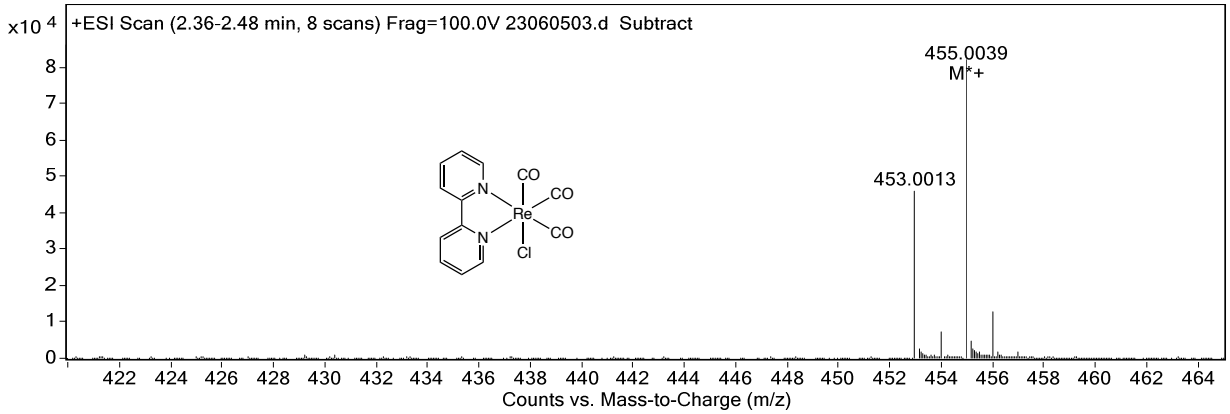

Figure S20. ^{1}H NMR spectrum of $Re(bpy)(CO)_3(acetone)$ in $(CD_3)_2CO$ (**5**).

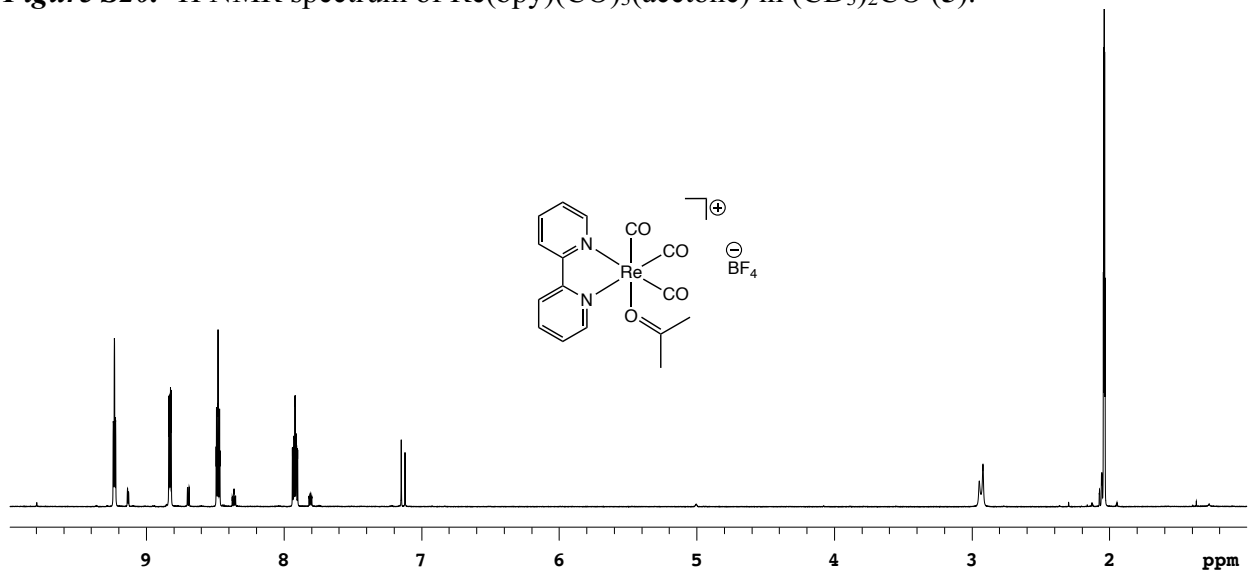

Figure S21. $^{13}C\{^{1}H\}$ NMR spectrum of $Re(bpy)(CO)_3(acetone)$ in $(CD_3)_2CO$ (**5**).

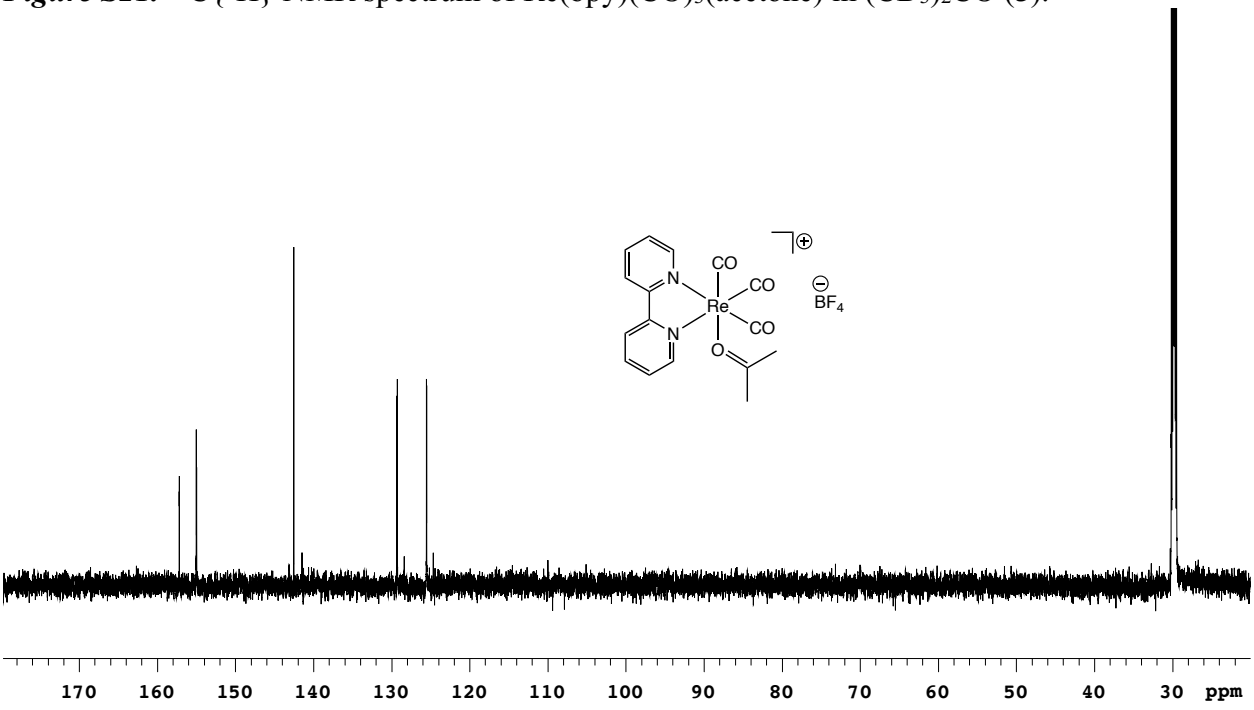

Figure S22. ^{1}H NMR spectrum of Re(bpy)$(CO)_3$(**2**) in $(CD_3)_2CO$.

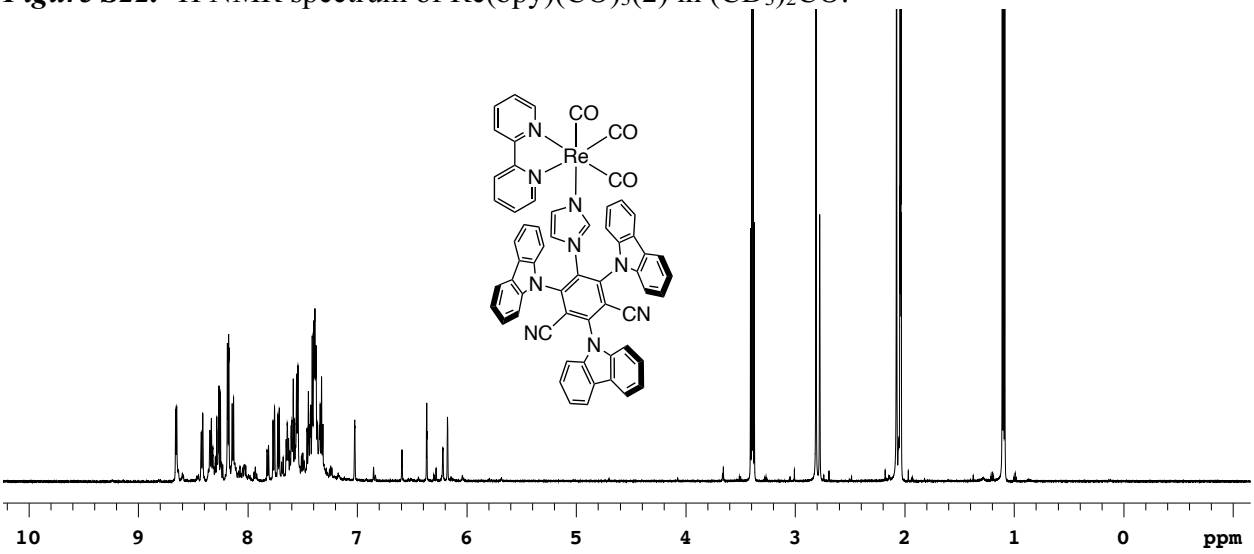

Figure S23. $^{13}C\{^{1}H\}$ NMR spectrum of Re(bpy)$(CO)_3$(**2**) in $(CD_3)_2CO$.

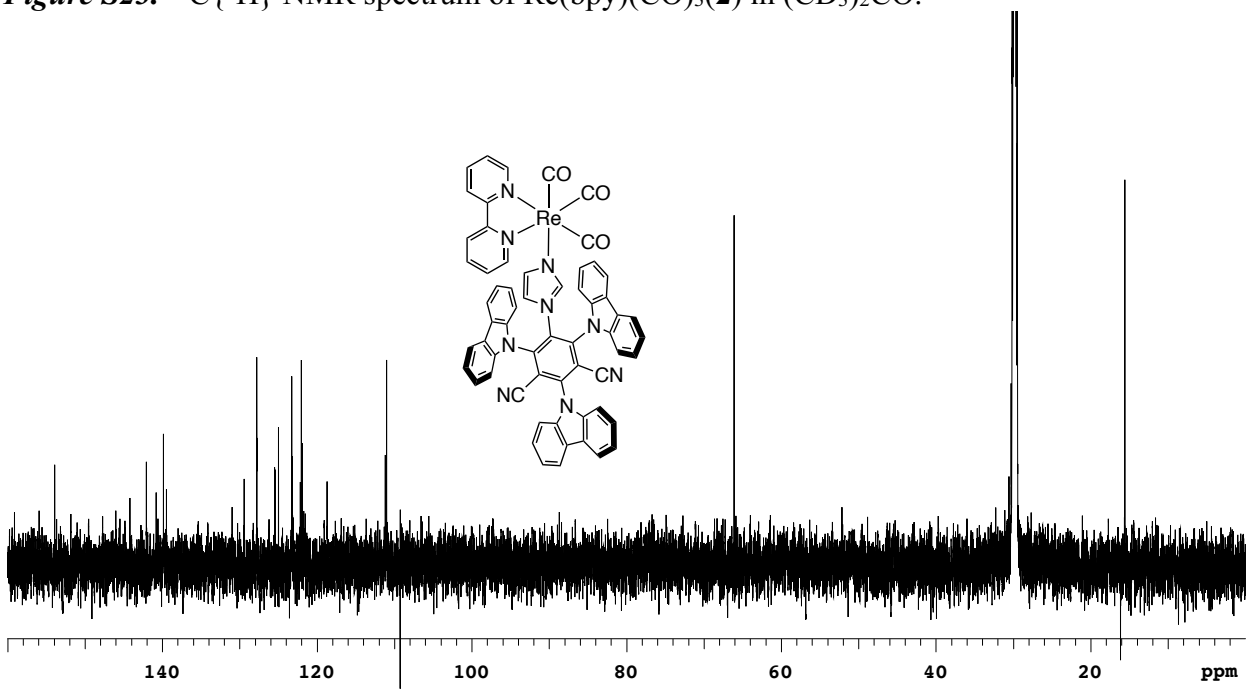

Figure S24. HRMS-ESI spectrum of Re(bpy)(CO)$_3$(**2**).

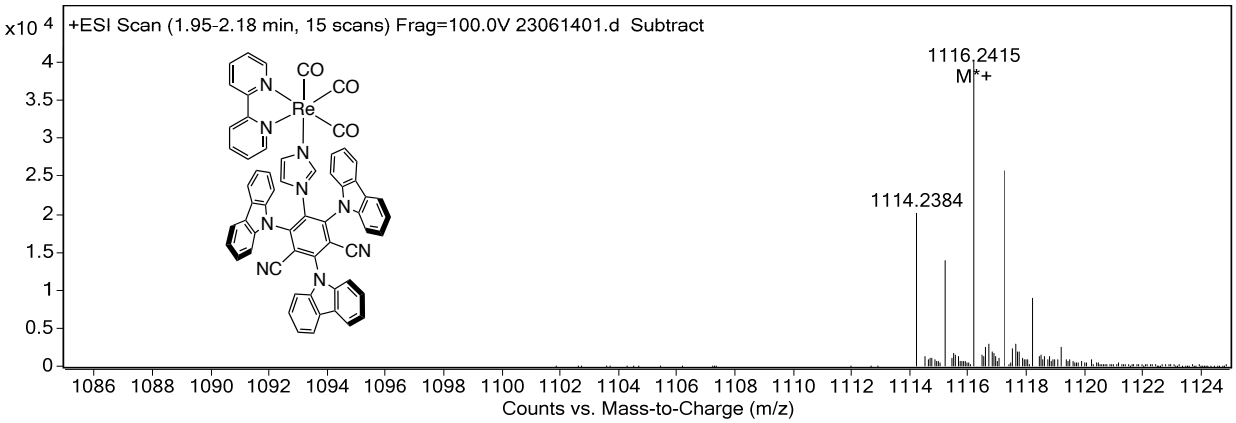

Figure S25. ^{1}H NMR spectrum of benzyl free NHC (**8**) in d_8-THF.

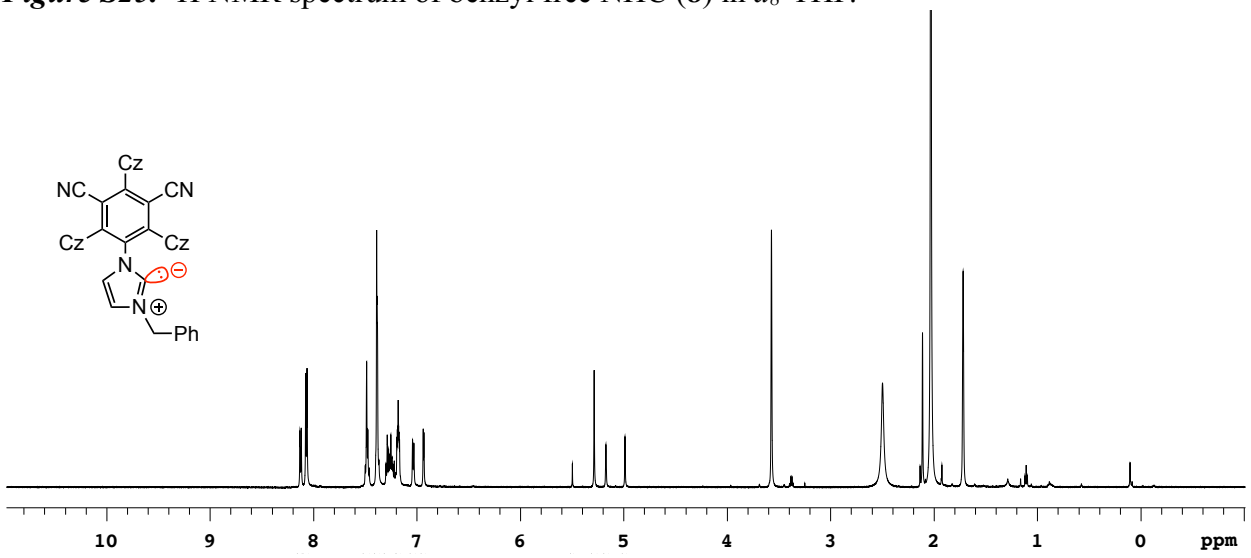

Figure S26. ^{1}H NMR spectrum of Re(bpy)(CO)$_3$(**8**) in d_8-THF.

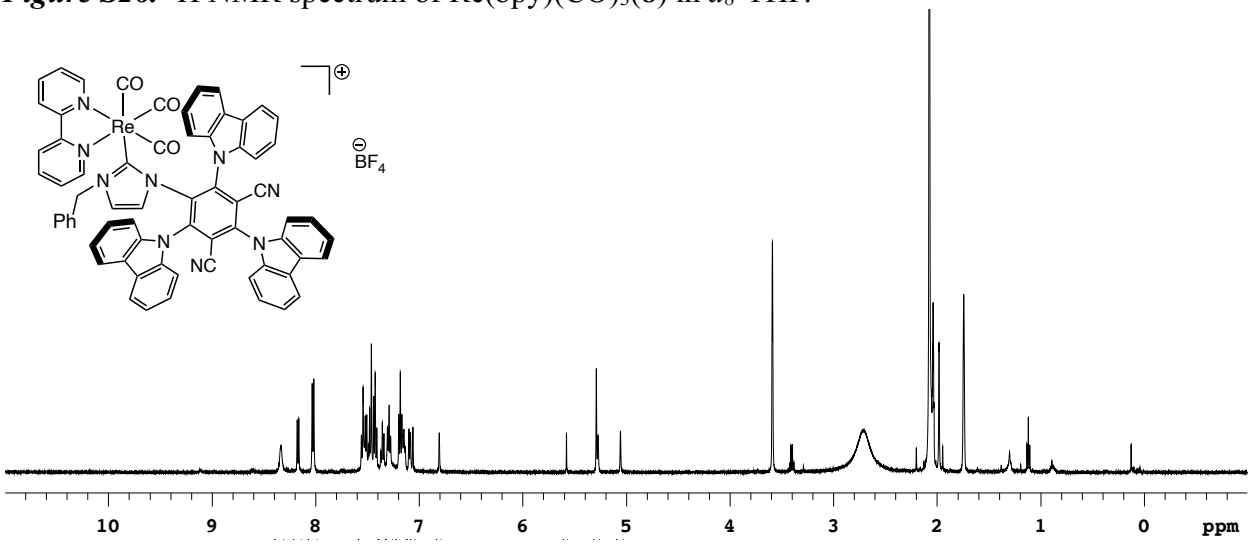

Figure S27. ^{13}C NMR spectrum of Re(bpy)(CO)$_3$(**8**) in d_8-THF.

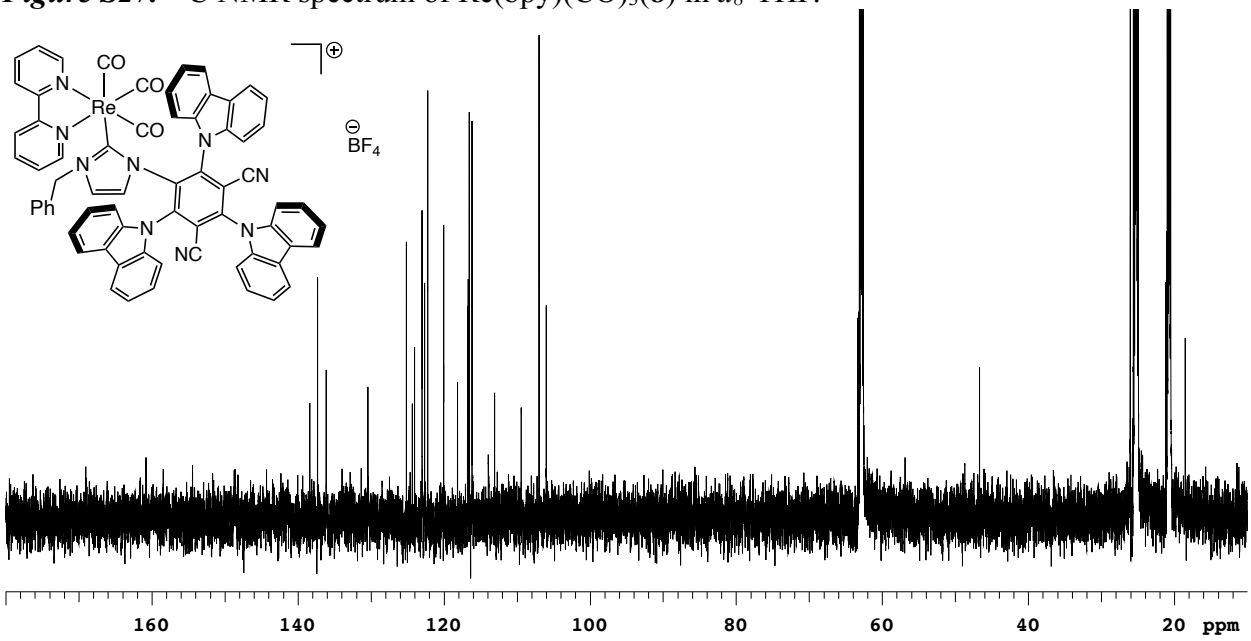

Figure S28. ^{1}H NMR spectrum of Re(bpy)(CO)$_3$(**9**) in $(CD_3)_2CO$.

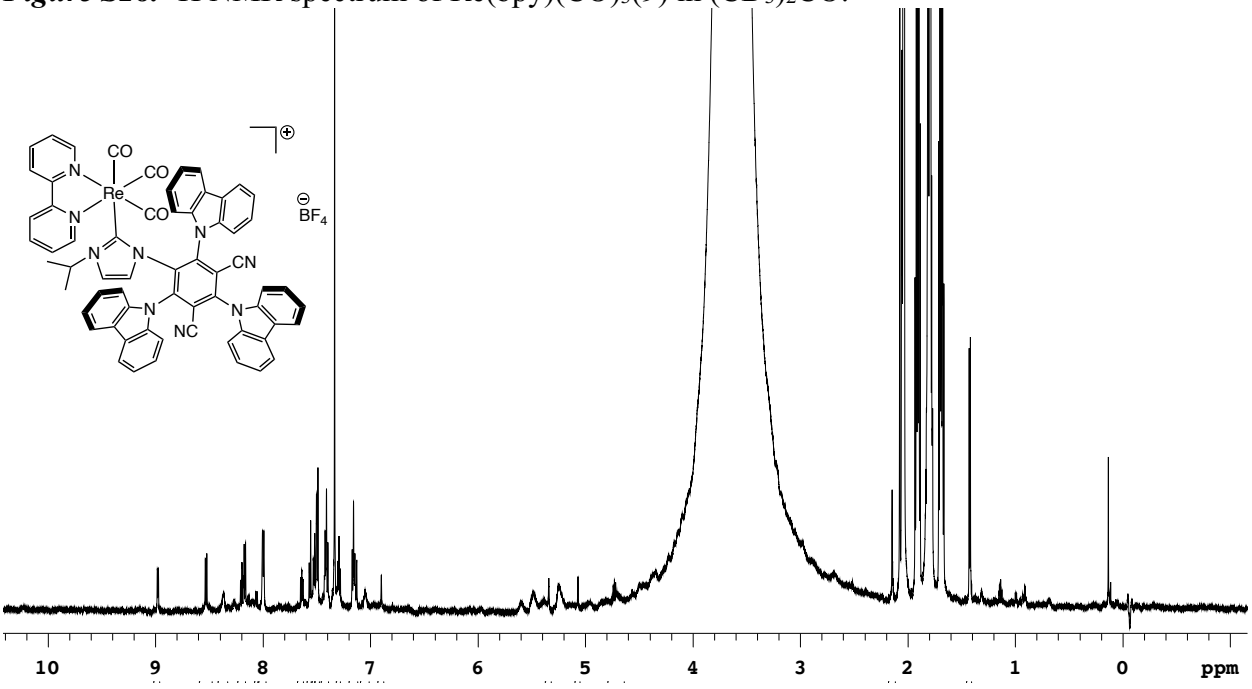

Figure S29. FTIR spectrum of Re(bpy)$(CO)_3$(**9**) in $(CD_3)_2CO$/THF.

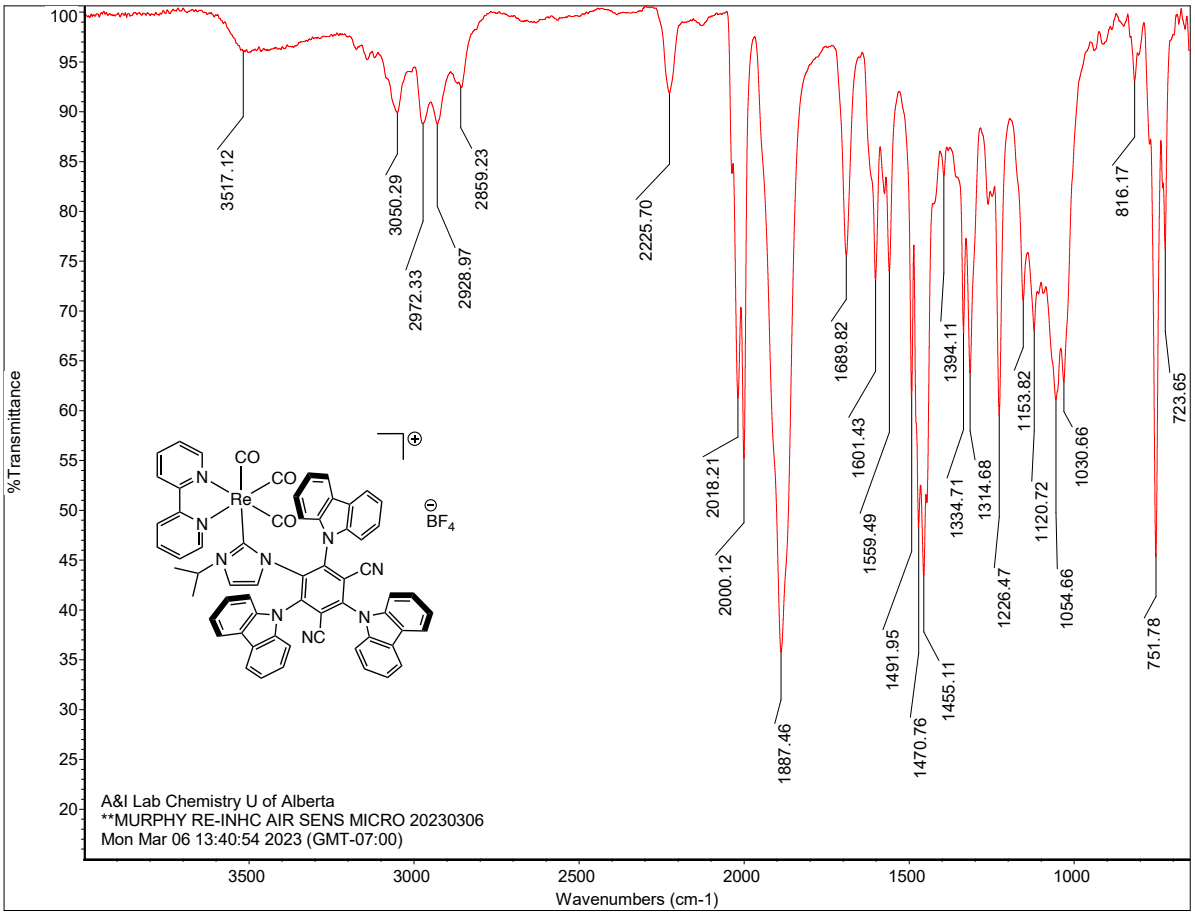

Figure S30. ^{1}H NMR spectrum of 1,3-dimethyl-2-phenylbenzimidazolium iodide in CD_3CN.

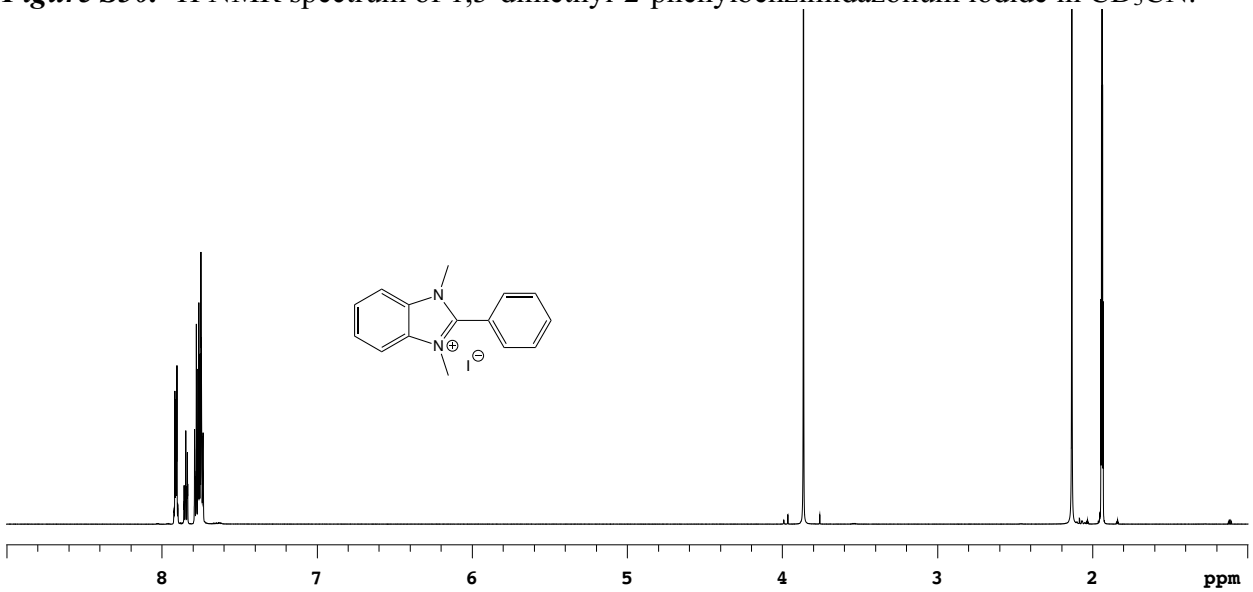

Figure S31. $^{13}C\{^{1}H\}$ NMR spectrum of 1,3-dimethyl-2-phenylbenzimidazolium iodide in CD_3CN.

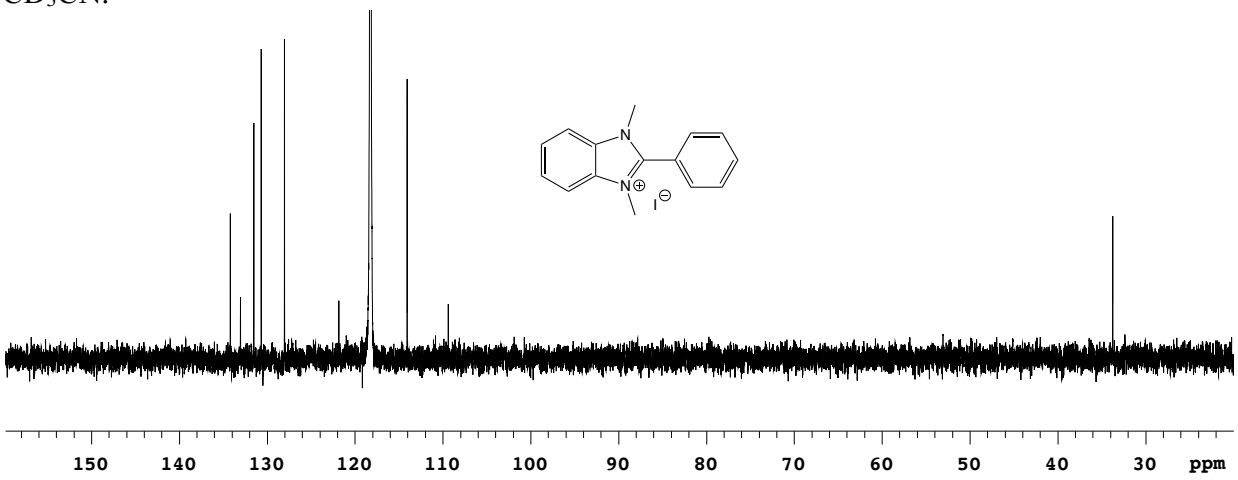

Figure S32. HRMS-ESI spectrum of 1,3-dimethyl-2-phenyl-benzimidazolium iodide.

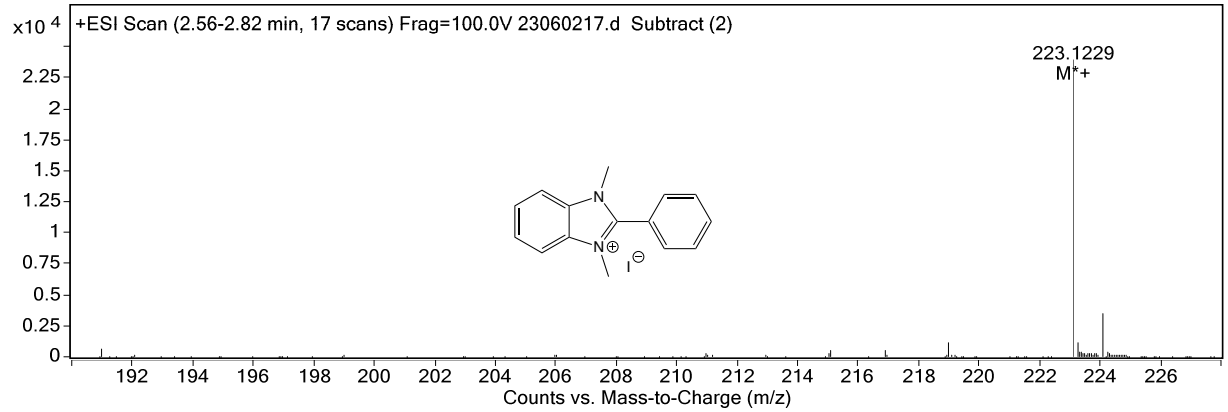

Figure S33. ^{1}H NMR spectrum of 1,3-dimethyl-2-phenyl-2,3-dihydro-1D-benzimidazole in CD_3CN (**10**).

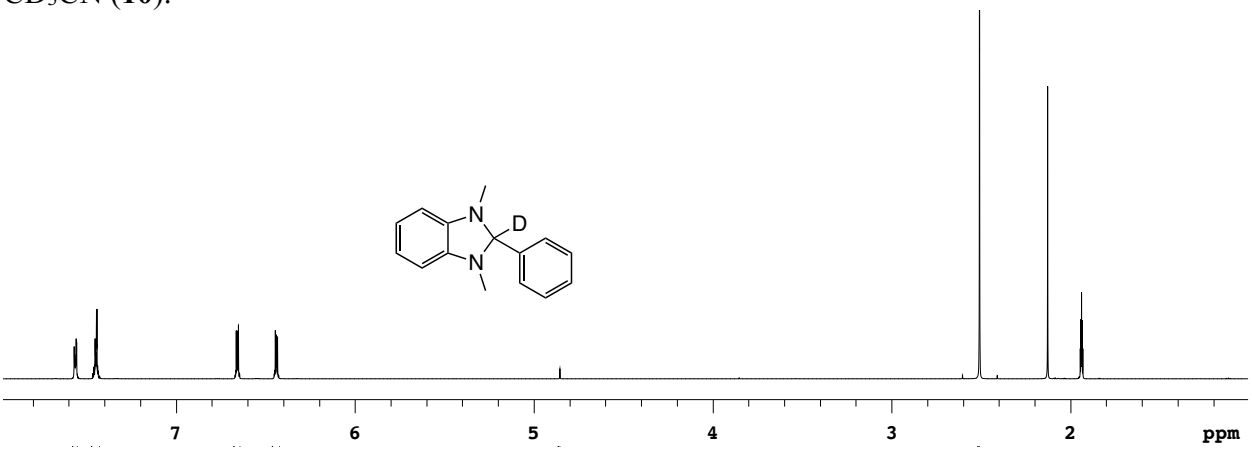

Figure S34. $^{13}C\{^{1}H\}$ NMR spectrum of 1,3-dimethyl-2-phenyl-2,3-dihydro-1D-benzimidazole in CD_3CN (**10**).

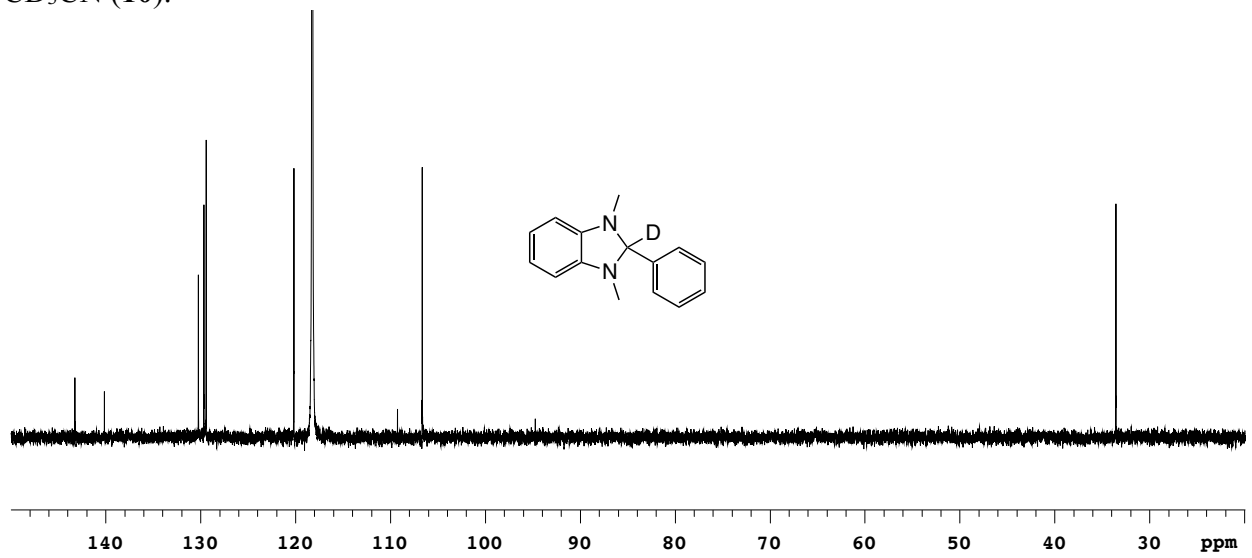

Figure S35. HRMS-ESI spectrum of 1,3-dimethyl-2-phenyl-2,3-dihydro-1D-benzimidazole (**10**).

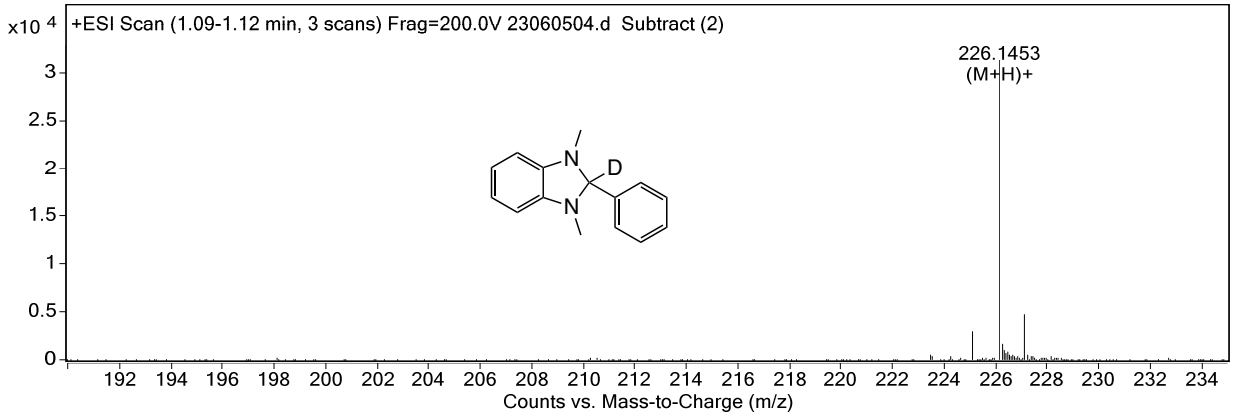

Figure S36. ^{1}H NMR spectrum of 1-methyl-2-phenylbenzimidazole in CD_3CN (**12**).

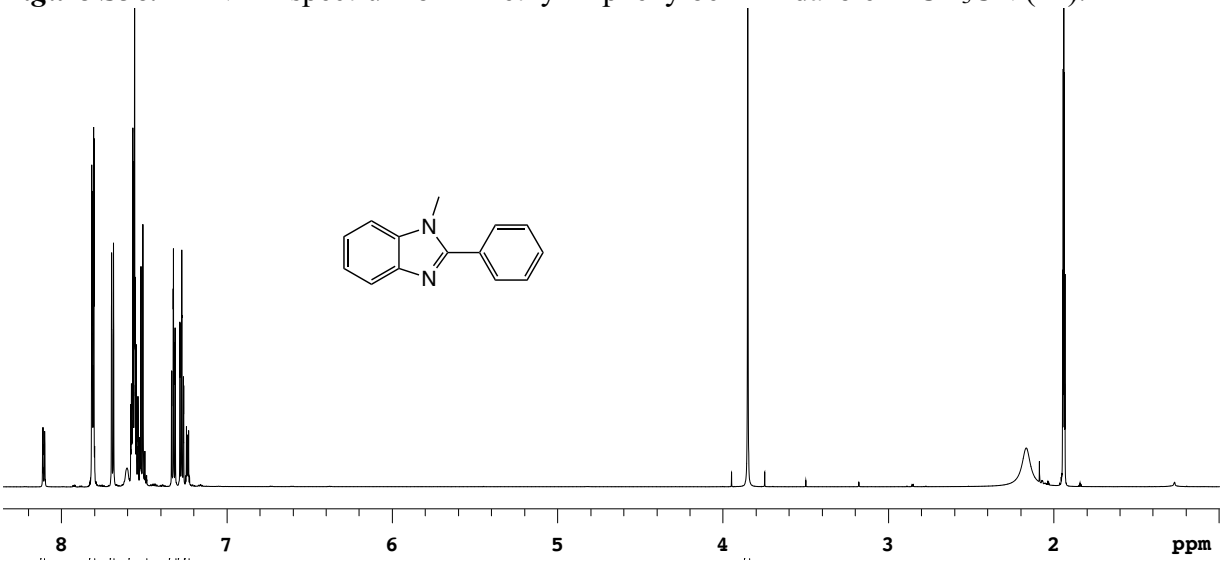

Figure S37. $^{13}C\{^{1}H\}$ NMR spectrum of 1-methyl-2-phenylbenzimidazole in CD_3CN (**12**).

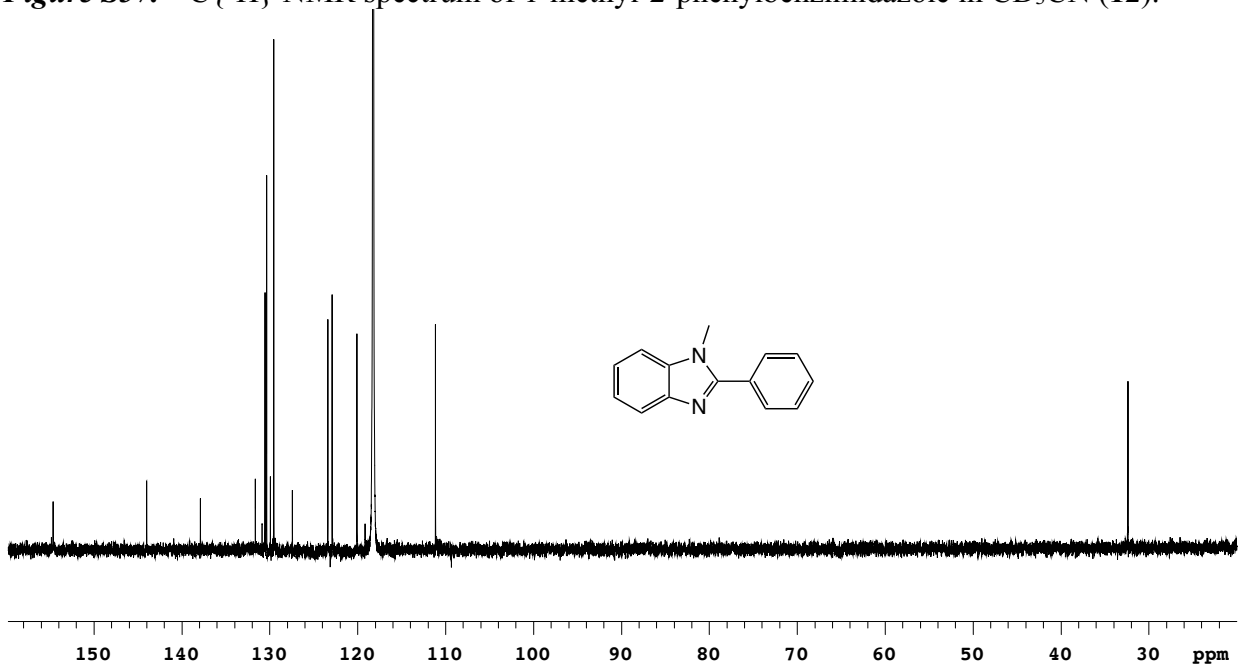

Figure S38. HRMS-ESI spectrum of 1-methyl-2-phenylbenzimidazole (**12**).

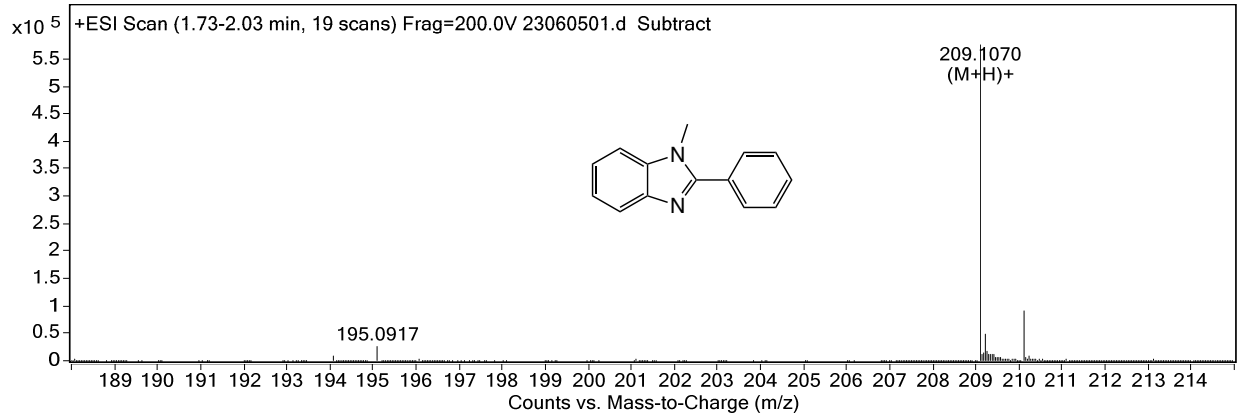

Figure S39. ^{1}H NMR spectrum of complex **5** after addition of D_2O in $(CD_3)_2CO$.

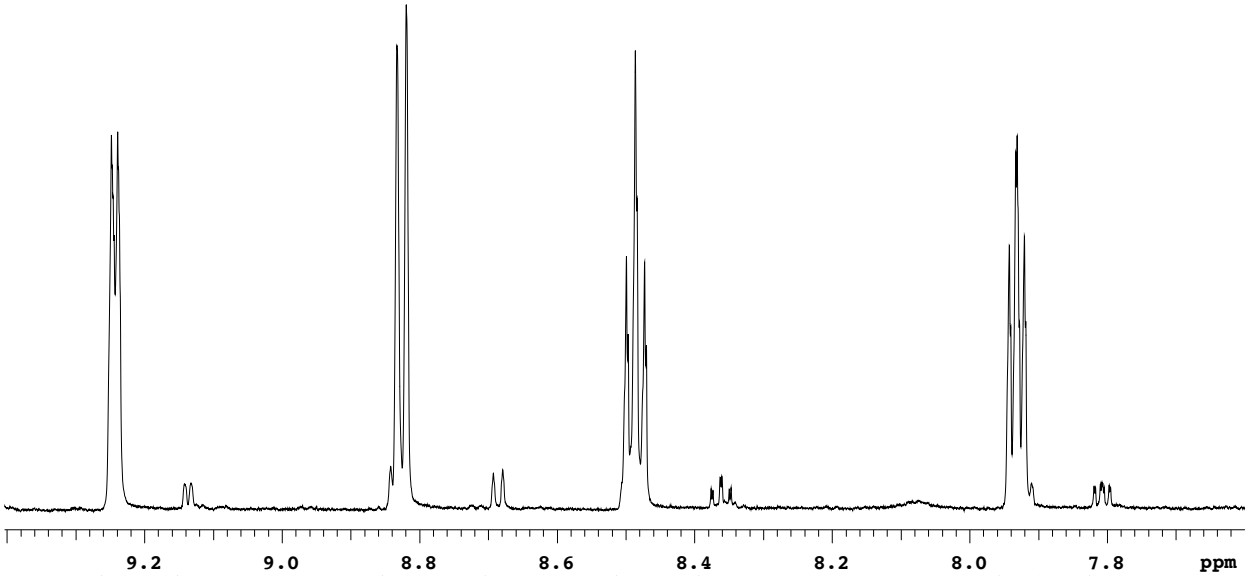

Figure S40. ^{1}H NMR spectrum of complex **5** after reaction with N-methyl imidazole in $(CD_3)_2CO$.

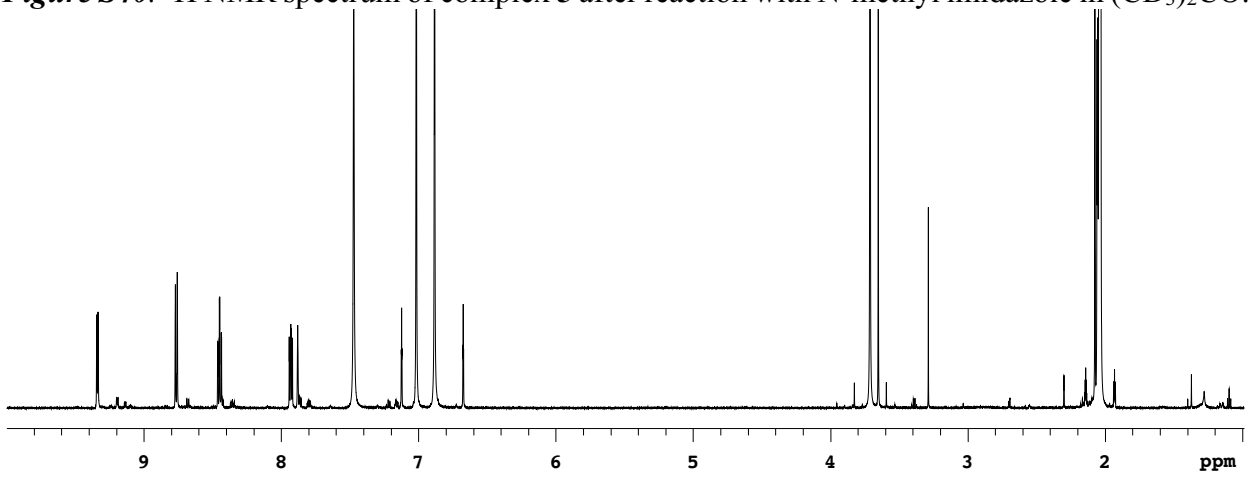

Figure S41. HRMS-ESI spectrum of [BI^+] [HCO_3^-] precipitate.

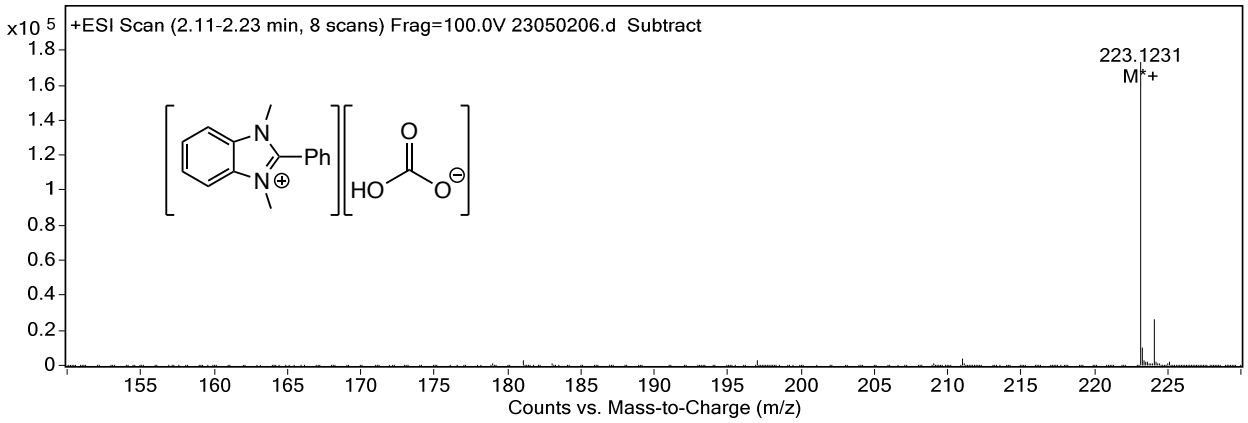

REFERENCES

1. Li, K.; An, X.; Park, K. H.; Khraisheh, M.; Tang, J. A Critical Review of CO2 Photoconversion: Catalysts and Reactors. *Catalysis Today* **2014**, *224*, 3–12. DOI:10.1016/j.cattod.2013.12.006.
2. NASA. Carbon Dioxide Concentration. https://climate.nasa.gov/vital-signs/carbon-dioxide/ (accessed 2023-05-26).
3. IPCC. Headline Statements. https://www.ipcc.ch/sr15/resources/headline-statements/ (accessed 2023-05-26).
4. Wang, W.-N.; Soulis, J.; Yang, Y. J.; Biswas, P. Comparison of CO2 Photoreduction Systems: A Review. *Aerosol and Air Quality Research* **2014**, *14* (2), 533–549. DOI:10.4209/aaqr.2013.09.0283.
5. Thompson, W. A.; Sanchez Fernandez, E.; Maroto-Valer, M. M. Review and Analysis of CO2 Photoreduction Kinetics. *ACS Sustainable Chemistry & Engineering* **2020**, *8* (12), 4677–4692. DOI:10.1021/acssuschemeng.9b06170.
6. Government of Alberta. Carbon Capture, Utilization and Storage – Development and Innovation. https://www.alberta.ca/carbon-capture-utilization-and-storage-development-and-innovation.aspx (accessed 2023-05-26).
7. Bizzarri, C. Homogeneous Systems Containing Earth-abundant Metal Complexes for Photoactivated CO2 Reduction: Recent Advances. *European Journal of Organic Chemistry* **2022**, *2022* (24). DOI:10.1002/ejoc.202200185.
8. Steinlechner, C.; Roesel, A. F.; Oberem, E.; Päpcke, A.; Rockstroh, N.; Gloaguen, F.; Lochbrunner, S.; Ludwig, R.; Spannenberg, A.; Junge, H.; Francke, R.; Beller, M. Selective Earth-Abundant System for CO2 Reduction: Comparing Photo- and Electrocatalytic Processes. *ACS Catalysis* **2019**, *9* (3), 2091–2100. DOI:10.1021/acscatal.8b03548.
9. Chang, X.; Wang, T.; Gong, J. Co2 Photo-Reduction: Insights Into Co2 Activation and Reaction on Surfaces of Photocatalysts. *Energy & Environmental Science* **2016**, *9* (7), 2177–2196. DOI:10.1039/c6ee00383d.
10. Kuramochi, Y.; Ishitani, O.; Ishida, H. Reaction Mechanisms of Catalytic Photochemical CO2 Reduction Using Re(I) and Ru(II) Complexes. *Coordination Chemistry Reviews* **2018**, *373*, 333–356. DOI:10.1016/j.ccr.2017.11.023.
11. Mikkelsen, M.; Jørgensen, M.; Krebs, F. C. The TERATON Challenge. A Review of Fixation and Transformation of Carbon Dioxide. *Energy Environ. Sci.* **2010**, *3* (1), 43–81. DOI:10.1039/b912904a.
12. Wang, W.-H.; Himeda, Y.; Muckerman, J. T.; Manbeck, G. F.; Fujita, E. Co2 Hydrogenation to Formate and Methanol as an Alternative to Photo- and Electrochemical CO_2 Reduction. *Chemical Reviews* **2015**, *115* (23), 12936–12973. DOI:10.1021/acs.chemrev.5b00197.
13. Schwarz, H. A.; Dodson, R. W. Reduction Potentials of CO_2- and the Alcohol Radicals. *The Journal of Physical Chemistry* **1989**, *93* (1), 409–414. DOI:10.1021/j100338a079.
14. Hildebrandt, D.; Glasser, D.; Hausberger, B.; Patel, B.; Glasser, B. J. Producing Transportation Fuels with Less Work. *Science* **2009**, *323* (5922), 1680–1681. DOI:10.1126/science.1168455.
15. Singh, A. K.; Singh, S.; Kumar, A. Hydrogen Energy Future with Formic Acid: A Renewable Chemical Hydrogen Storage System. *Catalysis Science & Technology* **2016**, *6* (1), 12–40. DOI:10.1039/c5cy01276g.

16. Takeda, H.; Ishitani, O. Development of Efficient Photocatalytic Systems for CO2 Reduction Using Mononuclear and Multinuclear Metal Complexes Based on Mechanistic Studies. *Coordination Chemistry Reviews* **2010**, *254* (3–4), 346–354. DOI:10.1016/j.ccr.2009.09.030.
17. Inoue, H.; Shimada, T.; Kou, Y.; Nabetani, Y.; Masui, D.; Takagi, S.; Tachibana, H. The Water Oxidation Bottleneck in Artificial Photosynthesis: How Can We Get through It? An Alternative Route Involving a Two-Electron Process. *ChemSusChem* **2011**. DOI:10.1002/cssc.201000385.
18. Kuramochi, Y.; Itabashi, J.; Fukaya, K.; Enomoto, A.; Yoshida, M.; Ishida, H. Unexpected Effect of Catalyst Concentration on Photochemical CO_2 Reduction by Trans(Cl)–Ru(Bpy)$(CO)_2Cl_2$: New Mechanistic Insight into the CO/$HCOO^-$ Selectivity. *Chemical Science* **2015**, 6 (5), 3063–3074. DOI:10.1039/c5sc00199d.
19. Ishida, H.; Terada, T.; Tanaka, K.; Tanaka, T. Photochemical Carbon Dioxide Reduction Catalyzed by Bis(2,2'-Bipyridine)Dicarbonylruthenium(2^+) Using Triethanolamine and 1-Benzyl-1,4-Dihydronicotinamide as an Electron Donor. *Inorganic Chemistry* **1990**, 29 (5), 905–911. DOI:10.1021/ic00330a004.
20. Kittler, L. Photoinduced Electron Transfer. Part C. Photoinduced Electron Transfer Reactions: Organic Substrates. *Bioelectrochemistry and Bioenergetics* **1989**, 22 (2), 170–171. DOI:10.1016/0302-4598(89)80051-0. 67 - 41
21. Tamaki, Y.; Morimoto, T.; Koike, K.; Ishitani, O. Photocatalytic Co2 Reduction with High Turnover Frequency and Selectivity of Formic Acid Formation Using Ru(II) Multinuclear Complexes. *Proceedings of the National Academy of Sciences* **2012**, *109* (39), 15673–15678. DOI:10.1073/pnas.1118336109.
22. Tamaki, Y.; Koike, K.; Morimoto, T.; Ishitani, O. Substantial Improvement in the Efficiency and Durability of a Photocatalyst for Carbon Dioxide Reduction Using a Benzoimidazole Derivative as an Electron Donor. *Journal of Catalysis* **2013**, *304*, 22–28. DOI:10.1016/j.jcat.2013.04.002.
23. Hasegawa, E.; Takizawa, S.; Seida, T.; Yamaguchi, A.; Yamaguchi, N.; Chiba, N.; Takahashi, T.; Ikeda, H.; Akiyama, K. Photoinduced Electron-Transfer Systems Consisting of Electron-Donating Pyrenes or Anthracenes and Benzimidazolines for Reductive Transformation of Carbonyl Compounds. *Tetrahedron* **2006**, *62* (27), 6581–6588. DOI:10.1016/j.tet.2006.03.061.
24. Kuramochi, Y.; Ishitani, O. Iridium(III) 1-Phenylisoquinoline Complexes as a Photosensitizer for Photocatalytic CO_2 Reduction: A Mixed System with a Re(I) Catalyst and a Supramolecular Photocatalyst. *Inorganic Chemistry* **2016**, *55* (11), 5702–5709. DOI:10.1021/acs.inorgchem.6b00777.
25. Yamazaki, Y.; Takeda, H.; Ishitani, O. Photocatalytic Reduction of CO_2 Using Metal Complexes. *Journal of Photochemistry and Photobiology C: Photochemistry Reviews* **2015**, *25*, 106–137. DOI:10.1016/j.jphotochemrev.2015.09.001.
26. Lv, M.; Wang, X.; Wang, D.; Li, X.; Liu, Y.; Pan, H.; Zhang, S.; Xu, J.; Chen, J. Unravelling the Role of Charge Transfer State during Ultrafast Intersystem Crossing in Compact Organic Chromophores. *Physical Chemistry Chemical Physics* **2021**, *23* (45), 25455–25466. DOI:10.1039/d1cp02912f.
27. Schultz, D. M.; Yoon, T. P. Solar Synthesis: Prospects in Visible Light Photocatalysis. *Science* **2014**, *343* (6174). DOI:10.1126/science.1239176.

28. Fukuzumi, S.; Ohkubo, K.; Suenobu, T. Long-Lived Charge Separation and Applications in Artificial Photosynthesis. *Accounts of Chemical Research* **2014**, *47* (5), 1455–1464. DOI:10.1021/ar400200u.
29. Romero, N. A.; Nicewicz, D. A. Organic Photoredox Catalysis. *Chemical Reviews* **2016**, *116* (17), 10075–10166. DOI:10.1021/acs.chemrev.6b00057.
30. Jiang, Y.; Weiss, E. A. Colloidal Quantum Dots as Photocatalysts for Triplet Excited State Reactions of Organic Molecules. *Journal of the American Chemical Society* **2020**, *142* (36), 15219–15229. DOI:10.1021/jacs.0c07421.
31. Xiang, H.; Cheng, J.; Ma, X.; Zhou, X.; Chruma, J. J. Near-Infrared Phosphorescence: Materials and Applications. *Chemical Society Reviews* **2013**, *42* (14), 6128. DOI:10.1039/c3cs60029g.
32. Kaji, H.; Suzuki, H.; Fukushima, T.; Shizu, K.; Suzuki, K.; Kubo, S.; Komino, T.; Oiwa, H.; Suzuki, F.; Wakamiya, A.; Murata, Y.; Adachi, C. Purely Organic Electroluminescent Material Realizing 100% Conversion from Electricity to Light. *Nature Communications* **2015**, *6* (1). DOI:10.1038/ncomms9476.
33. Li, Y.; Gecevicius, M.; Qiu, J. Long Persistent Phosphors—from Fundamentals to Applications. *Chemical Society Reviews* **2016**, *45* (8), 2090–2136. DOI:10.1039/c5cs00582e.
34. Yang, Z.; Mao, Z.; Xie, Z.; Zhang, Y.; Liu, S.; Zhao, J.; Xu, J.; Chi, Z.; Aldred, M. P. Recent Advances in Organic Thermally Activated Delayed Fluorescence Materials. *Chemical Society Reviews* **2017**, *46* (3), 915–1016. DOI:10.1039/c6cs00368k.
35. Englman, R.; Jortner, J. The Energy Gap Law for Radiationless Transitions in Large Molecules. *Molecular Physics* **1970**, *18* (2), 145–164. DOI:10.1080/00268977000100171.
36. Zhao, J.; Wu, W.; Sun, J.; Guo, S. Triplet Photosensitizers: From Molecular Design to Applications. *Chemical Society Reviews* **2013**, *42* (12), 5323. DOI:10.1039/c3cs35531d.
37. Takeda, H.; Cometto, C.; Ishitani, O.; Robert, M. Electrons, Photons, Protons and Earth-Abundant Metal Complexes for Molecular Catalysis of CO_2 Reduction. *ACS Catalysis* **2016**, *7* (1), 70–88. DOI:10.1021/acscatal.6b02181.
38. Kimura, E.; Wada, S.; Shionoya, M.; Okazaki, Y. New Series of Multifunctionalized Nickel(II)-Cyclam (Cyclam = 1,4,8,11-Tetraazacyclotetradecane) Complexes. Application to the Photoreduction of Carbon Dioxide. *Inorganic Chemistry* **1994**, *33* (4), 770–778. DOI:10.1021/ic00082a025.
39. Suzuki, K.; Kobayashi, A.; Kaneko, S.; Takehira, K.; Yoshihara, T.; Ishida, H.; Shiina, Y.; Oishi, S.; Tobita, S. Reevaluation of Absolute Luminescence Quantum Yields of Standard Solutions Using a Spectrometer with an Integrating Sphere and a Back-Thinned CCD Detector. *Physical Chemistry Chemical Physics* **2009**, 11 (42), 9850. DOI:10.1039/b912178a.
40. Tamaki, Y.; Watanabe, K.; Koike, K.; Inoue, H.; Morimoto, T.; Ishitani, O. Development of Highly Efficient Supramolecular CO_2 Reduction Photocatalysts with High Turnover Frequency and Durability. *Faraday Discuss* **2012**, *155*, 115–127. DOI:10.1039/c1fd00091h.
41. Tamaki, Y.; Koike, K.; Morimoto, T.; Yamazaki, Y.; Ishitani, O. Red-Light-Driven Photocatalytic Reduction of CO_2 Using Os(II)–Re(I) Supramolecular Complexes. *Inorganic Chemistry* **2013**, *52* (20), 11902–11909. DOI:10.1021/ic4015543.

42. Hay, P. J. Theoretical Studies of the Ground and Excited Electronic States in Cyclometalated Phenylpyridine Ir(III) Complexes Using Density Functional Theory. *The Journal of Physical Chemistry* **2002**, 106 (8), 1634–1641. DOI:10.1021/jp013949w.
43. Kapturkiewicz, A.; Angulo, G. Extremely Efficient Electrochemiluminescence Systems Based on Tris(2-Phenylpyridine)Iridium(III). *Dalton Transactions* **2003**, No. 20, 3907. DOI:10.1039/b308964a.
44. Garces, F. O.; King, K. A.; Watts, R. J. Synthesis, Structure, Electrochemistry, and Photophysics of Methyl-Substituted Phenylpyridine Ortho-Metalated Iridium(III) *Complexes. Inorganic Chemistry* **1988**, 27 (20), 3464–3471. DOI:10.1021/ic00293a008.
45. Colombo, M. G.; Brunold, T. C.; Riedener, T.; Guedel, H. U.; Fortsch, M.; Buergi, H.-B. Facial Tris Cyclometalated Rhodium(3^+) and Iridium(3^+) Complexes: Their Synthesis, Structure, and Optical Spectroscopic Properties. *Inorganic Chemistry* **1994**, *33* (3), 545–550. DOI:10.1021/ic00081a024.
46. King, K. A.; Spellane, P. J.; Watts, R. J. Excited-State Properties of a Triply Ortho-Metalated Iridium(III) Complex. *Journal of the American Chemical Society* **1985**, 107 (5), 1431–1432. DOI:10.1021/ja00291a064.
47. Morimoto, T.; Nishiura, C.; Tanaka, M.; Rohacova, J.; Nakagawa, Y.; Funada, Y.; Koike, K.; Yamamoto, Y.; Shishido, S.; Kojima, T.; Saeki, T.; Ozeki, T.; Ishitani, O. Ring-Shaped Re(I) Multinuclear Complexes with Unique Photofunctional Properties. *Journal of the American Chemical Society* **2013**, *135* (36), 13266–13269. DOI:10.1021/ja406144h.
48. Tsubaki, H.; Tohyama, S.; Koike, K.; Saitoh, H.; Ishitani, O. Effect of Intramolecular π–π and CH–π Interactions between Ligands on Structure, Electrochemical and Spectroscopic Properties of Fac-[Re(Bpy)$(CO)_3(PR_3)]^+$(Bpy = 2,2′-Bipyridine; PR_3= Trialkyl or Triarylphosphines). *Dalton Trans*. **2005**, No. 2, 385–395. DOI:10.1039/b407947g.
49. Kiyosawa, K.; Shiraishi, N.; Shimada, T.; Masui, D.; Tachibana, H.; Takagi, S.; Ishitani, O.; Tryk, D. A.; Inoue, H. Electron Transfer from the Porphyrin s2 State in a Zinc Porphyrin-Rhenium Bipyridyl Dyad Having Carbon Dioxide Reduction Activity. *The Journal of Physical Chemistry* **2009**, *113* (27), 11667–11673. DOI:10.1021/jp901548y.
50. Kou, Y.; Nakatani, S.; Sunagawa, G.; Tachikawa, Y.; Masui, D.; Shimada, T.; Takagi, S.; Tryk, D. A.; Nabetani, Y.; Tachibana, H.; Inoue, H. Visible Light-Induced Reduction of Carbon Dioxide Sensitized by a Porphyrin–Rhenium Dyad Metal Complex on P-Type Semiconducting NIO as the Reduction Terminal End of an Artificial Photosynthetic System. *Journal of Catalysis* **2014**, 310, 57–66. DOI:10.1016/j.jcat.2013.03.025.
51. Davis, G. A.; Gresser, J. D.; Carapellucci, P. A. Photoreduction of Nitrogen Heterocycles. I. Photoreduction Phenazine: Evidence for Singlet-State Reactivity. *Journal of the American Chemical Society* **1971**, 93 (9), 2179–2182. DOI:10.1021/ja00738a014.
52. Ogata, T.; Yamamoto, Y.; Wada, Y.; Murakoshi, K.; Kusaba, M.; Nakashima, N.; Ishida, A.; Takamuku, S.; Yanagida, S. Phenazine-Photosensitized Reduction of CO_2 Mediated by a Cobalt-Cyclam Complex through Electron and Hydrogen Transfer. *The Journal of Physical Chemistry* **1995**, 99 (31), 11916–11922. DOI:10.1021/j100031a020.
53. Bailey, D. N.; Roe, D. K.; Hercules, D. M. Photoreduction of Phenazine in Acidic Methanol. *Journal of the American Chemical Society* **1968**, 90 (23), 6291–6297. DOI:10.1021/ja01025a007.
54. Matsuoka, S.; Kohzuki, T.; Pac, C.; Ishida, A.; Takamuku, S.; Kusaba, M.; Nakashima, N.; Yanagida, S. Photocatalysis of Oligo(*p*-Phenylenes): Photochemical Reduction of Carbon

Dioxide with Triethylamine. *The Journal of Physical Chemistry* **1992**, 96 (11), 4437–4442. DOI:10.1021/j100190a057.

55. Matsuoka, S.; Fujii, H.; Yamada, T.; Pac, C.; Ishida, A.; Takamuku, S.; Kusaba, M.; Nakashima, N.; Yanagida, S. Photocatalysis of Oligo(*p*-Phenylenes): Photoreductive Production of Hydrogen and Ethanol in Aqueous Triethylamine. *The Journal of Physical Chemistry* **1991**, 95 (15), 5802–5808. DOI:10.1021/j100168a018.
56. Leung, C.-F.; Lau, T.-C. Organic Photosensitizers for Catalytic Solar Fuel Generation. *Energy & Fuels* **2021**, *35*(23), 18888–18899. DOI:10.1021/acs.energyfuels.1c02675.
57. Kuramochi, Y.; Kamiya, M.; Ishida, H. Photocatalytic CO_2 Reduction in *n*,*n*-Dimethylacetamide/Water as an Alternative Solvent System. *Inorganic Chemistry* **2014**, *53* (7), 3326–3332. DOI:10.1021/ic500050q.
58. Rosas-Hernández, A.; Junge, H.; Beller, M. Photochemical Reduction of Carbon Dioxide to Formic Acid Using Ruthenium(II)-Based Catalysts and Visible Light. *ChemCatChem* **2015**, 7 (20), 3316–3321. DOI:10.1002/cctc.201500494.
59. Ishida, H.; Sakaba, A. Temperature Dependence of Photocatalytic CO_2 Reduction by Trans(Cl)–Ru(Bpy)$(CO)_2Cl_2$: Activation Energy Difference between CO and Formate Production. *Faraday Discussions* **2017**, *198*, 263–277. DOI:10.1039/c6fd00242k.
60. Voyame, P.; Toghill, K. E.; Méndez, M. A.; Girault, H. H. Photoreduction of CO_2 Using $[Ru(Bpy)_2(CO)L]^{n+}$ Catalysts in Biphasic Solution/Supercritical CO_2 Systems. *Inorganic Chemistry* **2013**, 52 (19), 10949–10957. DOI:10.1021/ic401031j.
61. Lehn, J.-M.; Ziessel, R. Photochemical Reduction of Carbon Dioxide to Formate Catalyzed by 2,2'-Bipyridine- or 1,10-Phenanthroline-Ruthenium(II) Complexes. *Journal of Organometallic Chemistry* **1990**, 382 (1–2), 157–173. DOI:10.1016/0022-328x(90)85224-m.
62. Sekizawa, K.; Maeda, K.; Domen, K.; Koike, K.; Ishitani, O. Artificial Z-Scheme Constructed with a Supramolecular Metal Complex and Semiconductor for the Photocatalytic Reduction of CO_2. *Journal of the American Chemical Society* **2013**, 135 (12), 4596–4599. DOI:10.1021/ja311541a.
63. Hawecker, J.; Lehn, J.-M.; Ziessel, R. Efficient Photochemical Reduction of CO2to CO by Visible Light Irradiation of Systems Containing Re(Bipy)$(CO)_3X$ or $Ru(Bipy)_3^{2+}$–Co^{2+} Combinations as Homogeneous Catalysts. *Journal of the Chemical Society, Chemical Communications* **1983**, 9, 536–538. DOI:10.1039/c39830000536.
64. Ziessel, R.; Hawecker, J.; Lehn, J.-M. Photogeneration of Carbon Monoxide and of Hydrogenvia Simultaneous Photochemical Reduction of Carbon Dioxide and Water by Visible-Light Irradiation of Organic Solutions Containing Tris(2,2'-Bipyridine)Ruthenium(II) and Cobalt(II) Species as Homogeneous Catalysts. *Helvetica Chimica Acta* **1986**, 69 (5), 1065–1084. DOI:10.1002/hlca.19860690514.
65. Fisher, B. J.; Eisenberg, R. Electrocatalytic Reduction of Carbon Dioxide by Using Macrocycles of Nickel and Cobalt. *Journal of the American Chemical Society* **1980**, 102 (24), 7361–7363. DOI:10.1021/ja00544a035.
66. Tinnemans, A. H.; Koster, T. P.; Thewissen, D. H.; Mackor, A. Tetraaza-Macrocyclic Cobalt(II) and Nickel(II) Complexes as Electron-Transfer Agents in the Photo(Electro)Chemical and Electrochemical Reduction of Carbon Dioxide. *Recueil des Travaux Chimiques des Pays-Bas* **2010**, 103 (10), 288–295. DOI:10.1002/recl.19841031004.

67. Matsuoka, S.; Yamamoto, K.; Pac, C.; Yanagida, S. Enhancedp-Terphenyl-Catalyzed Photoreduction of CO_2 to CO through the Mediation of Co(III)–Cyclam Complex. *Chemistry Letters* **1991**, 20 (12), 2099–2100. DOI:10.1246/cl.1991.2099.
68. Bourrez, M.; Molton, F.; Chardon-Noblat, S.; Deronzier, A. [Mn(Bipyridyl)$(CO)_3$Br]: An Abundant Metal Carbonyl Complex as Efficient Electrocatalyst for CO_2 Reduction. *Angewandte Chemie International Edition* **2011**, 50 (42), 9903–9906. DOI:10.1002/anie.201103616.
69. Sampson, M. D.; Nguyen, A. D.; Grice, K. A.; Moore, C. E.; Rheingold, A. L.; Kubiak, C. P. Manganese Catalysts with Bulky Bipyridine Ligands for the Electrocatalytic Reduction of Carbon Dioxide: Eliminating Dimerization and Altering Catalysis. *Journal of the American Chemical Society* **2014**, 136 (14), 5460–5471. DOI:10.1021/ja501252f.
70. Takeda, H.; Koizumi, H.; Okamoto, K.; Ishitani, O. Photocatalytic CO_2 Reduction Using a Mn Complex as a Catalyst. *Chemical Communications* **2014**, 50 (12), 1491–1493. DOI:10.1039/c3cc48122k.
71. Grant, J. L.; Goswami, K.; Spreer, L. O.; Otvos, J. W.; Calvin, M. Photochemical Reduction of Carbon Dioxide to Carbon Monoxide in Water Using a Nickel(II) Tetra-Azamacrocycle Complex as Catalyst. *Journal of the Chemical Society, Dalton Transactions* **1987**, No. 9, 2105. DOI:10.1039/dt9870002105.
72. Mochizuki, K.; Manaka, S.; Takeda, I.; Kondo, T. Synthesis and Structure of [6,6‘-Bi(5,7-Dimethyl-1,4,8,11-Tetraazacyclotetradecane)]Dinickel(II) Triflate and Its Catalytic Activity for Photochemical CO_2 Reduction. *Inorganic Chemistry* **1996**, 35 (18), 5132–5136. DOI:10.1021/ic960208e.
73. Sato, S.; Morikawa, T.; Kajino, T.; Ishitani, O. A Highly Efficient Mononuclear Iridium Complex Photocatalyst for CO_2 Reduction under Visible Light. *Angewandte Chemie International Edition* **2012**, *52* (3), 988–992. DOI:10.1002/anie.201206137.
74. Reithmeier, R. O.; Meister, S.; Rieger, B.; Siebel, A.; Tschurl, M.; Heiz, U.; Herdtweck, E. Mono- and Bimetallic Ir(III) Based Catalysts for the Homogeneous Photocatalytic Reduction of CO_2 under Visible Light Irradiation. New Insights into Catalyst Deactivation. *Dalton Transactions* **2014**, *43* (35), 13259. DOI:10.1039/c4dt01717j.
75. Bonin, J.; Robert, M.; Routier, M. Selective and Efficient Photocatalytic CO_2 Reduction to CO Using Visible Light and an Iron-Based Homogeneous Catalyst. *Journal of the American Chemical Society* **2014**, *136* (48), 16768–16771. DOI:10.1021/ja510290t.
76. Grodkowski, J.; Behar, D.; Neta, P.; Hambright, P. Iron Porphyrin-Catalyzed Reduction of CO_2. Photochemical and Radiation Chemical Studies. *The Journal of Physical Chemistry A* **1997**, *101* (3), 248–254. DOI:10.1021/jp9628139.
77. Bonin, J.; Chaussemier, M.; Robert, M.; Routier, M. Homogeneous Photocatalytic Reduction of CO_2 to CO Using Iron(0) Porphyrin Catalysts: Mechanism and Intrinsic Limitations. *ChemCatChem* **2014**, *6* (11), 3200–3207. DOI:10.1002/cctc.201402515.
78. Behar, D.; Dhanasekaran, T.; Neta, P.; Hosten, C. M.; Ejeh, D.; Hambright, P.; Fujita, E. Cobalt Porphyrin Catalyzed Reduction of CO_2. Radiation Chemical, Photochemical, and Electrochemical Studies. *The Journal of Physical Chemistry A* **1998**, *102* (17), 2870–2877. DOI:10.1021/jp9807017.
79. Hieber, W.; Fuchs, H. Über Metallcarbonyle. XXXIX. Aminsubstituierte Rheniumcarbonyle. *Zeitschrift für anorganische und allgemeine Chemie* **1941**, *248* (3), 269–275. DOI:10.1002/zaac.19412480305

80. Wrighton, M.; Morse, D. L. Nature of the Lowest Excited State in Tricarbonylchloro-1,10-Phenanthrolinerhenium(I) and Related Complexes. *Journal of the American Chemical Society* **1974**, *96* (4), 998–1003. DOI:10.1021/ja00811a008.
81. Luong, J. C.; Nadjo, L.; Wrighton, M. S. Ground and Excited State Electron Transfer Processes Involving *Fac*-Tricarbonylchloro(1,10-Phenanthroline)Rhenium(I). Electrogenerated Chemiluminescence and Electron Transfer Quenching of the Lowest Excited State. *Journal of the American Chemical Society* **1978**, *100* (18), 5790–5795. DOI:10.1021/ja00486a033.
82. Hawecker, J.; Lehn, J.-M.; Ziessel, R. Photochemical and Electrochemical Reduction of Carbon Dioxide to Carbon Monoxide Mediated by (2,2'-Bipyridine)Tricarbonylchlororhenium(I) and Related Complexes as Homogeneous Catalysts. *Helvetica Chimica Acta* **1986**, *69* (8), 1990–2012. DOI:10.1002/hlca.19860690824.
83. Caspar, J. V.; Meyer, T. J. Application of the Energy Gap Law to Nonradiative, Excited-State Decay. *The Journal of Physical Chemistry* **1983**, *87* (6), 952–957. DOI:10.1021/j100229a010.
84. Kutal, C.; Weber, M. A.; Ferraudi, G.; Geiger, D. A Mechanistic Investigation of the Photoinduced Reduction of Carbon Dioxide Mediated by Tricarbonylbromo(2,2'-Bipyridine)Rhenium(I). *Organometallics* **1985**, *4* (12), 2161–2166. DOI:10.1021/om00131a016.
85. Kalyanasundaram, K. Luminescence and Redox Reactions of the Metal-to-Ligand Charge-Transfer Excited State of Tricarbonylchloro-(Polypyridyl)Rhenium(I) Complexes. *Journal of the Chemical Society, Faraday Transactions* **1986**, *82* (12), 2401. DOI:10.1039/f29868202401.
86. Kaim, W.; Kohlmann, S. EPR Evidence for Related Electronic Structures of α-Diimine Complexes with $[Ru(Bpy)_2]^{2+}$ and $Re(CO)_3(Halide)$ Fragments. *Chemical Physics Letters* **1987**, *139* (3–4), 365–369. DOI:10.1016/0009-2614(87)80574-2.
87. Juris, A.; Campagna, S.; Bidd, I.; Lehn, J. M.; Ziessel, R. Synthesis and Photophysical and Electrochemical Properties of New Halotricarbonyl(Polypyridine)Rhenium(I) Complexes. *Inorganic Chemistry* **1988**, *27* (22), 4007–4011. DOI:10.1021/ic00295a022.
88. Stufkens, D. J. The Remarkable Properties of α-Diimine Rhenium Tricarbonyl Complexes in Their Metal-to-Ligand Charge-Transfer (MLCT) Excited States. *Comments on Inorganic Chemistry* **1992**, *13* (6), 359–385. DOI:10.1080/02603599208048467.
89. Wallace, L.; Rillema, D. P. Photophysical Properties of Rhenium(I) Tricarbonyl Complexes Containing Alkyl- and Aryl-Substituted Phenanthrolines as Ligands. *Inorganic Chemistry* **1993**, *32* (18), 3836–3843. DOI:10.1021/ic00070a012.
90. Ishitani, O.; George, M. W.; Ibusuki, T.; Johnson, F. P.; Koike, K.; Nozaki, K.; Pac, C.; Turner, J. J.; Westwell, J. R. Photophysical Behavior of a New CO_2 Reduction Catalyst, $Re(CO)_2(Bpy)\{P(OEt)_3\}^{2+}$. *Inorganic Chemistry* **1994**, *33* (21), 4712–4717. DOI:10.1021/ic00099a022.
91. Hori, H.; Johnson, F. P. A.; Koike, K.; Ishitani, O.; Ibusuki, T. Efficient Photocatalytic CO_2 Reduction Using $[Re(Bpy)(CO)_3\{P(OEt)_3\}]^{+}$. *Journal of Photochemistry and Photobiology A: Chemistry* **1996**, *96* (1–3), 171–174. DOI:10.1016/1010-6030(95)04298-9.
92. Koike, K.; Hori, H.; Ishizuka, M.; Westwell, J. R.; Takeuchi, K.; Ibusuki, T.; Enjouji, K.; Konno, H.; Sakamoto, K.; Ishitani, O. Key Process of the Photocatalytic Reduction of CO_2

Using [Re(4,4'-X_2-Bipyridine)$(CO)_3PR_3]^+$ (X = CH_3, H, CF_3; PR_3 = Phosphorus Ligands): Dark Reaction of the One-Electron-Reduced Complexes with CO_2. *Organometallics* **1997**, *16* (26), 5724–5729. DOI:10.1021/om970608p.

93. Hori, H.; Ishihara, J.; Koike, K.; Takeuchi, K.; Ibusuki, T.; Ishitani, O. Photocatalytic Reduction of Carbon Dioxide Using [*Fac*-Re(Bpy)$(CO)_3$(4-xpy)]+ (xpy = pyridine Derivatives). *Journal of Photochemistry and Photobiology A: Chemistry* **1999**, *120* (2), 119–124. DOI:10.1016/s1010-6030(98)00430-4.
94. Kurz, P.; Probst, B.; Spingler, B.; Alberto, R. Ligand Variations in [ReX(Diimine)$(CO)_3$] Complexes: Effects on Photocatalytic CO_2 Reduction. *European Journal of Inorganic Chemistry* **2006**, *2006* (15), 2966–2974. DOI:10.1002/ejic.200600166.
95. Takeda, H.; Koike, K.; Inoue, H.; Ishitani, O. Development of an Efficient Photocatalytic System for CO_2 Reduction Using Rhenium(I) Complexes Based on Mechanistic Studies. *Journal of the American Chemical Society* **2008**, *130*(6), 2023–2031. DOI:10.1021/ja077752e.
96. Chauvin, J.; Lafolet, F.; Chardon-Noblat, S.; Deronzier, A.; Jakonen, M.; Haukka, M. Towards New Molecular Photocatalysts for CO_2 Reduction: Photo-Induced Electron Transfer versus CO Dissociation within [Os(NN)$(CO)_2Cl_2$] Complexes. *Chemistry - A European Journal* **2011**, *17* (15), 4313–4322. DOI:10.1002/chem.201003098.
97. Bian, Z.-Y.; Wang, H.; Fu, W.-F.; Li, L.; Ding, A.-Z. Two Bifunctional Ru(II)/Re(I) Photocatalysts for CO_2 Reduction: A Spectroscopic, Photocatalytic, and Computational Study. *Polyhedron* **2012**, *32* (1), 78–85. DOI:10.1016/j.poly.2011.08.037.
98. Ettedgui, J.; Diskin-Posner, Y.; Weiner, L.; Neumann, R. Photoreduction of Carbon Dioxide to Carbon Monoxide with Hydrogen Catalyzed by a Rhenium(I) Phenanthroline−polyoxometalate Hybrid Complex. *Journal of the American Chemical Society* **2010**, *133* (2), 188–190. DOI:10.1021/ja1078199.
99. Yu, B.; Li, L.; Liu, S.; Wang, H.; Liu, H.; Lin, C.; Liu, C.; Wu, H.; Zhou, W.; Li, X.; Wang, T.; Chen, B.; Jiang, J. Robust Biological Hydrogen-bonded Organic Framework with Post-functionalized Rhenium(I) Sites for Efficient Heterogeneous Visible-light-driven CO_2 Reduction. *Angewandte Chemie International Edition* **2021**, *133* (16), 9065–9071. DOI:10.1002/ange.202016710.
100. Gao, S.; Zhang, Q.; Su, X.; Wu, X.; Zhang, X.-G.; Guo, Y.; Li, Z.; Wei, J.; Wang, H.; Zhang, S.; Wang, J. Ingenious Artificial Leaf Based on Covalent Organic Framework Membranes for Boosting CO_2 Photoreduction. *Journal of the American Chemical Society* **2023**, *145* (17), 9520–9529. DOI:10.1021/jacs.2c11146.
101. Liang, H.-P.; Acharjya, A.; Anito, D. A.; Vogl, S.; Wang, T.-X.; Thomas, A.; Han, B.-H. Rhenium-Metalated Polypyridine-Based Porous Polycarbazoles for Visible-Light CO_2 Photoreduction. *ACS Catalysis* **2019**, *9* (5), 3959–3968. DOI:10.1021/acscatal.8b04032.
102. Li, J.; Zhao, D.; Liu, J.; Liu, A.; Ma, D. Covalent Organic Frameworks: A Promising Materials Platform for Photocatalytic CO_2 Reductions. *Molecules* **2020**, *25* (10), 2425. DOI:10.3390/molecules25102425.
103. Nguyen, H. L.; Alzamly, A. Covalent Organic Frameworks as Emerging Platforms for CO_2 Photoreduction. *ACS Catalysis* **2021**, *11* (15), 9809–9824. DOI:10.1021/acscatal.1c02459.
104. Fujita, E.; Grills, D. C.; Manbeck, G. F.; Polyansky, D. E. Understanding the Role of Inter- and Intramolecular Promoters in Electro- and Photochemical CO_2 Reduction Using Mn,

Re, and Ru Catalysts. *Accounts of Chemical Research* **2022**, *55* (5), 616–628. DOI:10.1021/acs.accounts.1c00616.
105. Müller, A. V.; Faustino, L. A.; de Oliveira, K. T.; Patrocinio, A. O.; Polo, A. S. Visible-Light-Driven Photocatalytic CO_2 Reduction by Re(I) Photocatalysts with N-Heterocyclic Substituents. *ACS Catalysis* **2022**, *13* (1), 633–646. DOI:10.1021/acscatal.2c05521.
106. Uoyama, H.; Goushi, K.; Shizu, K.; Nomura, H.; Adachi, C. Highly Efficient Organic Light-Emitting Diodes from Delayed Fluorescence. *Nature* **2012**, *492* (7428), 234–238. DOI:10.1038/nature11687.
107. Yang, Z.; Mao, Z.; Xie, Z.; Zhang, Y.; Liu, S.; Zhao, J.; Xu, J.; Chi, Z.; Aldred, M. P. Recent Advances in Organic Thermally Activated Delayed Fluorescence Materials. *Chemical Society Reviews* **2017**, *46* (3), 915–1016. DOI:10.1039/c6cs00368k.
108. Rasu, L.; Amiri, M.; Bergens, S. H. Carbazole–Cyanobenzene Dyes Electrografted to Carbon or Indium-Doped Tin Oxide Supports for Visible Light-Driven Photoanodes and Olefin Isomerizations. *ACS Applied Materials & Interfaces* **2021**, *13* (15), 17745–17752. DOI:10.1021/acsami.1c05064.
109. Herman, B.; Davidson, M. W.; Johnson, I. D.; Lakowicz, J. R. Solvent Effects on Fluorescence Emission. https://www.olympus-lifescience.com/en/microscope-resource/primer/java/jablonski/solventeffects/#:~:text=Solvent%20molecules%20assist%20in%20stabilizing,between%2010%20and%20100%20picoseconds (accessed 2023-07-04).
110. Snyder, L. R. Classification off the Solvent Properties of Common Liquids. *Journal of Chromatographic Science* **1978**, *16*(6), 223–234. DOI:10.1093/chromsci/16.6.223.
111. Jacobs, F. J.; Venter, G. J.; Fourie, E.; Kroon, R. E.; Brink, A. Substitution Reactivity and Structural Variability Induced by Tryptamine on the Biomimetic Rhenium Tricarbonyl Complex. *RSC Advances* **2021**, *11* (39), 24443–24455. DOI:10.1039/d1ra03750a.
112. Mukuta, T.; Simpson, P. V.; Vaughan, J. G.; Skelton, B. W.; Stagni, S.; Massi, M.; Koike, K.; Ishitani, O.; Onda, K. Photochemical Processes in a Rhenium(I) Tricarbonyl N-Heterocyclic Carbene Complex Studied by Time-Resolved Measurements. *Inorganic Chemistry* **2017**, *56* (6), 3404–3413. DOI:10.1021/acs.inorgchem.6b02936.
113. Koizumi, H.; Chiba, H.; Sugihara, A.; Iwamura, M.; Nozaki, K.; Ishitani, O. CO_2 Capture by Mn(I) and Re(I) Complexes with a Deprotonated Triethanolamine Ligand. *Chemical Science* **2019**, *10* (10), 3080–3088. DOI:10.1039/c8sc04389b.
114. Kurtz, D. A.; Brereton, K. R.; Ruoff, K. P.; Tang, H. M.; Felton, G. A.; Miller, A. J.; Dempsey, J. L. Bathochromic Shifts in Rhenium Carbonyl Dyes Induced through Destabilization of Occupied Orbitals. *Inorganic Chemistry* **2018**, *57*(9), 5389–5399. DOI:10.1021/acs.inorgchem.8b00360.
115. Greenwood, N. N.; Earnshaw, A. Manganese, Technetium and Rhenium. *Chemistry of the Elements* **1997**, 1040–1069. DOI:10.1016/b978-0-7506-3365-9.50030-4.
116. Liyanage, N. P.; Yang, W.; Guertin, S.; Sinha Roy, S.; Carpenter, C. A.; Adams, R. E.; Schmehl, R. H.; Delcamp, J. H.; Jurss, J. W. Photochemical CO_2 Reduction with Mononuclear and Dinuclear Rhenium Catalysts Bearing a Pendant Anthracene Chromophore. *Chemical Communications* **2019**, *55* (7), 993–996. DOI:10.1039/c8cc09155b.
117. Feng, Y.; Ng, C.-O.; Tong, K.-M.; Cheng, S.-C.; Chan, L.-L.; Ko, C.-C. Study of Re(I) Carbene Complexes for Photocatalytic Reduction of Carbon Dioxide. *Energy & Fuels* **2021**, *35* (23), 19170–19177. DOI:10.1021/acs.energyfuels.1c02372.

118. Rotundo, L.; Grills, D. C.; Gobetto, R.; Priola, E.; Nervi, C.; Polyansky, D. E.; Fujita, E. Photochemical CO_2 Reduction Using Rhenium(I) Tricarbonyl Complexes with Bipyridyl-type Ligands with and without Second Coordination Sphere Effects. *ChemPhotoChem* **2021**, *5* (6), 526–537. DOI:10.1002/cptc.202000307.
119. Teesdale, J. J.; Pistner, A. J.; Yap, G. P. A.; Ma, Y.-Z.; Lutterman, D. A.; Rosenthal, J. Reduction of CO2 Using a Rhenium Bipyridine Complex Containing Ancillary BODIPY Moieties. *Catalysis Today* **2014**, *225*, 149–157. DOI:10.1016/j.cattod.2013.10.091.
120. Zhao, Q.; Meng, G.; Nolan, S. P.; Szostak, M. N-Heterocyclic Carbene Complexes in C–H Activation Reactions. *Chemical Reviews* **2020**, *120* (4), 1981–2048. DOI:10.1021/acs.chemrev.9b00634.
121. Jalal, M.; Hammouti, B.; Touzani, R.; Aouniti, A.; Ozdemir, I. Metal-NHC Heterocycle Complexes in Catalysis and Biological Applications: Systematic Review. *Materials Today: Proceedings* **2020**, *31*. DOI:10.1016/j.matpr.2020.06.398.
122. Peris, E. Smart N-Heterocyclic Carbene Ligands in Catalysis. *Chemical Reviews* **2017**, *118* (19), 9988–10031. DOI:10.1021/acs.chemrev.6b00695.
123. Tests for Anions - Chemical Analysis - (CCEA) - GCSE Chemistry (Single Science) Revision - CCEA - BBC Bitesize. https://www.bbc.co.uk/bitesize/guides/zmbmrj6/revision/16 (accessed 2023-07-31).
124. Malato-Rodríguez, S. Solar Detoxification and Disinfection. *Encyclopedia of Energy* **2004**, 587–596. DOI:10.1016/b0-12-176480-x/00323-5.
125. Zhang, W.; Li, H.; Li, X.; Zou, Z.; Huang, M.; Liu, J.; Wang, X.; Ni, S.; Pan, Y.; Wang, Y. A Practical Fluorosulfonylating Platform via Photocatalytic Imidazolium-Based SO_2F Radical Reagent. *Nature Communications* **2022**, *13* (1). DOI:10.1038/s41467-022-31296-2.
126. Lakowicz, J. R. Quenching of Fluorescence. In *Principles of fluorescence spectroscopy*; Springer, 2006; pp 277–330.
127. Gehlen, M. H. The Centenary of the Stern-Volmer Equation of Fluorescence Quenching: From the Single Line Plot to the SV Quenching Map. *Journal of Photochemistry and Photobiology C: Photochemistry Reviews* **2020**, *42*, 100338. DOI:10.1016/j.jphotochemrev.2019.100338.
128. John, D. A. Rhenium: A Rare Metal Critical in Modern Transportation. *Fact Sheet* **2015**. DOI:10.3133/fs20143101.
129. Lucchini, R. G.; Aschner, M.; Yangho kim; Šarić, M. Manganese. *Handbook on the Toxicology of Metals* **2015**, 975–1011. DOI:10.1016/b978-0-444-59453-2.00045-7.
130. Liu, J.; Perez, O.M.; Lavergne, D.; Rasu, L.; Murphy, E.; Galvez-Rodriguez, A.; Bergens, S.H. One-Step Electropolymerization of a Dicyanobenzene-Carbazole-Imidazole Dye to Prepare Photoactive Redox Polymer Films. *Polymers* **2023**, *15*, 3340. DOI:10.3390/polym15163340
131. Matsuda, S.; Niitsuma, Y.; Yoshida, Y.; Umeda, M. H_2-CO_2 Polymer Electrolyte Fuel Cell That Generates Power While Evolving CH4 at the Pt0.8ru0.2/C Cathode. *Scientific Reports* **2021**, *11* (1). DOI:10.1038/s41598-021-87841-4.
132. Liu, Y.; Li, Y.; Chen, Y.; Qu, T.; Shu, C.; Yang, X.; Zhu, H.; Guo, S.; Zhao, S.; Asefa, T.; Liu, Y. A CO_2/H_2 Fuel Cell: Reducing CO_2 While Generating Electricity. *Journal of Materials Chemistry A* **2020**, *8* (17), 8329–8336. DOI:10.1039/d0ta02855j.